Freshwater influence on the hydrography and dissolved CO_2 of the Northeast Greenland shelf

by Esdoorn Willcox

In partial fulfilment of the degree of

Doctor of Philosophy

A thesis submitted to
the Faculty of Graduate and Postdoctoral Studies
University of Manitoba

Department of Environment and Geography
C.H.R. Faculty of Environment, Earth, and Resources
University of Manitoba Winnipeg, Manitoba, Canada

Esdoorn Wander Sylvan Tijl

Willcox

Abstract

The Northeast Greenland shelf and the associated fjords are an extremely dynamic Arctic environment. It is influenced by Arctic Ocean processes, the Greenland Ice Sheet, and the North Atlantic. In turn, any modifications that occur in the region are exported south, back into the North Atlantic. This thesis addresses some of the open questions in the region regarding regional water mass distribution, carbon dynamics, and fjord processes.

The first research chapter presents an updated hydrography for the Northeast Greenland shelf, including observations from latitudes that were not included in previous work. We look at the sources for the water masses identified and find a clear link between the Polar Surface Water found on the Northeast Greenland shelf and the Laptev Sea region in the Siberian Arctic using geochemical tracers.

The second research chapter is an investigation of the effect of the hydrographical configuration identified in the previous chapter on the carbon system. We determine that the region can act as a source of CO_2 to the atmosphere rather than a sink, challenging the prior understanding of the Northeast Greenland shelf as a strong atmospheric CO_2 sink.

The third and last research chapter focuses on a mooring and novel automated stable water isotope sampler deployed, with a weather station, in a fjord linked to the Northeast Greenland shelf. After the maximum discharge occurs in autumn, driven by a change from along-shelf winds to piteraq, the salinity increases steadily. Nonetheless, the fjord remains stratified throughout winter between depths of 11 m and 50 m, even recovering after two high salinity events. This very stably stratified water column will be exported onto the shelf, where it will add to an already highly stratified surface water identified in the first research chapter.

Together these results provide a new synoptic view of changes associated with Northeast Greenland freshwater, that will open up new avenues of research in the region.

Acknowledgements

This thesis marks the end of the long and winding road that this PhD process has been. It has been a period of profound change, in terms of the focus of my programme as well as of the world as a whole. I started work on sea ice microstructure and brine networks and ended up writing this thesis on the topic of Northeast Greenland synoptic-scale oceanography and freshwater interactions. I am grateful that during pandemic lockdowns I had an opportunity to change direction and so to continue to work while so much of the world was at standstill.

First and foremost, I am grateful to my primary supervisor Dr. Søren Rysgaard, who has been instrumental in providing me with a broad set of opportunities and guidance throughout my PhD. A source of unerring support and openness to change, I was encouraged to choose new directions to investigate several times before settling into the project presented here. This is a luxury not many students have and has been pivotal in maintaining and developing my interdisciplinary interests and will stand me in good stead in future. I would like to thank co-supervisor Dr. Ryan Galley for his attention to detail and thorough questioning of my ideas during the initial phase of my PhD programme. Following 'the bouncing ball' has allowed me to stay on course and not be as distracted from pursuing a core idea as I otherwise might have been. I would like to thank PhD advisory committee member Dr. Feiyue Wang for being available in person to answer the litany of questions I have had on all manner of chemistry topics over the years, and Dr Roberta Hamme for the detailed feedback I received on the wide variety of work I have presented.

I would like to highlight the staff, faculty, and students at the Centre for Earth Observation Science (CEOS). In particular, I would like to thank Dr. Marcos Lemes for many hours spent guiding me in the lab and providing practical and logistical support and direction. My lab and field efforts were also supported by Debbie Armstrong, Ashley Soloway and David Binne. All the times I almost got stuck in

administrative quagmire could have ended in disaster if it had not been for the tireless efforts of Celia Mellinger and Linda Chow. Additionally, Dr. C.J. Mundy, Dr. Norm Kenkel, Dr. Jens Ehn, Dr. Igor Dmitrenko, and Dr. Kristina Brown each made an effort to provide me with additional guidance.

The list of fellow students in CEOS who influenced my path by providing advice or the opportunity to brainstorm is extensive, including (but not limited to) Dongyoung Back for being one of my first friends at UM, Durell Desmond for poetry and friendship, Kaushik Gupta and Atreya Basu for long and in depth conversations on culture and politics. Also thanks to Monojit Saha, Emma Ausen, and Aura Diaz for making my time at UM memorable. I would be remiss if I did not make particular mention of Tonya Burgers, who not only shares my passion for chemical tracers and oceanic carbon but also spent several weeks caring for me while I was recovering from surgery. You went above and beyond, thank you.

I would like to thank Bear Clan Patrol (West Broadway and North End) for allowing me to walk with you. Before I did I felt somewhat disconnected and you provided me with the grounding in community that I needed to find my place in Winnipeg. I would also like to thank everyone at Winnipeg Circus Club for all the fun. It was great hanging out with you. Special thanks to my Winnipeg trans family, Ashley Gawne, Mateo Llanillos, and Kai Solomon. You're awesome, thank you for everything you do for our community.

To my closest friends and chosen family, wherever you are in the world: You know who you are, I love you and I have your back, whatever happens next.

Land Acknowledgement

The University of Manitoba, at which much of the work for this thesis was done, is located on lands belonging to the Anishinaabeg, Cree, Ojibwe-Cree, Dakota and Dene peoples and on the homeland of the Métis Nation.

The land on which the university stands is part of the Peguis-Selkirk Treaty of 1917, a land-sharing agreement that was willfully misinterpreted by the Hudson Bay Company. Subsequently in 1871, the land was covered by Treaty 1, the first of the numbered treaties. I acknowledge that promises were made to the signatory First Nations during the negotiations of this treaty that were broken, particularly pertaining to the ownership, rather than sharing of, lands and in respecting First Nations ways of life.

In addition, I acknowledge that the country of my birth, the Netherlands, entered into the Two Row Wampum Treaty with the Nations of the Haudenosaunee in 1613 to establish kaswentha relations between our peoples, as conferred in the oral Iroquois tradition.

I have been welcomed to sit by sacred fires, listen to the Bear Song, and share in Country Food. I have been shown such genuine care and generosity in the light of current and historical wrongs that I can not be anything but grateful and I will carry their lessons within me for the rest of my life.

Contents

List of Figures

List of Tables

1 Introduction

1.1 Thesis motivation

The Northeast Greenland shelf is one of two outflow shelves of the Arctic Ocean. Between 2000 and 2010 57 % of Arctic Ocean freshwater was exported via Fram Strait, 23 % via sea ice export and 34 % as liquid freshwater (Haine et al., 2015). This freshwater is buoyant compared to the Atlantic Water (AW) on which it is superimposed, and can be advected onto the relatively shallow shelf through Ekman and geostrophic driven transport (Vianco, 2024). Since 2010, each of the different sources of freshwater to and in the Arctic Ocean has undergone extensive change.

Freshwater discharge from rivers has increased (Shiklomanov et al., 2021), and 12.5 % of sea ice volume was lost between 2018 and 2021 (Kacimi and Kwok, 2022). Precipitation is set to increase associated with the increase in global temperatures and associated poleward moisture transport (McCrystall et al., 2021). It is estimated that up to 7.5 % of global atmospheric carbon dioxide (CO_2) uptake occurs in the Arctic Ocean (Bates et al., 2009), a larger component of global carbon exchange than expected for this relatively small ocean. Each freshwater component, including sea ice melt, terrestrial discharge, and direct precipitation, influences the carbon inventory in a unique way. In the rapidly changing Arctic Ocean this can lead to complex and potentially unpredictable] consequences for Arctic outflow shelves, including the Northeast Greenland shelf, potentially negatively influencing the life found there (Kikuchi et al., 2021).

Seasons of successive sea ice melting and freezing as water is transported across the Arctic Ocean, dilute the surface water with respect to many of its dissolved

constituents. These constituents are transported from inside the ice within drained brine which mixes with water at the ice-ocean interface. This constituent-rich and denser than ambient water eventually sinks to a depth where it achieves neutral buoyancy (Jones et al., 1983; Rysgaard et al., 2007; Miller et al., 2011). This process separates constituents found in seawater such as salts and other impurities by freezing. Separation of those impurities (with respect to a pure ice matrix) which are more likely to remain in the ice from those that are rejected is considered a leading cause for the higher buffer capacity found in Arctic Ocean surface water which have a high sea ice melt fraction. The higher buffer capacity associated with seasonal sea ice melting into the surface layer, is thought to allow more CO_2 to be dissolved without increasing acidification by lowering the pH. Contrary to this, there has been some evidence of aragonite (a metastable form of calcium carbonate) undersaturation in the Western Arctic in newly melted regions (Robbins et al., 2013; Qi et al., 2022).

Terrestrial freshwater discharge from rivers contains particulate and dissolved organic and inorganic matter (Holmes et al., 2000; Tank et al., 2023). Arctic rivers also supply much of the alkalinity found in the Arctic Ocean (Tank et al., 2016; Drake et al., 2018). Around 11 % of global freshwater is discharged into the Arctic Ocean (Shiklomanov et al., 2000) even though it contains a mere 1 % of global ocean volume and only 3 % of global ocean surface area (Dai and Trenberth, 2002; Carmack et al., 2016). This results in a strong influence of terrestrial freshwater on processes occurring in the Arctic Ocean, and in a strong coupling between bioavailable and photolabile materials, and alkalinity, with freshwater content. This is especially pronounced on the continental shelves and within the photic zone where photosynthesis and photochemical reactions can take place. Since these materials and the processes that act on them all involve the carbon cycle, the determination of the relative quantities of these is important in the entire Arctic Ocean domain, including on the Northeast Greenland outflow shelf.

The Northeast Greenland shelf is generally considered to be an annual net sink for atmospheric CO_2. This is a result of theory surrounding increased buffering capacity per fraction of sea ice melt present in the surface layer (Jones and Coote, 1981) and early observations which established the important role of sea ice cover

as a seasonal barrier between atmosphere and ocean during the dark season (Jones et al., 1983; Jones et al., 1983; Yager et al., 1995). Whether this is true has not been verified for the Northeast Greenland shelf to date. After the initial observations were made in the 1990s, only two datasets contain measurements on the Northeast Greenland shelf. One is a collection of measurements of the fugacity of CO_2 by an underway system (Bakker et al., 2023), and the others are part of CARINA (CARbon IN the Atlantic) where several full-depth sections cross onto the Northeast Greenland shelf (Olsen, 2009). The former comprises the most recent results, going up to 2014 but has a strong late-spring and early-summer bias,with most measurements between late May and late July.

Very little is known about the interaction between the water sources introduced to the Arctic Ocean upstream and their interaction with water sources and relevant processes input along the Northeast Greenland shelf. This is primarily due to regional inaccessibility as a result of the formerly perennial sea ice cover. In addition, finding suitable mooring locations for monitoring the upper 70 m of the water column where much of these activities take place is challenging, especially close to the coast and inside the fjord systems, due to the presence of icebergs with a high risk of equipment loss.

The primary goal for this thesis was to use full depth field observations taken opportunistically during a low sea ice year in late summer/early autumn to infer carbon system changes associated with an open water season on the Northeast Greenland shelf. The presence of specific water masses and their relative spatial and temporal distribution on the shelf had only been quantified for the Northern part of the Northeast Greenland shelf (Budéus and Schneider, 1995; Bignami and Hopkins, 1997; Budéus et al., 1997; Falck, 2001; Dodd et al., 2012) which limited our ability to directly explain the factors driving the variability of the carbonate system.

Since the water mass fractions on the shelf are all variable, the determination of the water mass presence is a prerequisite to study the behaviour of CO_2 on the shelf, particularly near the surface where the water may be (seasonally) in touch with the atmosphere through convection. This thesis therefore first addresses

both the hydrography and the carbon system of the Northeast Greenland shelf and adds a complimentary study on seasonal exchanges that take place inside an East Greenland fjord system to determine possible temporal hydrographic variation.

1.2 Thesis objectives

The initial goal of the PhD work undertaken was to determine the drivers of the carbonate system on the Northeast Greenland Shelf. During initial investigations it became clear that an understanding of the carbonate system would first require a complete review of the local hydrography and freshwater sources. This resulted in two main objectives:

1. Determine which water masses are present on the Northeast Greenland shelf, their characteristics, and how they might be locally transformed.
2. Determine the main drivers of the carbonate system on the Northeast Greenland shelf.

1.3 Thesis outline

The initial goal upon which the data made available for this project was based was intended to determine the main controls on the carbon system on the Northeast Greenland shelf. Initial investigations of these data highlighted that the region had changed since prior hydrographic surveys (Budéus and Schneider, 1995; Bignami and Hopkins, 1997; Budéus et al., 1997). and that the hydrography on the shelf would have to be revisited before the regional variability in CO_2 could be fully understood.

Therefore this manuscript is divided into several sections. After this introduction (chapter 1), there are five additional chapters. A background chapter (chapter 2) describes water masses in the Arctic Ocean, an overview of the hydrography of the Northeast Greenland shelf and fjords, and the associated carbon system.

Two published manuscripts, titled "An Updated View of the Water Masses on the Northeast Greenland Shelf and Their Link to the Laptev Sea and Lena River" (chapter 3) and "The Northeast Greenland Shelf as a potential late-summer CO_2 source to the atmosphere" (chapter 4) have been published in peer reviewed journals. The first is a review of shelf hydrography and the second investigates the associated shelf carbon system. The review of the hydrograpohy is a pre-requisite to understanding the surface water source locations and any processes taking place there that might influence CO_2. The final manuscript is titled "A year of hydrographic variability in a fjord in Northeast Greenland" (chapter 5) which looks at the variability and trends of a fjord system bordering on the Northeast Greenland shelf during winter. This manuscript is still undergoing modifications prior to being submitted to a journal. Finally, my conclusions and future research avenues based on the overall thesis are presented in chapter 6.

In chapter 3 (Willcox et al., 2023), I address the first thesis objective by determining the water masses present and linking Northeast Greenland inexorably to the Laptev Sea via the Transpolar Drift (TPD) stream. I examined the Conductivity Temperature Depth device (CTD) profiles with mounted oxygen sensor observations, and data from the associated bottle chemistry, including phosphate, nitrate, and silicate, and the stable water hydrogen $\delta^2 H$ and oxygen $\delta^{18} O$ isotopes. We grouped CTD profiles by their shape in a TS diagram, to determine the vertical order and mixing behaviour of water types on the shelf. Variations in the average profiles of (potential) temperature and salinity are associated with five different geographical regions, and showed mixing is enhanced along the slope near the East Greenland Current (EGC) where Atlantic Water (AW) from the West Spitsbergen Current (WSC) meets cold Arctic-sourced water, including Polar Surface Water (PSW), Polar Surface Water (warm) (PSWw), and Arctic Atlantic Water (AAW). Nitrogen is entirely depleted in the surface layer. The highest dissolved oxygen concentrations are found in the remnant of the winter mixed layer at around 30 m where nutrients, in particular nitrogen, also start to become available. This layer is not ventilated to the atmosphere due to the strongly stratified summer mixed layer.

This chapter does not address the subglacial meltwater component from the Greenland Ice Sheet in the surface water in the Northeast Greenland shelf. The volume

of water produced by the Greenland Ice Sheet is small compared to that of the Eurasian river input transported via the TPD (Haine et al., 2015). Further, it has been shown that even near the glacial front of Niogerhalvfjerdsbrae (or the 79N glacier) which discharges onto the shelf, the subglacial discharge only amounts to 1.8 % and is not measured near the shelf edge, and is less influential than the sea ice melt component (Huhn et al., 2021).

In chapter 4 (Willcox et al., 2024) I utilise the information gleaned in the first paper to look at the processes controlling the carbon system through measurements of dissolved inorganic carbon and total alkalinity. To be able to determine these processes, I normalize the carbonate data by the application of a polynomial, a novel method which compares well to an initial normalization by sea ice meltwater fraction followed by a salinity normalization for the dilution of dissolved constituents by meteoric freshwater. The data can be separated into two periods, and each have a different spatial scope. These two groupings show different patterns. Data obtained in late August and early September and is obtained from stations closer to the slope has a higher fugacity of CO_2 than the stations from late September and nearer to the coast. The controlling factor of this change is a reduction in dissolved inorganic carbon. The total alkalinity is adequately predicted by the algorithm written by Arrigo et al. (2010) which was based on data collected in the Northeast Water Polynya in the early 1990s by Wallace et al. (1995). I was unable to match any algorithm to the observed dissolved inorganic carbon concentration, which could lead to mistakes in modeling efforts. Below the surface mixed layer which is nitrogen depleted, the fugacity of CO_2 is inversely correlated with dissolved oxygen. The highest dissolved oxygen and lowest dissolved CO_2 are found in the unventilated remnant of the winter mixed layer. Gas exchange with the atmosphere is limited to the summer surface mixed layer, at least until this layer deepens to the depths of the previous winter.

In chapter 5, I discuss a full year (2022/2023) of hydrographical observations inside a Northeast Greenland fjord system that borders on the Northeast Greenland shelf based on weather station data combined with current data from an upward facing Acoustic Doppler Current Profiler (ADCP), two Conductivity Temperature Depth device (CTD), and a stable water isotopic sampler set to store one new sample each

week. Water at depths as shallow as 11 m remains above freezing temperatures (based on their salinity) until January, indicating that the mixed layer deepens slowly throughout winter. The wind system is dominated by piteraq in winter and shifts to along-shelf winds during spring. The system remains stratified between 11 m and 50 m depth throughout winter. This supports a depth of shallower than 50 m for the maximum winter mixed layer depth in winter which was found in Willcox et al. (2023) to be at ~ 30 m.

References

Arrigo KR, Pabi S, van Dijken GL, Maslowski W. 2010. Air-sea flux of CO2 in the Arctic Ocean, 1998 – 2003. *Journal of Geophysical Research* **115**(G4): G04024. doi: 10.1029/2009jg001224

Bakker DCE, Alin SR, Bates N, Becker M, Feely RA, Gkritzalis T, Jones SD, Kozyr A, Lauvset SK, Metzl N, et al. 2023. Surface Ocean CO2 Atlas Database Version 2023 (SOCATv2023) (NCEI Accession 0278913). NOAA National Centers for Environmental Information. doi: 10.25921/R7XA-BT92

Bates NR, Mathis JT, Cooper LW. 2009. Ocean acidification and biologically induced seasonality of carbonate mineral saturation states in the western Arctic Ocean. *Journal of Geophysical Research* **114**(C11): C11007. doi: 10.1029/2008jc004862

Bignami F, Hopkins TS. 1997. The water mass characteristics of the Northeast Water Polynya: Polar Sea data 1992 – 1993. *Journal of Marine Systems* **10**(1-4): 139 – 156. doi: 10.1016/S0924-7963(96)00079-6

Budéus G, Schneider W. 1995. On the hydrography of the Northeast Water Polynya. *Journal of Geophysical Research* **100**(C3): 4287. doi: 10.1029/94jc02024

Budéus G, Schneider W, Kattner G. 1997. Distribution and exchange of water masses in the Northeast Water polynya (Greenland Sea). *Journal of Marine Systems*

10(1): 123 – 138. doi: 10.1016/s0924-7963(96)00074-7

Carmack EC, Yamamoto-Kawai M, Haine TWN, Bacon S, Bluhm BA, Lique C, Melling H, Polyakov IV, Straneo F, Timmermans M-L, et al. 2016. Freshwater and its role in the Arctic Marine System: Sources, disposition, storage, export, and physical and biogeochemical consequences in the Arctic and global oceans. *Journal of Geophysical Research: Biogeosciences* **121**(3): 675 – 717. doi: 10.1002/2015jg003140

Dai A, Trenberth KE. 2002. Estimates of Freshwater Discharge from Continents: Latitudinal and Seasonal Variations. *Journal of Hydrometeorology* **3**(6): 660 – 687. doi: 10.1175/1525-7541(2002)003<0660:EOFDFC>2.0.CO;2

Dodd PA, Rabe B, Hansen E, Falck E, Mackensen A, Rohling E, Stedmon C, Kristiansen S. 2012. The freshwater composition of the Fram Strait outflow derived from a decade of tracer measurements: COMPOSITION OF THE FRAM STRAIT OUTFLOW. *Journal of Geophysical Research: Oceans* **117**(C11): n/a – n/a. doi: 10.1029/2012JC008011

Drake TW, Tank SE, Zhulidov AV, Holmes RM, Gurtovaya T, Spencer RGM. 2018. Increasing Alkalinity Export from Large Russian Arctic Rivers. *Environmental Science & Technology* **52**(15): 8302 – 8308. doi: 10.1021/acs.est.8b01051

Falck E. 2001. Contribution of waters of Atlantic and Pacific origin in the Northeast Water Polynya. *Polar Research* **20**(2): 193 – 200. doi: 10.3402/polar.v20i2.6517

Haine TWN, Curry B, Gerdes R, Hansen E, Karcher M, Lee C, Rudels B, Spreen G, de Steur L, Stewart KD, et al. 2015. Arctic freshwater export: Status, mechanisms, and prospects. *Global and Planetary Change* **125**: 13 – 35. doi: 10.1016/j.gloplacha.2014.11.013

Holmes RM, Peterson BJ, Gordeev VV, Zhulidov AV, Meybeck M, Lammers RB, Vörösmarty CJ. 2000. Flux of nutrients from Russian rivers to the Arctic Ocean:

Can we establish a baseline against which to judge future changes? *Water Resources Research* **36**(8): 2309 – 2320. doi: 10.1029/2000wr900099

Huhn O, Rhein M, Kanzow T, Schaffer J, Sültenfuß J. 2021. Submarine Meltwater From Nioghalvfjerdsbræ (79 North Glacier), Northeast Greenland. *Journal of Geophysical Research: Oceans* **126**(7). doi: 10.1029/2021JC017224

Jones EP, Coote AR. 1981. Oceanic CO_2 produced by the precipitation of $CaCO_3$ from brines in sea ice. *Journal of Geophysical Research* **86**(C11): 11041. doi: 10.1029/JC086iC11p11041

Jones EPeter, Coote AR, Levy EM. 1983. Effect of sea ice meltwater on the alkalinity of seawater. *Journal of Marine Research* **41**(1): 43 – 52. doi: 10.1357/002224083788223063

Kacimi S, Kwok R. 2022. Arctic Snow Depth, Ice Thickness, and Volume From ICESat-2 and CryoSat-2: 2018 – 2021. *Geophysical Research Letters* **49**(5): e2021GL097448. doi: 10.1029/2021GL097448

Kikuchi T, Nishino S, Fujiwara A, Onodera J, Yamamoto-Kawai M, Mizobata K, Fukamachi Y, Watanabe E. 2021. Status and trends of Arctic Ocean environmental change and its impacts on marine biogeochemistry: Findings from the ArCS project. *Polar Science* **27**: 100639. doi: 10.1016/j.polar.2021.100639

McCrystall MR, Stroeve J, Serreze M, Forbes BC, Screen JA. 2021. New climate models reveal faster and larger increases in Arctic precipitation than previously projected. *Nature Communications* **12**(1): 6765. doi: 10.1038/s41467-021-27031-y

Miller LA, Papakyriakou TN, Collins RE, Deming JW, Ehn JK, Macdonald RW, Mucci A, Owens O, Raudsepp M, Sutherland N. 2011. Carbon dynamics in sea ice: A winter flux time series. *Journal of Geophysical Research* **116**(C2): C02028. doi: 10.1029/2009JC006058

Olsen A. 2009. Nordic Seas total alkalinity data in CARINA. *Earth System Science Data* **1**(1): 77 – 86. doi: 10.5194/essd-1-77-2009

Qi D, Ouyang Z, Chen L, Wu Y, Lei R, Chen B, Feely RA, Anderson LG, Zhong W, Lin H, et al. 2022. Climate change drives rapid decadal acidification in the Arctic Ocean from 1994 to 2020. *Science* **377**(6614): 1544 – 1550. doi: 10.1126/science.abo0383

Robbins LL, Wynn JG, Lisle JT, Yates KK, Knorr PO, Byrne RH, Liu X, Patsavas MC, Azetsu-Scott K, Takahashi T. 2013. Baseline Monitoring of the Western Arctic Ocean Estimates 20% of Canadian Basin Surface Waters Are Undersaturated with Respect to Aragonite. Paranhos R, editor. *PLoS ONE* **8**(9): e73796. doi: 10.1371/journal.pone.0073796

Rysgaard S, Glud RN, Sejr MK, Bendtsen J, Christensen PB. 2007. Inorganic carbon transport during sea ice growth and decay: A carbon pump in polar seas. *Journal of Geophysical Research* **112**(C3): C03016. doi: 10.1029/2006JC003572

Shiklomanov A, Déry S, Tretiakov M, Yang D, Magritsky D, Georgiadi A, Tang W. 2021. River freshwater flux to the arctic ocean. In: Yang D, Kane DL, editors. *Arctic Hydrology, Permafrost and Ecosystems*. Cham: Springer International Publishing. p. 703 – 738. doi: 10.1007/978-3-030-50930-9₂4

Shiklomanov AI, Lammers RB, Peterson BJ, Vorosmarty CJ. 2000. The Dynamics of River Water Inflow to the Arctic Ocean. In: Lewis EL, Jones EP, Lemke P, Prowse TD, Wadhams P, editors. *The Freshwater Budget of the Arctic Ocean*. Dordrecht: Springer Netherlands. p. 281 – 296. doi: 10.1007/978-94-011-4132-1_13

Tank SE, McClelland JW, Spencer RGM, Shiklomanov AI, Suslova A, Moatar F, Amon RMW, Cooper LW, Elias G, Gordeev VV, et al. 2023. Recent trends in the chemistry of major northern rivers signal widespread Arctic change. *Nature Geoscience* **16**(9): 789 – 796. doi: 10.1038/s41561-023-01247-7

Tank SE, Striegl RG, McClelland JW, Kokelj SV. 2016. Multi-decadal increases in dissolved organic carbon and alkalinity flux from the Mackenzie drainage basin to the Arctic Ocean. *Environmental Research Letters* **11**(5): 054015. doi: 10.1088/1748-9326/11/5/054015

Vianco SL. 2024. The origins of the East Greenland Coastal Current on the Northeast Greenland Shelf: A comparison of two reanalysis products [PhD thesis]. the Massachusetts Institute of Technology; the Woods Hole Oceanographic Institution. doi: 10.1575/1912/70545

Wallace DWR, Minnett PJ, Hopkins TS. 1995. Nutrients, oxygen, and inferred new production in the Northeast Water Polynya, 1992. *Journal of Geophysical Research* **100**(C3): 4323. doi: 10.1029/94JC02203

Willcox E, Bendtsen J, Mortensen J, Mohn C, Lemes M, Pedersen T-J, Holding J, Møller EF, Sejr MK, Seidenkrantz M-S, et al. 2023. An Updated View of the Water Masses on the Northeast Greenland Shelf and Their Link to the Laptev Sea and Lena River. *Journal of Geophysical Research: Oceans* **128**(4): e2022JC019052. doi: 10.1029/2022JC019052

Willcox E, Lemes M, Juul-Pedersen T, Sejr MK, Holding JM, Rysgaard S. 2024. The Northeast Greenland Shelf as a potential late-summer CO_2 source to the atmosphere. *Biogeosciences* **21**(17): 4037 – 4050. doi: 10.5194/bg-21-4037-2024

Yager PL, Wallace DWR, Johnson KM, Smith WO, Minnett PJ, Deming JW. 1995. The Northeast Water Polynya as an atmospheric CO_2 sink: A seasonal rectification hypothesis. *Journal of Geophysical Research* **100**(C3): 4389. doi: 10.1029/94JC01962

2 Background

To be able to understand the hydrography of the Northeast Greenland shelf it is necessary to look at water mass sources and their transformations upstream in the Arctic Ocean, and how they are advected to Fram Strait and eventually onto the Northeast Greenland shelf (Figure 2.1).

In this thesis I focus on the part of the water column at depths which can be advected onto our region of interest, the Northeast Greenland shelf and its adjoining fjord systems. Like most of the Arctic continental shelves, the Northeast Greenland shelf is a shallow and broad shelf region, interspersed with deeper troughs created by previous episodes of extensive glaciation. The troughs found on the shelf extend down to a maximum of ~ 300 - 370 m (Arndt et al., 2015), though water from somewhat deeper depths can be brought up via along-slope mixing.

The water masses which have access to the shelf are modified by the various processes described below in roughly counter-clockwise direction from Fram Strait and the Barents Sea where AW enters the Arctic Ocean. While journeying northward, water is modified by cooling, by the addition of freshwater, and the addition of brine. The modified water can be identified by using chemical profiles based on the signatures of source waters or of the relevant modification processes as input into systems of linear equations. I discuss these in section 2.1. Some of the more prominent tracers used to source these water masses by their biogeochemical singature are described in section 2.2.

The carbon system on the Northeast Greenland shelf is closely linked to water mass properties and to changes in physical conditions such as temperature and pressure. The carbon system in the Arctic Ocean is described in Section 2.3. This includes

a brief description of alkalinity, which is commonly used to determine the buffer capacity of the ocean with respect to CO_2, but we use as a tracer of Arctic water masses.

Once the water arrives on the Northeast Greenland shelf, it is transported by different currents and interacts with the warm AW which crosses Fram Strait directly, without first being transported around the Arctic Ocean. Water from melted snow and ice is added in the region and advected further south which I discuss in Section 2.4 and concludes this chapter.

2.1 Water masses and their transformations

The Arctic Ocean is the region where the effects of climate change are likely the most pronounced of all of Earths oceans (Eldevik et al., 2020). AW heated at lower latitudes is transported northward in the Atlantic Ocean by the North Atlantic Current (NAC). Between the north coast of Norway and Bjorn Øya (Bear Island), in a region termed the Barents Sea Opening (BSO), a portion of the AW is advected by the North Cape Current (NCaC) onto the shelf through Bear Island Trough and Hopen Trench (Kolås et al., 2024). The remainder becomes the West Spitsbergen Current which flows northward along the East side of Fram Strait (Aagaard et al., 1987). Around Yermak Plateau this current is split into three branches, one of which veers west, while the other two enter the Arctic where they circulate in an anti-clockwise direction (Rudels et al., 2005).

The AW from both pathways into the Arctic Ocean (via BSO and Yermak Plateau (YP)) are cooled through the loss of heat to the atmosphere and by the melting of sea ice. These processes modify the surface water and form a fresh upper layer which is mixed into a homogeneous surface layer during winter convection (Rudels et al., 1996). When this process is repeated annually, the layer eventually forms the Arctic halocline layer which insulates the cold fresh surface water from the warmer saltier AW below. During transport around the Arctic basin, the water continues to cool and is modified further by the addition of freshwater from rivers and the Pacific

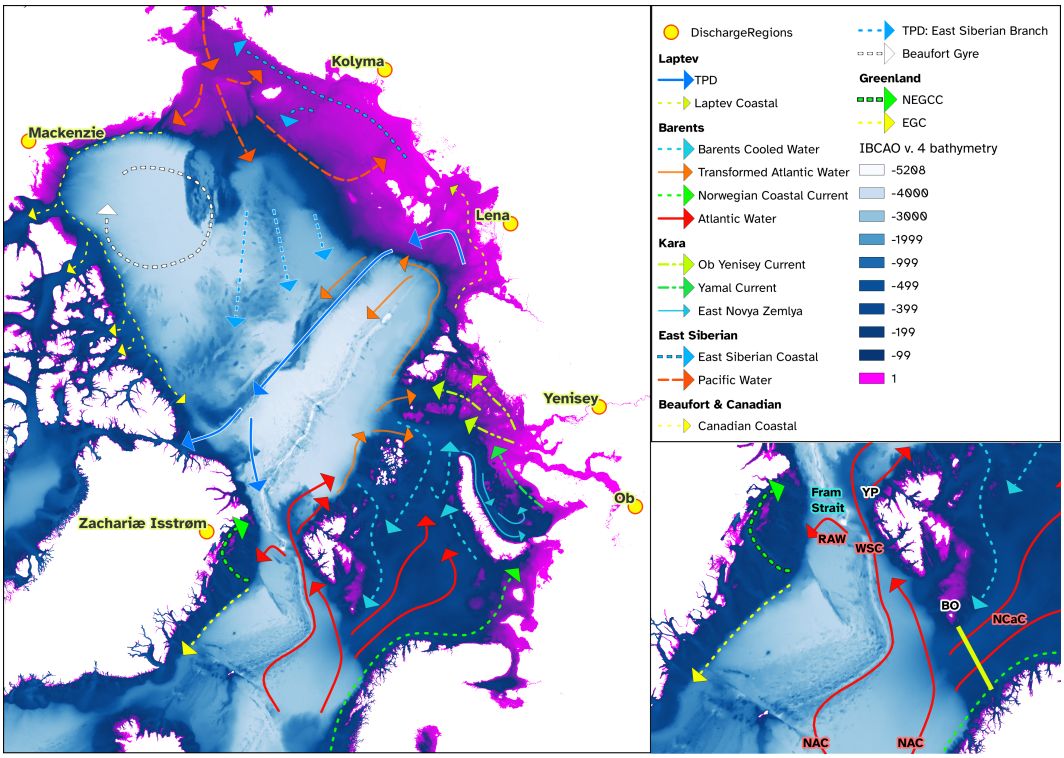

Figure 2.1: Main surface currents and discharge input locations of the Arctic Ocean. YP: Yermak Plateau, RAW: Return Atlantic Water, WSC: West Spitsbergen Current, BO: Bjørn Oya, NCaC: North Cape Current, NAC: North Atlantic Current. The yellow line indicates the BSO: Barents Sea Opening. Currents obtained from maps in literature, including Kolås et al. (2024), McPherson et al. (2023), Dvoretsky and Dvoretsky (2015), and Kolås et al. (2024), as well as data and discussion provided in the papers associated with the NEWP 1992 Cruise to the Northeast Greenland shelf described in Wallace, Behrens, et al. (1995)

Ocean, and brine from seawater freezing. Eventually the water exits the Arctic via two gateways connected to the Atlantic Ocean, the Canadian Arctic Archipelago and the western side of Fram Strait.

Water from Fram Strait is advected laterally onto the Northeast Greenland Shelf. In the Westwind Trough this is water from the Arctic Ocean, but at latitudes at and south of 79°N recirculating AW, also termed Return Atlantic Water (RAW) joins with the EGC and can be advected onto the shelf.

2.1.1 Heat loss to atmosphere and the melting of ice

As northward flowing AW encounters cold atmospheric temperatures and sea ice near the surface, it loses heat. The heat that is lost between two points in a northward flowing current can be approximated by comparing the water properties for water shallower than a certain depth and applying Equation 2.1

$$Q_{loss} = c \cdot \rho \cdot \Delta T \cdot H \tag{2.1}$$

Here, Q_{loss} ($J \cdot m^{-2}$) is the heat energy loss, c ($J \cdot kg^{-1} \cdot K^{-1}$) is the specific heat capacity of the ocean water, ρ ($kg \cdot m^{-3}$) is the density of the seawater at the depth, ΔT ($^{\circ}K$) is the change in temperature between the two locations, and H (m) is the depth to which the change is being measured (Rudels et al., 2005). If the water velocity is known, it can be used in conjuction with the distance to calculate the heat loss over time for a particular transect. How much of the heat is lost due to the melting of sea ice can be approximated by determining the amount of freshwater added using the salinity.

The observed salinity of the mixed layer that forms north of Svalbard, where the AW near the surface is initially cooled and the Lower Halocline Water (LHW) (described below) forms, is higher than would be expected if all the heat lost by the AW went into the melting of sea ice (Rudels et al., 1999; Rudels et al., 2005). This finding led to the testing of a hypothesis that the partitioning of sensible heat loss from an

ocean that is above freezing between an atmosphere below freezing and (sea) ice melt, is such that the energy lost to ice melt is at a minimum, while neglecting the presence of brine. First the fraction of heat lost by a surface water layer with a temperature that is above freezing to an atmosphere that has a temperature below freezing is calculated, and the remainder is assigned to sea ice melting (Steele et al., 1995; Rudels et al., 1999; Rudels et al., 2005). The reduction in salinity associated with this melt can be compared with observations though this requires ignoring any brine contained in the volume, decreasing the usefulness of this method the further the water layer travels in the Arctic under freezing conditions. Since the Northeast Greenland Shelf is an outflow shelf, such a method is not directly applicable there.

The method does provide an important clue regarding the formation of the LHW. The LHW is an important feature in the Arctic Ocean as it forms the base of the so-called Cold Halocline Layer (CHL), initially described by Aagaard et al. (1981), with further hypotheses regarding its formation developed by Steele et al. (1995) and Rudels et al. (1996). The CHL is of interest since it acts as a barrier between warm AW and the sea ice above, inhibiting sea ice melt from below (Stigebrandt, 1981 a). Two potential mechanisms for the formation of the CHL were originally described, one being the salinization of freshwater at the surface by brine expelled during sea ice formation, for example in polynyas, the second the cooling and freshening of AW. This was first associated with continental slope upwelling but turned out to be primarily associated with the Marginal Ice Zone (MIZ) (Steele et al., 1995) in the Barents Sea regions and north of Svalbard where AW meets PSW and sea ice at the surface. Although cooling from the surface would be expected to cause thermal convection, this is counteracted by the sea ice melt related freshening. In a cold and salinity-stratified θ-ocean (Carmack, 2007), freshening makes the water more buoyant than the saltier AW though still more dense than the sea ice melt influenced layer directly below the sea ice and therefore dives below this water mass as it continues its journey through the Arctic.

The salinity of the LHW is determined by the temperature of the AW from which it is formed because it depends on the thermal expansion coefficient as well as on the difference in temperature between it and the ice melt layer near the surface (Rudels et al., 1996). If the AW is colder, the resulting LHW should have higher

salinity. This is considered one factor that causes the observed differences between the LHW formed in the Barents Sea versus that formed North of Svalbard, which are named the denser and colder Barents Sea Branch Water (BSBW) and the more buoyant and warmer Fram Strait Branch Water (FSBW) respectively.

The calculations underlying the hypothesis may oversimplify the issue in the Barents Sea since although temperatures there have increased, the branch water has become more saline (Lien and Trofimov, 2013). Nonetheless, one consequence of increased AW temperatures into the Arctic Ocean (Atlantification) can be a reduction in the salinity of the LHW and impacting the stratification.

2.1.2 Riverine input

Since AW is transported around the Arctic in an anti-clockwise pattern, water from the Barents Sea containing the newly formed LHW is transported toward the Kara, Laptev, East Siberian, and Chukchi seas. Here large volumes of freshwater are added to the surface by river discharge from the rivers Ob', Yenisey, Lena, and Kolyma which drain the extensive Eurasian catchment with an area of over $9.1 \cdot 10^6$ km^2 (Speetjens et al., 2023). This freshwater is more buoyant than the circulating AW, even after it has been freshened by LHW formation, and initially forms fresh surface river plumes at the surface before being mixed down to depths of the LHW and cooled in winter and creating the bulk of the PSW.

In the area of the Kara Sea near Novaya Zemlya, away from the river plume, *TS* diagrams show that the LHW, marked by a drop in water temperature from those associated with the AW and generally following the density contour at 1027 kg m^{-3}, has formed in this locations while the broader CHL, along the freezing line to lower salinities (e.g. Figure 3 in Drozdova et al. (2021)) is absent. The CHL becomes apparent at stations in more eastern and northern parts of the Kara Sea, including St Anna Trough in the areas influenced by discharge from the rivers Ob' and Yenisey (Dmitrenko et al., 2015). Across Vilkitsky trough on the western side of the Laptev Sea, a layer of so-called summer warmed surface water is present in years where

this water is advected to the Laptev instead of northward into the Arctic Ocean (Janout et al., 2017).

At least a portion of the freshwater that collects in the Kara Sea during summer is advected into the Laptev Sea in winter between October and January with any remainder being advected northward on the western side of the Kara Sea via Anna Trough toward Nansen Basin (Dmitrenko et al., 2015; Osadchiev et al., 2023). The Nansen Basin freshwater layer is not influenced by river input but solely by sea ice melt (Rudels, 2022) which supports the hypothesis of westward advection of the river plume in winter toward the eastward Laptev Sea rather than the northern Nansen Basin.

The Laptev Sea receives additional discharge from the Lena river. Similarly to the situation in the Kara Sea, a portion of this is advected northward where it is entrained into the TPD. In winter such shelf waters are modified by sea ice formation and convection (Namyatov, 2021), increasing the salinity before being advected further toward the East Siberian Sea or northward into the TPD. The relative proportion of sea ice meltwater to meteoric input decreases from the Barents to Kara to Laptev shelves (Namyatov, 2021) as the proportion of discharge increases.

The direction of the river plumes is largely determined by wind direction (Johnson and Polyakov, 2001; Kubryakov et al., 2016; Osadchiev et al., 2020). The diversion of more water in the along-shore direction, for example from the Laptev to the East Siberian Sea rather than into the Arctic Ocean, can lead to large difference in terms of the distribution of Arctic Ocean surface salinity. This behaviour of river plumes will determine where precisely river-influenced surface water is at the onset of winter and therefore on the main source location of the PSW in any particular year.

In the East Siberian Sea more freshwater from the Kolyma river is added, as well as PW transported from the Bering Strait across the Chukchi Sea. Along with the Laptev Sea, this region is a major source for the TPD (Constantin and Johnson, 2024). Through upwelling of cold water in Anadyr strait (Kawaguchi et al., 2020), and subsequent winter convection in the Bering, Chukchi, and East Siberian seas,

the water taking this pathway has some identifiable geochemical characteristics (Kinney et al., 1970) that will be discussed in Section 2.2.

Freshwater input into the Arctic Ocean is experiencing large shifts under the influence of climate change. River discharge from the Eurasian landmass intensified by 7% between 1936 and 1999 (Rawlins et al., 2021), and has consequences for the global ocean through its influence on Atlantic Meridional Overturning Circulation (AMOC) and by extension on global circulation (Gjelstrup et al., 2024).

2.1.3 Seawater freezing

Though the sea ice melt fraction reduces compared to the meteoric freshwater fraction with eastward transport along the Eurasian continental shelf seas (Namyatov, 2021), the formation of sea ice has a strong influence on water mass characteristics in the Eurasian Arctic and the associated salinization was the first process hypothesized to create the CHL (Aagaard et al., 1981). This process is particularly relevant to the formation of Upper Halocline Water (UHW) which lies above the LHW in the Makarov and Canadian Basins (Steele and Boyd, 1998) and is formed by salinization of the Pacific inflow through Bering Strait (Shimada, 2005) and subsequent advection from the shelf (Anderson et al., 2013; Wang et al., 2021).

For seawater with salinities above 24.7 to start freezing the entire surface mixed layer needs to be at temperatures below that associated with the maximum density for the salinity of that water type (Figure 2.2). This sets it apart from brackish waters with a salinity lower than 24.7 (Weeks, 2010) where the temperature of the maximum density of seawater is higher than the freezing temperature. During periods of below freezing atmospheric temperatures, especially where also associated with a lack of incoming shortwave solar radiation, the surface will lose heat and start to convect, bringing up the warmer water from below. Once the entire Surface Mixed Layer (SML) is at freezing temperature, further heat loss will result in ice crystal formation[1].

[1]This is an oversimplification, the chaining of water molecules at cold temperatures is complex and outside the scope of this manuscript

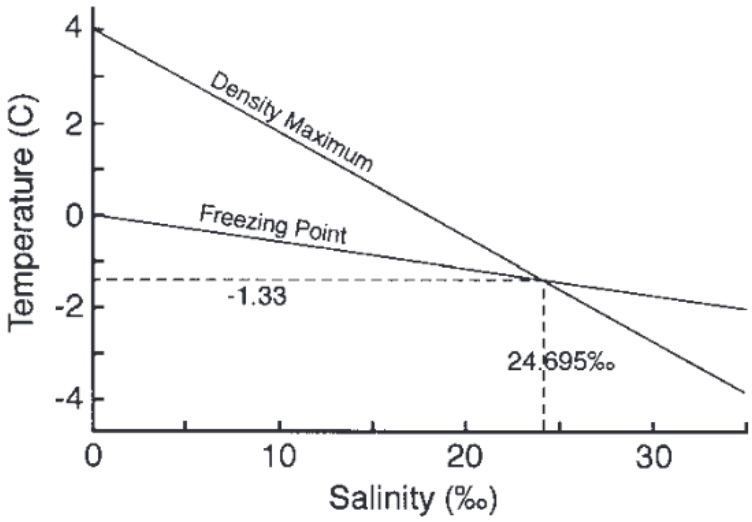

Figure 2.2: Intersection between the freezing point and the maximum density on a *TS* diagram from Weeks (2010)

The ice crystals will float to the surface and form a thin layer of frazil ice which, after a certain thickness has been achieved, will consolidate and start forming congelation ice, characterized by crystal growth in a specific (c-axis) direction. Since the ice crystals are made up primarily of pure water ice[2] the salts found in seawater are rejected during this process. This increases the salinity of the water below, with most salt lost during frazil ice formation in open water in the water column and further brine lost during additional ice growth (Thomas and Dieckmann, 2010).

Open water such as that found in leads and polynyas has therefore been considered to be 'ice factories' (Smith and Barber, 2007) which also makes them brine factories. Associated with many of the Arctic continental shelf seas are so-called flaw leads which exist between the fast ice and pack ice and where much of the UHW is thought to be formed by sea ice associated haline convection which is then advected to a depth of neutral buoyancy off shelf into the Arctic Ocean (Anderson et al., 2013). Due to its interaction with benthic sediments (Sun et al., 2021) the UHW can be identified by its nutrient signature across the Arctic Ocean, and on the Northeast Greenland Shelf (Jones et al., 1991; Jones et al., 1998; Falck, 2001; Dodd et al.,

[2]Some molecules can be included in the sea ice lattice, depending on their shape and surface energy. One example of this is Ammonium Fluoride.

2012).

2.2 Water mass tracers

Water mass tracing is the process of using observations of specific geochemical characteristics to determine the source location, often in fractions, of a water mass or water mass mixture or shed light on mixing processes. *TS* diagrams are the most common form, highlighting isopycnal and diapycnal mixing between end members that have distinguishable potential temperature and salinity. *TS* space is also valuable because it describes two out of the three components required to thermodynamically describe the state of a seawater parcel if approximated as a binary geophysical fluid, with the most frequently used being temperature, salinity, and pressure.

In Arctic outflow regions, including Fram Strait, Nares Strait, and their associated outflow shelves (Michel et al., 2015), where so many water masses with a varied mixing history are superimposed, additional tracers are often required to separate end-members, processes, or transport and residence times. These tracers are either associated with direct input into the Arctic Ocean or by processes taking place there. Some of the most frequently used passive biogeochemical tracers are described below, after the basic principle is described in Section 2.2.1.

2.2.1 Water mass fraction calculations

Water mass fraction calculations are systems of linear equations which assume that a specified number of water masses make up a water sample and their fractions sum to 1. If this is the case, each measured parameter should reflect the sum of that parameter by water mass and a set of measured parameters can be used to obtain a set of water mass fraction solutions:

$$
\begin{aligned}
f_{m1} + f_{m2} + f_{m3} + ... + f_{mn} &= 1 \\
f_{m1}X_1 + f_{m2}X_1 + f_{m3}X_1 + ... + f_{m1}X_n &= X_{1,obs} \\
f_{m1}X_2 + f_{m2}X_2 + f_{m3}X_2 + ... + f_{m2}X_n &= X_{2,obs} \\
f_{m1}X_3 + f_{m2}X_3 + f_{m3}X_3 + ... + f_{m3}X_n &= X_{3,obs} \\
&... \\
f_{m1}X_n + f_{m2}X_n + f_{m3}X_n + ... + f_{mn}X_n &= X_{n,obs}
\end{aligned}
$$

Here f refers to the fraction for water masses m1, m2, m3 , ⋯ mn, and X (1,2,3, ⋯n) refers to a measured parameter such as salinity, $\delta^{18}O$, or the equation between two nutrient concentrations with respect to one another as associated with a particular water source, and obs refers to the observation or measured value of the variable in the sample. A more complex variation on this basic scheme exists called Optimum Multiparameter Analysis which was developed by Tomczak (1981). It has only been applied to the Arctic Ocean a few times (Jeansson et al., 2008; Burgers et al., 2023).

2.2.2 The NO and PO tracers

The NO tracer was first proposed as a tracer by Broecker (1974). They defined it per Equation 2.2 based on earlier work by Redfield (1934) who determined nutrient ratios could be related to productivity.

$$NO = 9[NO_3^-] + [O_2] \tag{2.2}$$

Here NO is the tracer, $[NO_3^-]$ is the concentration of nitrate in the seawater sample, and $[O_2]$ is the concentration of dissolved oxygen. This tracer is closely related to so-called preformed nutrients which are dissolved nutrient concentrations at the location of subduction as separate from remineralized nutrients which are nutrients that are regenerated by organisms post-subduction by microbial and

archaeal decomposition. The assumption is that oxygen saturation with respect to the atmosphere at the surface during ventilation is at or very near 100%. Since remineralization by biota consumes oxygen and releases nitrogen as NO_3^- (at a rate of 1 O_2 to approximately 1/9 NO_3^-), respiration and remineralization in a water mass no longer exposed to the atmosphere is canceled out (Broecker, 1974), allowing the use of the tracer as a conservative properties even though both measured variables are not. The full ventilation of the SML by diffusion or bubbles requires time and therefore is not always an appropriate assumption for each water mass. Although this tracer has been applied to the Arctic, there is evidence of non-Redfield uptake of nutrients from the Chukchi Sea (Ouyang et al., 2022) to the Northeast Greenland shelf (Daly et al., 1999).

Similar to NO is the PO tracer, which relies on comparable motivation but uses the Redfield relationship of phosphate PO_4^{3-} instead of NO_3^- and shown in Equation 2.3. PO_4^{3-} is not limiting in the Arctic Ocean so it may more accurately reflect the preformed component of the nutrient concentrations with respect to O_2.

$$PO = 135[PO_4^{3-}] + [O_2] \tag{2.3}$$

Low values of both NO and PO can be used to identify the LHW, particularly the shelf-derived BSBW (Wilson and Wallace, 1990; Jones et al., 1991; Alkire et al., 2017; Alkire et al., 2021), after its subduction and the formation of the CHL ensures the layer is no longer ventilated even in winter. Meanwhile PW, including UHW will have high NO and PO. This difference is primarily due to low versus high oxygen concentrations in the respective water masses due to their most recent time of ventilation, e.g. on the Barents Sea shelf, Nansen Basin along the Barents Sea slope, or in the East Siberian Sea and sedimentary interactions that consume oxygen (Alkire et al., 2021). The ratio of NO/PO will also produce an intermediate minimum at the LHW (Wilson and Wallace, 1990; McLaughlin et al., 1996; Min et al., 2003). There are additional tracers which exploit the redfield nutrient relationship to trace water masses of interest, including N* proposed by Gruber and Sarmiento (1997) to trace water with a history of denitrification, PO_4* (Broecker et al., 1985), and nitrate to phosphate ratio frequently used in the Arctic Ocean.

2.2.3 The N/P tracer

The nitrate (NO_3^-) to phosphate (PO_4^{3-}) ratio is used as a tracer primarily to obtain the fraction of PW in a water sample. This ratio was first used by Jones et al. (1998) who determined that the slope of the ratio was different for AW and PW respectively and mixing relationships between them were clearly represented (Figure 2.3). A physical basis for the change in slope was found when denitrification processes were identified in the Chukchi Sea sediments (Devol et al., 1997; Tanaka et al., 2004; Chang and Devol, 2009; Zeng et al., 2017) involving PW that is already low in nitrogen (Yamamoto-Kawai et al., 2006). Higher rates of denitrification are associated with shallower depths (Chang and Devol, 2009), the MIZ (Codispoti et al., 1991)], and with under ice blooms (UIBs) (Ardyna et al., 2020; Payne and Arrigo, 2022).

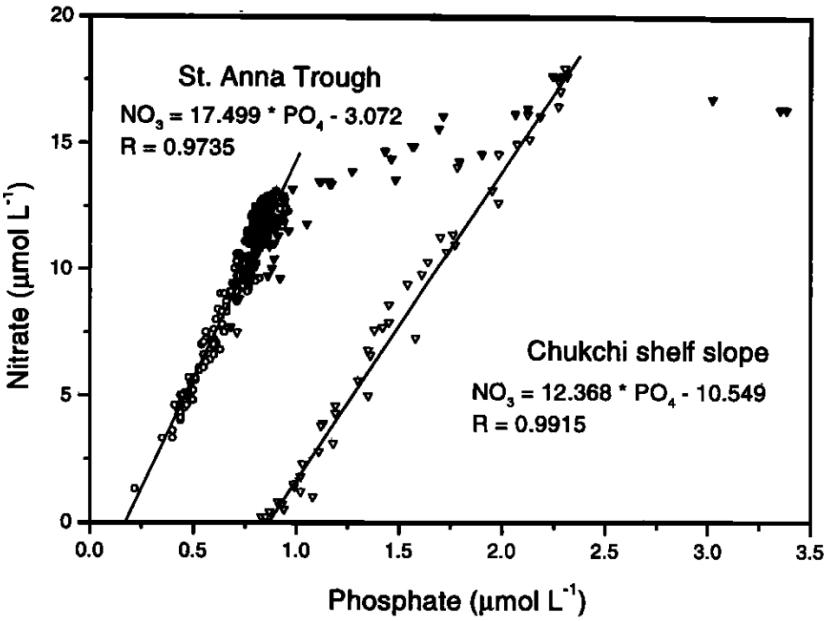

Figure 2.3: Nitrate to phosphate ratio for the Chukchi shelf (PW) and St. Anna Trough (AW) in the Arctic Ocean as determined by Jones et al. (1998)

This ratio is not without problems as a tracer however, particularly since questions remain regarding the extent of denitrification in Eurasian shelf sediments and this region is undergoing extreme changes. The MIZ is moving to deeper waters, as are

springtime UIBs. Furthermore, denitrification in sediments has been found further west where no PW should exist, potentially leading to the overestimation of this water mass in downstream regions to the water mass formation area(s) (Nitishinsky et al., 2007; Bauch et al., 2011; Sun et al., 2021). Another factor is that the base premise of Redfield ratio compliant primary productivity may not be valid for the Arctic (Daly et al., 1999). Discrepancies in the use of different techniques for the nutrient-based PW fraction in particular are discussed in Alkire et al. (2015) and Forryan et al. (2019).

Nevertheless the Atlantic and Pacific nitrate to salinity ratio equations are frequently used in mass fraction calculations in Arctic Ocean outflow regions to determine water mass origins. Such calculations take the form of systems of linear equations of the form described in Section 2.2.1, especially in combination with the salinity and stable water oxygen isotopic ratio ($\delta^{18}O$).

2.2.4 Stable water isotopes ($\delta^{18}O$ and $\delta^{2}H$)

The fractionation of stable water isotopes occurs primarily during phase changes of water. There are two main types of fractionation which affect stable water isotopes, equilibrium and kinetic fractionation (Young et al., 2002; Ferronskiĭ and Polîakov, 2012). Equilibrium fractionation refers to the bidirectional replacement of heavy and light isotopes of two substances in equilibrium, and kinetic fractionation is a unidirectional transfer of isotopes between two substances. Three examples of phase changes at the ocean surface are the evaporation of water into the atmosphere (Craig et al., 1963), the freezing of seawater (O'Neil, 1968), and the forming of snow from vapour in the atmosphere (Souchez et al., 2000). As a result of evaporation which favours lighter isotopes near the equator and the subsequent transfer of this vapour by winds towards more northern latitudes where it is deposited, there is an observable relationship between isotopic composition in freshwater reservoirs and their latitude (Craig, 1961; Dansgaard, 1964). In the Arctic Ocean several of these influences overlap and are used to differentiate between water sources. Foremost, the AW which has a nominal $\delta^{18}O$ of ~ 0.3 ‰ (Östlund and Hut, 1984; Bauch et al., 1995) is the dominant water mass that fills the Arctic Basin, with additional

water discharge in the form of freshwater contributions of PW through the Bering Strait and river discharge. Subsequent modification of the stable water isotope ratio in the surface water occurs in the form of sea ice freezing and evaporation and precipitation. The effect this change has when diluted into a larger body of water is small relative to the change in salinity associated with the same process (Figure 2.4).

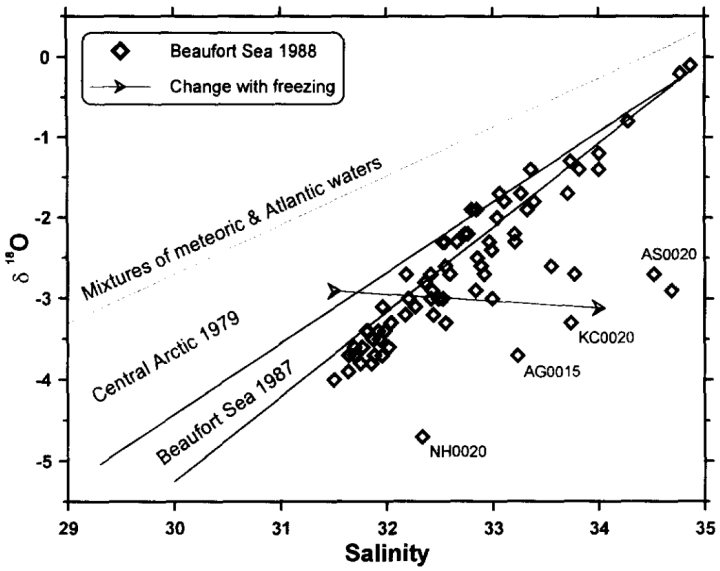

Figure 2.4: Example of an Arctic Ocean δ^{18}O-S relationship that shows the increase in salinity resulting from the extrusion of brine during ice formation. From Melling and Moore (1995)

The original water mass tracing experiments utilising stable water isotopes in the Arctic Ocean were performed by Östlund and Hut (1984) who separated AW from river discharge (runoff) and sea ice brine (negative sea ice melt) by solving a set of three linear equations of the form described in Section 2.2.1 with salinity and δ^{18}O as tracers. The salinity and δ^{18}O for AW and sea ice melt were obtained from literature and the value of δ^{18}O for river discharge was obtained via a standardization method utilising tritium measurements rather than by linear extrapolation between a salinity of 0 and 35 to make sure that multiple possible freshwater sources could be represented. They used this to determine the long term average halocline water residence time (10 ± 1 years) and average ice production (0.59 m/y) and the meteoric freshwater contribution through Bering Strait, river discharge, and precipitation

(1.16 m/y) based on measurements made in Fram Strait.

Since then stable water isotopes have continued to be used as part of mass balance equations for water masses, especially focused on water mass transformations and modification of halocline waters (Östlund, 1994; Bauch et al., 1995; Melling and Moore, 1995), and for tracing source locations for water found on Arctic outflow shelves (Dodd et al., 2009; Dodd et al., 2012; Burgers et al., 2017). Individual Arctic rivers have their own biogeochemical signature depending on that of the precipitation in their catchments (Cooper et al., 2008; McClelland et al., 2008; Yi et al., 2012) and these signatures can be traced into the shelf seas they discharge onto (Östlund, 1994) and beyond.

One of the main assumptions such three-component calculations are based on is that the sea ice and the underlying SML carrying its brine signature are travelling in the same direction (Bauch et al., 1995) and therefore would not be applicable where ice and the underlying water have diverged. Although frequently unmentioned, the underlying assumption for mass balance studies on outflow shelves is therefore that the TPD transports both toward Fram Strait and the Canadian Arctic, and equally partitions them in the freshwater switchyard by the Lincoln Sea. This region is undergoing rapid change, particularly as a result of freshening (De Steur et al., 2013) and the earlier and more frequent collapse of the northern ice bridge (Moore et al., 2021) which allows more ice to be exported south into Baffin Bay (Bi et al., 2019).

A commonly encountered error is that of negative fractions of a non-sea ice melt water mass. This is frequently attributed to an error in end-member input, non-conservative behaviour, or lack of the negative fraction in the sample (Abrahamsen et al., 2009; Bauch et al., 2011). What is less frequently discussed is the potential impact of direct precipitation, either in the form of rain or snow, even though snow precipitating on sea ice in the Arctic Ocean has a very negative $\delta^{18}O$ (Mellat et al., 2024) and may explain some of the observed variance observed in summer (Rysgaard et al., 2024), depending on the relative volumes of (water equivalent) precipitation and the SML. Due to losses in sea ice cover, Arctic snow is becoming less depleted with respect to $\delta^{18}O$ (Song et al., 2023), and when combined with

increases in Arctic precipitation (Bintanja et al., 2020) could lead to unpredictable changes in this tracer.

2.2.5 Silicon

Silicon bearing minerals are a common mineral found in the Earth's lithosphere (Tréguer et al., 1995). They experience geological weathering when they are brought in contact with gaseous carbon dioxide (CO_2) and water. The mineral wollastonite (a single chain inosilicate mineral, $CaSiO_3$) is frequently used as an example of such weathering using Equation 2.4, though variations exist for each silicate bearing mineral.

$$CaSiO_{3(s)} + 2CO_{2(g)} + 3H_2O \rightarrow H_4SiO_{4(aq)} + 2HCO_3^- + Ca^{2+} \tag{2.4}$$

The products of this reaction, orthosilicic acid ($Si(OH)_4$), bicarbonate ions, and calcium ions, are transported to the oceans by river water along with other minerals and organic materials (Tréguer and De La Rocha, 2013). This is the primary pathway for silicon to enter the ocean, with aeolian inputs as a secondary source. River inputs give rise to unique and often seasonal signatures for each catchment with respect to dissolved chemistry that can be traced onto the shelves (Min et al., 2003; Cooper et al., 2005; Raymond et al., 2007; Cooper et al., 2008; McClelland et al., 2008; Yi et al., 2012; Makkaveev et al., 2015; Tank et al., 2023) and into the TPD (Charette et al., 2020; Liguori et al., 2021; Paffrath et al., 2021; Laukert et al., 2022). Once in the ocean, the bicarbonate can be precipitated by biology and the resulting calcium carbonate affects the ocean buffering capacity. These will be discussed in Section 2.3. The orthosilicic acid can be precipitated by primary producers as biogenic opal (biogenically hydrated silica, $SiO_2 \cdot nH_2O$) per equation 2.5 (Quéguiner, 2016; Penman et al., 2020).

$$H_4SiO_{4(aq)} \rightarrow SiO_{2(s)} + 2H_2O \tag{2.5}$$

The diatoms that are the main primary producers in the Arctic Ocean (Ardyna and Arrigo, 2020) and in Arctic sea ice (Arrigo, 2016), produce silacious biogenic opal frustules. Phytoplankton can be both light and nutrient limited in the Arctic Ocean which affects orthosilicate uptake when away from open water and the input of other nutrients in the continental shelf seas.

The use of dissolved silicon dioxide (SiO_2), frequently referred to as silica, as a tracer, has a long history in the Arctic Ocean with early expeditions like that of the Northwind including it as a measured parameter (Codispoti and Richards, 1968), and the measurement of silicate was used as a parameter in early investigations of the formation of the CHL (Aagaard et al., 1981). Since high concentrations of silicate have been associated with the presence of UHW, along with high concentrations of other nutrients (Jones et al., 1991), it has been used to identify this water mass since the first studies of water masses in Fram Strait and on the Northeast Greenland shelf (Deming and The NEWATER Steering Committee and Principle Investigators, 1993; Budéus and Schneider, 1995; Wallace, Minnett, et al., 1995; Budéus et al., 1997; Falck, 2001). Here it tends to exist as a maximum peaking at a salinity of around 32.5 when present (Falck et al., 2005).

Although the regions of the Arctic Ocean outside the TPD may be nutrient limited by silicate and by iron (Liguori et al., 2021), the photic zone inside the TPD is nitrate limited. As a result, silicate may be a better tracer of PW and the UHW in particular than tracers based on nitrate. This tracer is primarily sourced from river input, and large changes in river input are expected as a result of increasing global temperatures and atmospheric humidity, implying associated changes in the tracer. Particularly changes in humic input and source catchment as a result of melting permafrost are likely to impact river chemistry (Tank et al., 2023).

2.3 Arctic CO_2 exchange

CO_2 is an important gas to the Earth's climate. Together with H_2O vapour, O_3, N_2O and CH_4 it absorbs longwave radiation from the Earth where it is re-emitted

in all directions rather than being reflected to space (Arrhenius, 1869; Anderson et al., 2016; IPCC, 2023). Out of this group, CO_2 has the longest lifetime in the atmosphere. Carbon is also the fundamental building block of life on Earth and is therefore involved in much of its biogeochemistry. The biotic and abiotic parts of the ocean CO_2 exchange are frequently referred to as the biological pump and the solubility pump respectively.

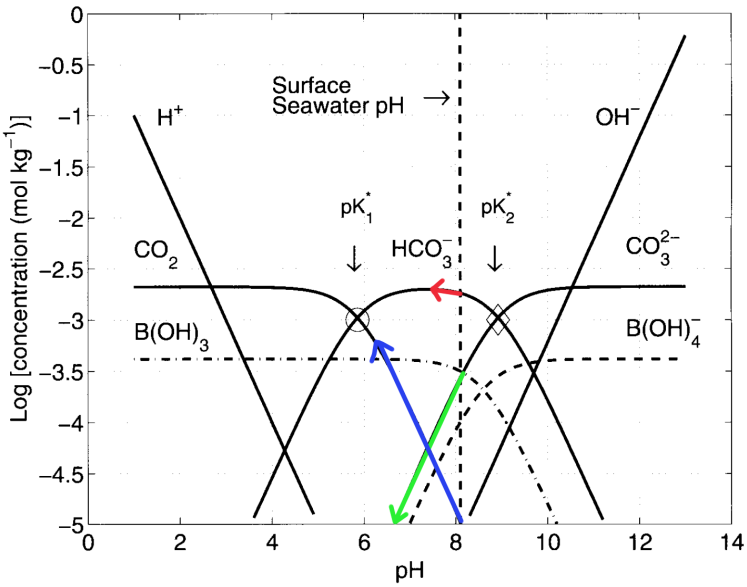

Figure 2.5: Bjerrum plot showing the equilibrium relationships affecting the pH in seawater at 25°C, a salinity of 35, and atmospheric pressure from Zeebe and Wolf-Gladrow (2001). The arrows that show the direction of the change in CO_2, HCO_3^-, and CO_3^{2-} in the system that are related to (but not caused by) a drop in pH have been coloured in (in blue, red, and green respectively) to show the direction of these reactions associated with (not caused by) a drop in seawater pH.

The biological pump is involved in the cycling of carbon through organisms. Primary producers (primarily photoautotrophs) utilise energy (primarily from sunlight) to convert CO_2 into carbohydrates, proteins, and lipids. Primary producers can be consumed by primary consumers (e.g. grazing heterotrophs), can be infected with viruses, or die by lack of nutrient input or changes in ambient conditions not conducive to autotrophic life. Primary consumers are eaten by secondary consumers and so forth up the food chain. Each of these steps creates detritus which coagulate into particles under the influence of turbulence (Takeuchi et al., 2019). Once these

aggregates achieve a certain size they become dense enough to sink out of the photic zone and into deeper water. The aggregates are consumed by detritivores, initially in the water column as they sink and finally in the benthos. This consumption by microorganisms transforms organic matter back into inorganic matter. If this takes place in the water column, this leads to increased dissolved nutrients at the depth of decomposition. If this takes place in sediments these nutrients can be resuspended. This latter process is considered crucial to the high nutrient concentrations associated with PW, in particular with the UHW which are the product of resuspension through convection in winter polynyas.

The solubility pump describes the abiotic mechanism by which CO_2 is transported away from the atmosphere and into the deep ocean. The near-surface part of the pump, where the drawdown of CO_2 from the atmosphere takes place, consists of a sequence of chemical reactions that occur when gaseous CO_2 is dissolved into seawater per the equilibria in Equation 2.6 (Zeebe and Wolf-Gladrow, 2001). Each H^+ ion added to the ocean by the dissolution of CO_2 increases the ocean acidity by lowering the pH. DIC refers to the sum of the dissolved forms of CO_2 shown in Equation 2.6, e.g. the sum of $CO_{2(aq)}$ from the atmosphere or respiration, HCO_3^- which forms as a result of the first part of equilibrium dissociation or is sourced directly via river inputs as a result of the weathering of rock as discussed in Section 2.2.5, and CO_3^{2-}. The equilibrium constants shown in Equations 2.7 and 2.8 depend on temperature, salinity, and pressure.

$$CO_{2(aq)} + H_2O \rightleftharpoons H_2CO_3 \overset{K_1^*}{\rightleftharpoons} HCO_3^- + H^+ \overset{K_2^*}{\rightleftharpoons} CO_3^{2-} + 2H^+ \tag{2.6}$$

$$K_1^* = \frac{[HCO_3^-][H^+]}{[CO_2]} \tag{2.7}$$

$$K_2^* = \frac{[CO_3^{2-}][H^+]}{[HCO_3^-]} \tag{2.8}$$

The fraction of each component that makes up DIC to the whole is controlled by this equilibrium at a specific temperature, pressure, and salinity. DIC is frequently measured in bottle samples during oceanographic field work to determine whether

water is a source or sink of atmospheric CO_2 in conjunction with the TA[3] (Figure 2.5).

TA is a measure of the ability of the water to buffer additional acid without a large associated jump in pH and can be defined as the excess of proton acceptors over donors, or as the charge imbalance associated with the sum of the conservative cations and anions in solution. The TA works to neutralize (i.e. remove charge from) the solution when CO_2 is added to seawater to make it more acidic. TA is a conservative property in seawater and is affected by the addition and removal of ions, such as those resulting from terrestrial weathering associated runoff (Equation 2.4), from $CaCO_3$ biomineralization[4] (Okazaki (岡崎), 1993; Gilbert et al., 2022) or by the formation of $CaCO_3 \cdot 6H_2O$ during the freezing of sea ice (Dieckmann et al., 2008; Fischer, 2009; Nomura et al., 2013). The stoichiometry of the formation and dissolution of $CaCO_3$ are shown in the equilibrium reactions in Equations 2.9 to 2.11[5]. The HCO_3^- and CO_3^{2-} are the products of the reaction between H_2O and CO_2. As a result, when $CaCO_3$ is formed from HCO_3^- or CO_3^{2-}, the equilibrium in Equation 2.6 is shifted toward the left hand side, resulting in the production of CO_2 to maintain the equilibrium. Similarly, in the reverse direction, if CO_2 is dissolved into the surface water, the equilibrium moves the other way, dissolving $CaCO_3$ in the process in favour of HCO_3^-, and CO_3^{2-}.

$$H_2CO_3 + CaCO_3 \overset{K_{sp,1}^*}{\rightleftharpoons} 2HCO_3^- + Ca^{2+} \tag{2.9}$$

$$CaCO_3 \overset{K_{sp,2}^*}{\rightleftharpoons} CO_3^{2-} + Ca^{2+} \tag{2.10}$$

$$K_{sp,2}^* = [Ca^{2+}]_{sat} \cdot [CO_3^{2-}]_{sat} \tag{2.11}$$

$$\Omega = \frac{[Ca^{2+}][CO_3^{2-}]}{K_{sp,2}} \tag{2.12}$$

[3] A set of four equations and six unknowns describes the entire equilibrium, which means two measurements are required to determine the entire system. The unknown variables are CO_3^{2-}, HCO_3^-, CO_2, H^+, DIC, and CA.

[4] Through the use of carbonic anhydrase all forms of DIC can be used to create calcium carbonate.

[5] $\sum CO_2 \approx [HCO_3^-] + [CO_3^{2-}]$, while $TA \approx [HCO_3^-] + 2[CO_3^{2-}]$ since this is a measure of the charge. A substitution of $[HCO_3^-]$ can be made from the rearranged second equation into the first which results in $[CO_3^{2-}] \approx TA - \sum CO_2$

The stoichiometric equilibrium constant (here, $K_{sp,2*}$) used for the determination of the saturation state Ω is shown in Equation 2.11 and is the product of the concentrations of Ca^{2+} and CO_3^{2-} when the solution is saturated with respect to $CaCO_3$.

Ω is the ion concentration product divided by the stoichiometric equilibrium constant (Equation 2.12) (Mucci, 1983; Morse et al., 2007). This parameter is frequently calculated to infer acidification in ocean surface waters in the Arctic Ocean with respect to marine calcifiers (Jutterström and Anderson, 2005; Bates et al., 2009; Chierici and Fransson, 2009; Azetsu-Scott et al., 2010; Yamamoto-Kawai et al., 2011; Bates et al., 2013), though whether the equilibrium relationship is the primary reason (compared to kinetic processes) for the observed effects related to low Ω is still under debate (Waldbusser et al., 2016). In general, the consensus is that if Ω is below 1, the environment is considered to be corrosive to the particular mineral polymorph that K_{sp}^* (where sp stands for solubility product) was calculated for. The anhydrous polymorphs of $CaCO_3$ are vaterite, calcite, and aragonite, of which the latter is the most vulnerable to increases in acidification as a result of increases in dissolved CO_2.

Biological processes create all three polymorphs though vaterite is used as a metastable precursor and not generally included in $CaCO_3$ shells. Sea ice formation allows for the mineralisation and retention of $CaCO_3 \cdot 6H_2O$ in the ice lattice (Fischer, 2009; Nedashkovsky et al., 2009; Rysgaard et al., 2012; Nomura et al., 2013; Papadimitriou et al., 2013). Since brine extruded through freezing is exported to deeper layers while melt remains in the SML, this process allows TA to be used as a tracer.

2.3.1 TA as a tracer for Arctic Ocean freshwater

Since TA is not expected to vary with gas exchange, temperature, or pressure, but does vary with sea ice formation, it has been used as an Arctic Ocean water mass tracer since at least the 1980s (Jones et al., 1983; Tan et al., 1983; Anderson and Jones, 1985), even before Dieckmann et al. (2008) first identified ikaite crystals

in Arctic sea ice [6]. $CaCO_3$ precipitation had been identified in earlier laboratory studies (Nelson and Thompson, 1954) which led authors to suspect that TA might affect the uptake of CO_2 associated with sea ice meltwater in the SML if this $CaCO_3$ was retained inside the ice while the DIC was preferentially exported with extruded brine and exported to depths below the SML.

Subsequently, per-ocean relationships between alkalinity and salinity, temperature, and latitude were determined (Millero et al., 1998). This allowed their observation to be used more broadly, including in the Arctic Ocean and in combination with $\delta^{18}O$ (Yamamoto-Kawai et al., 2005). Besides the staggering 11% of global ocean river water being discharged into the Arctic Ocean, the TA received through this discharge is also twice as high per unit surface area compared to other oceans (Carter et al., 2014) and increasing (Drake et al., 2018). Similar to other tracers, each river has its own signature alkalinity (Cooper et al., 2008) and can be traced onto their respective shelf seas (Sun et al., 2024).

Besides varying input concentrations and subsequent modification by sea ice melt and brine extrusion, there are some issues pertaining to the use of TA as a tracer. These include the decomposition of DOM (Kim and Lee, 2009; Kerr et al., 2021), nitrification, denitrification, and various other processes (Middelburg et al., 2020) [7]. The effect of decomposition of DOM on alkalinity may be of particular importance in the Arctic Ocean. This is due to the fact that the large Eurasian rivers, besides higher TA also transport high volumes of DOC (Kaiser et al., 2017; Hölemann et al., 2021). So much so that fluorescent $CDOM$ can itself be used as a tracer of Siberian shelf waters as far afield as Fram Strait and the Northeast Greenland Shelf (Stedmon and Markager, 2001; Granskog et al., 2012; Stedmon et al., 2021).

2.4 Fjord and shelf dynamics

The processes and tracers described in the previous sections of this chapter superimpose in the TPD before being transported into the EGC and onto the Northeast

[6] It was first discoverd in tufa chimneys in cold water rather than in sea ice by Pauly (1963)
[7] Organic alkalinity may even influence certified reference materials (Sharp and Byrne, 2021).

Greenland shelf. Due to geographical restriction of deeper water by Ob bank to the north, combined with the flow of the Northeast Greenland Counter Current (NEGCC) which acts to push water toward the Westwind Trough, the northern part of the shelf and the Northeast Water Polynya (NEWP) have *TS* diagrams which show modification of the LHW. This is contrary to Belgica Trough which is where deeper water can enter the shelf, including AW, AAW, and PSW before being modified by local sea ice and glacial melt.

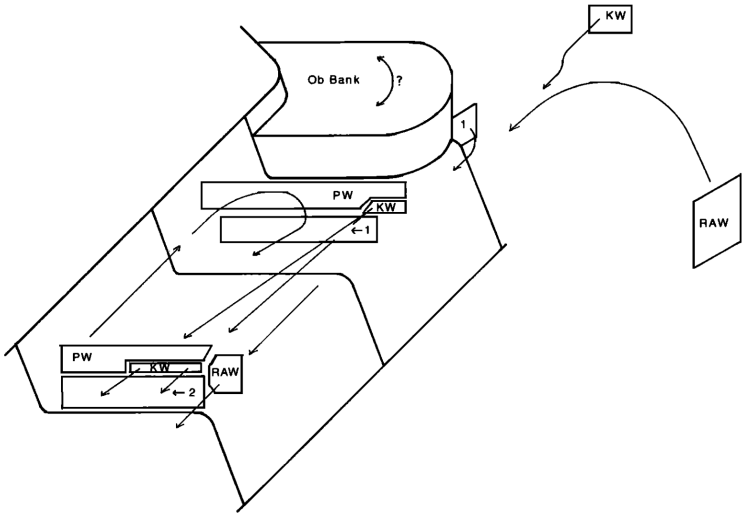

Figure 2.6: The water mass distribution on the Northeast Greenland shelf per Budéus and Schneider (1995)

The foundations of how we currently think about Northeast Greenland shelf hydrography and water masses was laid by Budéus and Schneider (1995) (Figure 2.6). They describe several water masses on the shelf, each Atlantic in origin though with different modifications. These water masses are the RAW and the PSW and a feature reminiscent of the LHW which they term 'knee water' due to its shape in *TS* space first described by Paquette et al. (1985) and Bourke et al. (1987). The knee was initially determined to be "undoubtedly" due to the subduction of Arctic Intermediate Water (AIW) from the Return Atlantic Current (RAC) under southward flowing PSW from the Arctic Ocean but later considered to be advected from the Arctic Ocean. Both could be true since, similarly to north of Svalbard, warm AW is available for sea ice melt at the surface in the RAC which would create a local LHW with the shape of the knee water in *TS* space while FSBW is also advected to the

region by the TPD. The water masses sourced off the Northeast Greenland Shelf are advected onto the shelf by Ekman pumping (Vianco, 2024).

This means that the water on the Northeast Greenland shelf falls somewhere in an area between a set of four relationships in *TS* space (Figure 2.7); The AW surface freshwater to the LHW or knee mixing line, the CHL which follows the freezing line from the LHW to the coldest of the previous winter SML, a line between the winter SML and the local runoff end-member which has a salinity of 0 and a temperature that is above the freshwater freezing temperature, and finally the mixing line between the runoff back to the AW.

As the 'knee' is advected north- and westward through the trough system (e.g. Belgica Trough →Westwind Trough), it becomes less pronounced (Bignami and Hopkins, 1997). This is reflected in more recent data as well (An et al., 2021; Huhn et al., 2021) where the water in Belgica Trough shows a clear knee or LHW but the water in front of the Zachariae Isstrøm and Niogerhalvfjerdbrae outlet glaciers does not. The precise cause of the erosion of this feature has not been convincingly shown, though it is likely similar to what occurs in tidewater glacier fjords in other parts of Greenland where water from plume pools gets progressively mixed into ambient water with distance away from the pool (Mortensen et al., 2020). The feature also erodes with latitude. While still prominent at 68.3 °N, it becomes less pronounced within the East Greenland Coastal Current (CC), entirely disappearing by the time it reaches Cape Farewell (60 °N) (Sutherland and Pickart, 2008). These lines of evidence indicate that increasing freshwater fractions play a role.

Apart from the two aforementioned Zachariae Isstrøm outlet glaciers, there are no glaciers directly discharging onto the shelf so the water masses are advected into the fjords without LHW or knee water erosion where depth permits (Straneo and Cenedese, 2015). Once near the coast and inside the fjords local processes will further modify the incoming water. These local modifications occur due to local freshwater input at the head, due to friction and flow interactions with fjord topography, and due to wind forcing and ice melt (sea and glacial ice) at the surface. The extent of each of these modifications will vary on a per-fjord basis.

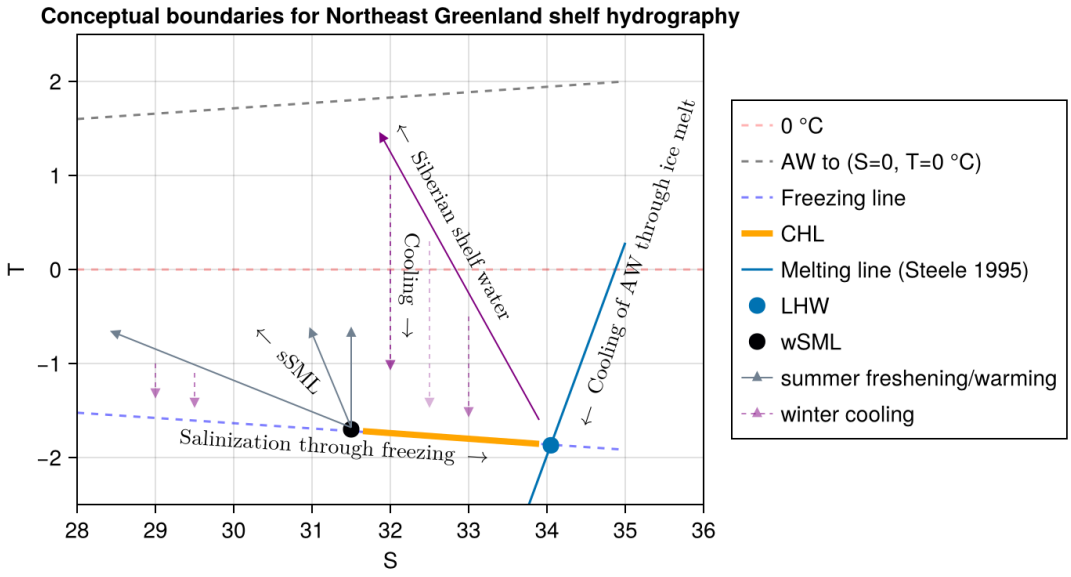

Figure 2.7: *TS* diagram showing the processes responsible for the hydrography generally found on the Northeast Greenland shelf. The cold halocline layer is highlighted in orange and between the two points of the winter Summer Mixed Layer (black) and the Lower Halocline Water or knee (blue). The boundaries of the CHL can vary depending on the amount of freshwater in the system at various points in the water mass history

Traditional fjord models (Stigebrandt, 1981 b; Farmer and Freeland, 1983) tend to consist of a two-layer estuarine model modified for fjords by the addition of a sill at the entrance that limits the inflow of water and creates an additional watermass inside the fjord at depths below the sill termed the basin water. Flow is controlled by a balance between intruding shelf waters and river runoff at the head. This creates a brackish surface layer overlying an intermediate layer which exists between the brackish layer and the sill. The thickness of the brackish layer is controlled by discharge volumes, and the horizontal surface area of the fjord for high specific runoff. For low runoff it is proportional to the Monin-Obukov length, which relates the friction velocity to the buoyancy to describe the impact of turbulence on a homogeneous environment. The maximum salinity of the brackish layer in the fjord is similarly governed by the freshwater discharge volume and the geometrical constriction formed by the geometry and dimensions of the fjord mouth (Stigebrandt, 1981 b). Wind mixing, tidal forcing, and the effect of Earths rotation influence mixing of the brackish and intermediate layers and circulation of the water inside fjords (Valle-Levinson, 2010).

The circulation inside Northeast Greenland fjords differentiates itself from traditional fjord models primarily through sill depth and stratification. Sills in Northeast Greenland are frequently deep, resulting in hydraulic activity across them having a comparatively lesser role. Shelf water that enters these fjords is already stratified into AW and PW, rather than a single ambient water mass. These factors mean that the classic two layer estuarine circulation model cannot necessarily be applied without modification (Straneo and Cenedese, 2015) unless sill depths restrict the denser AW from entering a fjord. In addition to the traditional model, freshwater is added by sea ice melt and ice bergs rather than solely at its head and received subglacial discharge at depth, entraining AW and entering the water column at intermediate to surface depths, depending on entrainment-controlled buoyancy and discharge velocity. Layers inside these fjords are therefore (from the surface); Surface water (in the form of a shallow ≈10 m SML), PW, AW, and basin water (Straneo and Cenedese, 2015). Intermediary flows, i.e. flows occuring in the water below the brackish surface layer, can have a large influence in Greenland fjords, in some cases replacing all the water inside a fjord in only a few months (Straneo et

al., 2010; Sutherland and Straneo, 2012; Straneo and Cenedese, 2015).

First and second baroclinic Rossby radii at high latitudes are small (Nurser and Bacon, 2014; Schaffer et al., 2017). Nonetheless many Northeast Greenland fjords are narrow enough to inhibit circulation driven by Earths rotation. That this is not the entire story is clear from observations of eddies at fjord surfaces and cross-fjord variations in flow [Rysgaard, personal communication, 2020]. These variations may be caused by wind, tides or remote forcing (Valle-Levinson, 2010; Valle-Levinson et al., 2014). At this time these secondary drivers of cross-fjord flow have not been fully described for the Northeast Greenland shelf.

2.5 Conclusions

Northeast Greenland shelf waters are at the centre of many of our current questions with regards to the influence of climate change on our oceans. Water advected onto the shelf is sourced from the rapidly warming Arctic and North Atlantic oceans. This water is locally modified through shelf and fjord processes, in terms of freshwater and chemistry. Downstream from the region deep water formation takes place and is influenced by the amount of stratification in the water column. This water is transported around the world oceans and is part of the global ocean conveyor. The associated export of atmospheric carbon into intermediate and deep water is a main sink for CO_2 on the order of ≈1000 years. The determination of water sources and processes affecting surface waters in this region are pivotal in our understanding of a changing Arctic and its influence on the atmosphere and ocean.

Water measurements in this region are difficult, particularly of the surface water due to logistical challenges. In particular, the difficulty and expense in accessing the region due to its remoteness, and the frequent passage of ice bergs whose keels will drag any moored equipment it can reach, means observations are limited in both time and space. Measurements tend to be taken in summer once sea ice has become passable, and from moorings placed deeper in the water column. Furthermore, many of the long term programmes have focused on either the Northeast Water

Polynya region, or on specific fjords. Any effort to broaden our understanding of this region, be it at a synoptic or local scale, that focuses our understanding of surface water processes, can be considered an important piece of the climate puzzle.

References

Aagaard K, Coachman LK, Carmack E. 1981. On the halocline of the Arctic Ocean. *Deep Sea Research Part A Oceanographic Research Papers* **28**(6): 529 – 545. doi: 10.1016/0198-0149(81)90115-1

Aagaard K, Foldvik A, Hillman SR. 1987. The West Spitsbergen Current: Disposition and water mass transformation. *Journal of Geophysical Research* **92**(C4): 3778. doi: 10.1029/JC092iC04p03778

Abrahamsen EP, Meredith MP, Falkner KK, Torres-Valdes S, Leng MJ, Alkire MB, Bacon S, Laxon SW, Polyakov I, Ivanov V. 2009. Tracer-derived freshwater composition of the Siberian continental shelf and slope following the extreme Arctic summer of 2007. *Geophysical Research Letters* **36**(7): 2009GL037341. doi: 10.1029/2009GL037341

Alkire MB, Morison J, Andersen R. 2015. Variability in the meteoric water, sea-ice melt, and P acific water contributions to the central A rctic O cean, 2000 – 2014. *Journal of Geophysical Research: Oceans* **120**(3): 1573 – 1598. doi: 10.1002/2014JC010023

Alkire MB, Polyakov I, Rember R, Pnyushkov A, Ivanov V, Ashik I. 2017. Combining physical and geochemical methods to investigate lower halocline water formation and modification along the Siberian continental slope. *Ocean Science* **13**(6): 983 – 995. doi: 10.5194/os-13-983-2017

Alkire MB, Rember R, Polyakov I. 2021. The Pacific-Atlantic Front in the East Siberian Sea of the Arctic Ocean. In: Belkin IM, editor. *Chemical Oceanography*

of Frontal Zones. Berlin, Heidelberg: Springer Berlin Heidelberg. p. 63 – 94. doi: 10.1007/698_2021_795

An L, Rignot E, Wood M, Willis JK, Mouginot J, Khan SA. 2021. Ocean melting of the Zachariae Isstrøm and Nioghalvfjerdsfjorden glaciers, northeast Greenland. *Proceedings of the National Academy of Sciences* **118**(2): e2015483118. doi: 10.1073/pnas.2015483118

Anderson LG, Andersson PS, Björk G, Peter Jones E, Jutterström S, Wåhlström I. 2013. Source and formation of the upper halocline of the Arctic Ocean. *Journal of Geophysical Research: Oceans* **118**(1): 410 – 421. doi: 10.1029/2012JC008291

Anderson LG, Jones EP. 1985. Measurements of total alkalinity, calcium, and sulfate in natural sea ice. *Journal of Geophysical Research* **90**(C5): 9194. doi: 10.1029/JC090iC05p09194

Anderson TR, Hawkins E, Jones PD. 2016. CO2, the greenhouse effect and global warming: From the pioneering work of Arrhenius and Callendar to today' s Earth System Models. *Endeavour* **40**(3): 178 – 187. doi: 10.1016/j.endeavour.2016.07.002

Ardyna M, Arrigo KR. 2020. Phytoplankton dynamics in a changing Arctic Ocean. *Nature Climate Change* **10**(10): 892 – 903. doi: 10.1038/s41558-020-0905-y

Ardyna M, Mundy CJ, Mayot N, Matthes LC, Oziel L, Horvat C, Leu E, Assmy P, Hill V, Matrai PA, et al. 2020. Under-Ice Phytoplankton Blooms: Shedding Light on the "Invisible" Part of Arctic Primary Production. *Frontiers in Marine Science* **7**: 608032. doi: 10.3389/fmars.2020.608032

Arndt JE, Jokat W, Dorschel B, Myklebust R, Dowdeswell JA, Evans J. 2015. A new bathymetry of the Northeast Greenland continental shelf: Constraints on glacial and other processes. *Geochemistry, Geophysics, Geosystems* **16**(10): 3733 – 3753. doi: 10.1002/2015gc005931

Arrhenius S. 1869 Apr. On the Influence of Carbonic Acid in the Air upon the Temperature of the Ground, in press.

Arrigo KR. 2016. Sea ice as a habitat for primary producers. In: Thomas DN, editor. *Sea Ice*. Chichester, UK: John Wiley & Sons, Ltd. p. 352 – 369. doi: 10.1002/9781118778371.ch14

Azetsu-Scott K, Clarke A, Falkner K, Hamilton J, Jones EP, Lee C, Petrie B, Prinsenberg S, Starr M, Yeats P. 2010. Calcium carbonate saturation states in the waters of the Canadian Arctic Archipelago and the Labrador Sea. *Journal of Geophysical Research: Oceans* **115**(C11). doi: 10.1029/2009JC005917

Bates NR, Mathis JT, Cooper LW. 2009. Ocean acidification and biologically induced seasonality of carbonate mineral saturation states in the western Arctic Ocean. *Journal of Geophysical Research* **114**(C11): C11007. doi: 10.1029/2008jc004862

Bates NR, Orchowska MI, Garley R, Mathis JT. 2013. Summertime calcium carbonate undersaturation in shelf waters of the western Arctic Ocean – how biological processes exacerbate the impact of ocean acidification. *Biogeosciences* **10**(8): 5281 – 5309. doi: 10.5194/bg-10-5281-2013

Bauch D, van der Loeff MR, Andersen N, Torres-Valdes S, Bakker K, Abrahamsen EP. 2011. Origin of freshwater and polynya water in the Arctic Ocean halocline in summer 2007. *Progress in Oceanography* **91**(4): 482 – 495. doi: 10.1016/j.pocean.2011.07.017

Bauch D, Schlosser P, Fairbanks RG. 1995. Freshwater balance and the sources of deep and bottom waters in the Arctic Ocean inferred from the distribution of H218O. *Progress in Oceanography* **35**(1): 53 – 80. doi: 10.1016/0079-6611(95)00005-2

Bi H, Zhang Z, Wang Y, Xu X, Liang Y, Huang J, Liu Y, Fu M. 2019. Baffin Bay sea ice inflow and outflow: 1978 – 1979 to 2016 – 2017. *The Cryosphere* **13**(3): 1025

– 1042. doi: 10.5194/tc-13-1025-2019

Bignami F, Hopkins TS. 1997. The water mass characteristics of the Northeast Water Polynya: Polar Sea data 1992 – 1993. *Journal of Marine Systems* **10**(1-4): 139 – 156. doi: 10.1016/S0924-7963(96)00079-6

Bintanja R, Van Der Wiel K, Van Der Linden EC, Reusen J, Bogerd L, Krikken F, Selten FM. 2020. Strong future increases in Arctic precipitation variability linked to poleward moisture transport. *Science Advances* **6**(7): eaax6869. doi: 10.1126/sciadv.aax6869

Bourke RH, Newton JL, Paquette RG, Tunnicliffe MD. 1987. Circulation and water masses of the East Greenland shelf. *Journal of Geophysical Research* **92**(C7): 6729. doi: 10.1029/jc092ic07p06729

Broecker WS. 1974. "NO," a conservative water-mass tracer. *Earth and Planetary Science Letters* **23**(1): 100 – 107. doi: 10.1016/0012-821X(74)90036-3

Broecker WS, Takahashi T, Takahashi T. 1985. Sources and flow patterns of deep-ocean waters as deduced from potential temperature, salinity, and initial phosphate concentration. *Journal of Geophysical Research: Oceans* **90**(C4): 6925 – 6939. doi: 10.1029/JC090iC04p06925

Budéus G, Schneider W. 1995. On the hydrography of the Northeast Water Polynya. *Journal of Geophysical Research* **100**(C3): 4287. doi: 10.1029/94jc02024

Budéus G, Schneider W, Kattner G. 1997. Distribution and exchange of water masses in the Northeast Water polynya (Greenland Sea). *Journal of Marine Systems* **10**(1): 123 – 138. doi: 10.1016/s0924-7963(96)00074-7

Burgers TM, Miller LA, Rysgaard S, Mortensen J, Else B, Tremblay J-É, Papakyriakou T. 2023. Distinguishing Physical and Biological Controls on the Carbon Dynamics in a High-Arctic Outlet Strait. *Journal of Geophysical Research: Oceans* **128**(3):

e2022JC019393. doi: 10.1029/2022JC019393

Burgers TM, Miller LA, Thomas H, Else BGT, Gosselin M, Papakyriakou T. 2017. Surface Water CO2 Variations and Sea-Air CO2 Fluxes During Summer in the Eastern Canadian Arctic. *Journal of Geophysical Research: Oceans* **122**(12): 9663 – 9678. doi: 10.1002/2017jc013250

Carmack EC. 2007. The alpha/beta ocean distinction: A perspective on freshwater fluxes, convection, nutrients and productivity in high-latitude seas. *Deep Sea Research Part II: Topical Studies in Oceanography* **54**(23-26): 2578 – 2598. doi: 10.1016/j.dsr2.2007.08.018

Carter BR, Toggweiler JR, Key RM, Sarmiento JL. 2014. Processes determining the marine alkalinity and calcium carbonate saturation state distributions. *Biogeosciences* **11**(24): 7349 – 7362. doi: 10.5194/bg-11-7349-2014

Chang BX, Devol AH. 2009. Seasonal and spatial patterns of sedimentary denitrification rates in the Chukchi sea. *Deep Sea Research Part II: Topical Studies in Oceanography* **56**(17): 1339 – 1350. doi: 10.1016/j.dsr2.2008.10.024

Charette MA, Kipp LE, Jensen LT, Dabrowski JS, Whitmore LM, Fitzsimmons JN, Williford T, Ulfsbo A, Jones E, Bundy RM, et al. 2020. The Transpolar Drift as a Source of Riverine and Shelf-Derived Trace Elements to the Central Arctic Ocean. *Journal of Geophysical Research: Oceans* **125**(5). doi: 10.1029/2019JC015920

Chierici M, Fransson A. 2009. Calcium carbonate saturation in the surface water of the Arctic Ocean: Undersaturation in freshwater influenced shelves. *Biogeosciences* **6**(11): 2421 – 2431. doi: 10.5194/bg-6-2421-2009

Codispoti LA, Friederich GE, Sakamoto CM, Gordon LI. 1991. Nutrient cycling and primary production in the marine systems of the Arctic and Antarctic. *Journal of Marine Systems* **2**(3-4): 359 – 384. doi: 10.1016/0924-7963(91)90042-S

Codispoti LA, Richards FA. 1968. Micronutrient Distributions in the East Siberian and Laptev Seas during summer 1963. *ARCTIC* **21**(2): 67 – 83. doi: 10.14430/arctic3251

Constantin A, Johnson RS. 2024. The dynamics of the transpolar drift current. *Geophysical & Astrophysical Fluid Dynamics* **118**(3): 165 – 182. Taylor & Francis. doi: 10.1080/03091929.2024.2351919

Cooper LW, Benner R, McClelland JW, Peterson BJ, Holmes RM, Raymond PA, Hansell DA, Grebmeier JM, Codispoti LA. 2005. Linkages among runoff, dissolved organic carbon, and the stable oxygen isotope composition of seawater and other water mass indicators in the Arctic Ocean. *Journal of Geophysical Research: Biogeosciences* **110**(G2). doi: 10.1029/2005JG000031

Cooper LW, McClelland JW, Holmes RM, Raymond PA, Gibson JJ, Guay CK, Peterson BJ. 2008. Flow-weighted values of runoff tracers (d18O, DOC, Ba, alkalinity) from the six largest Arctic rivers. *Geophysical Research Letters* **35**(18): L18606. doi: 10.1029/2008gl035007

Craig H. 1961. Isotopic Variations in Meteoric Waters. *Science* **133**(3465): 1702 – 1703. American Association for the Advancement of Science. doi: 10.1126/science.133.3465.1702

Craig H, Gordon LI, Horibe Y. 1963. Isotopic exchange effects in the evaporation of water: 1. Low-temperature experimental results. *Journal of Geophysical Research* **68**(17): 5079 – 5087. doi: 10.1029/JZ068i017p05079

Daly KL, Wallace DWR, Smith Jr. WO, Skoog A, Lara R, Gosselin M, Falck E, Yager PL. 1999. Non-Redfield carbon and nitrogen cycling in the Arctic: Effects of ecosystem structure and dynamics. *Journal of Geophysical Research: Oceans* **104**(C2): 3185 – 3199. doi: 10.1029/1998JC900071

Dansgaard W. 1964. Stable isotopes in precipitation. *Tellus* **16**(4): 436 – 468. doi:

10.1111/j.2153-3490.1964.tb00181.x

De Steur L, Steele M, Hansen E, Morison J, Polyakov I, Olsen SM, Melling H, McLaughlin FA, Kwok R, Smethie WM, et al. 2013. Hydrographic changes in the Lincoln Sea in the Arctic Ocean with focus on an upper ocean freshwater anomaly between 2007 and 2010. *Journal of Geophysical Research: Oceans* **118**(9): 4699 – 4715. doi: 10.1002/jgrc.20341

Deming J, The NEWATER Steering Committee and Principle Investigators. 1993. Northeast water polynya: Polar sea cruise results. *Eos, Transactions American Geophysical Union* **74**(16): 185 – 196. doi: 10.1029/93EO00264

Devol AH, Codispoti LA, Christensen JP. 1997. Summer and winter denitrification rates in western Arctic shelf sediments. *Continental Shelf Research* **17**(9): 1029 – 1050. doi: 10.1016/S0278-4343(97)00003-4

Dieckmann GS, Nehrke G, Papadimitriou S, Göttlicher J, Steininger R, Kennedy H, Wolf-Gladrow D, Thomas DN. 2008. Calcium carbonate as ikaite crystals in Antarctic sea ice. *Geophysical Research Letters* **35**(8): L08501. doi: 10.1029/2008GL033540

Dmitrenko IA, Rudels B, Kirillov SA, Aksenov YO, Lien VS, Ivanov VV, Schauer U, Polyakov IV, Coward A, Barber DG. 2015. Atlantic water flow into the Arctic Ocean through the St. Anna Trough in the northern Kara Sea: ATLANTIC WATER FLOW TO THE ARCTIC OCEAN. *Journal of Geophysical Research: Oceans* **120**(7): 5158 – 5178. doi: 10.1002/2015JC010804

Dodd PA, Heywood KJ, Meredith MP, Naveira-Garabato AC, Marca AD, Falkner KK. 2009. Sources and fate of freshwater exported in the East Greenland Current. *Geophysical Research Letters* **36**(19): 2009GL039663. doi: 10.1029/2009GL039663

Dodd PA, Rabe B, Hansen E, Falck E, Mackensen A, Rohling E, Stedmon C, Kristi-

ansen S. 2012. The freshwater composition of the Fram Strait outflow derived from a decade of tracer measurements: COMPOSITION OF THE FRAM STRAIT OUTFLOW. *Journal of Geophysical Research: Oceans* **117**(C11): n/a – n/a. doi: 10.1029/2012JC008011

Drake TW, Tank SE, Zhulidov AV, Holmes RM, Gurtovaya T, Spencer RGM. 2018. Increasing Alkalinity Export from Large Russian Arctic Rivers. *Environmental Science & Technology* **52**(15): 8302 – 8308. doi: 10.1021/acs.est.8b01051

Drozdova AN, Nedospasov AA, Lobus NV, Patsaeva SV, Shchuka SA. 2021. CDOM Optical Properties and DOC Content in the Largest Mixing Zones of the Siberian Shelf Seas. *Remote Sensing* **13**(6): 1145. doi: 10.3390/rs13061145

Dvoretsky VG, Dvoretsky AG. 2015. Regional differences of mesozooplankton communities in the Kara Sea. *Continental Shelf Research* **105**: 26 – 41. doi: 10.1016/j.csr.2015.06.004

Eldevik T, Smedsrud LH, Li C, Årthun M, Madonna E, Svendsen L. 2020. The Arctic Mediterranean. In: Mechoso CR, editor. *Interacting Climates of Ocean Basins*1st ed. Cambridge University Press. p. 186 – 215. doi: 10.1017/9781108610995.007

Falck E. 2001. Contribution of waters of Atlantic and Pacific origin in the Northeast Water Polynya. *Polar Research* **20**(2): 193 – 200. doi: 10.3402/polar.v20i2.6517

Falck E, Kattner G, Budéus G. 2005. Disappearance of Pacific Water in the northwestern Fram Strait: DISAPPEARANCE OF PACIFIC WATER. *Geophysical Research Letters* **32**(14). doi: 10.1029/2005gl023400

Farmer DM, Freeland HJ. 1983. The physical oceanography of Fjords. *Progress in Oceanography* **12**(2): 147 – 219. doi: 10.1016/0079-6611(83)90004-6

Ferronskiĭ VI, Polîakov VA. 2012. *Isotopes of the Earth' s Hydrosphere*. 1st ed.

Dordrecht New York: Springer Science+Business Media.

Fischer M. 2009. Carbonate chemistry and $CaCO_3$ precipitation as ikaite in Antarctic sea ice [Diplom-{{Geograph}}]. [Leipzig]: Universität Leipzig.

Forryan A, Bacon S, Tsubouchi T, Torres-Valdés S, Naveira Garabato AC. 2019. Arctic freshwater fluxes: Sources, tracer budgets and inconsistencies. *The Cryosphere* **13**(8): 2111 – 2131. doi: 10.5194/tc-13-2111-2019

Gilbert PUPA, Bergmann KD, Boekelheide N, Tambutté S, Mass T, Marin F, Adkins JF, Erez J, Gilbert B, Knutson V, et al. 2022. Biomineralization: Integrating mechanism and evolutionary history. *Science Advances* **8**(10): eabl9653. doi: 10.1126/sciadv.abl9653

Gjelstrup CVB, Myers PG, Lee CM, Azetsu-Scott K, Stedmon CA. 2024. Connectivity between Siberian river runoff and the lower limb of the Atlantic Meridional Overturning Circulation. *Limnology and Oceanography* **69**(11): 2680 – 2687. doi: 10.1002/lno.12696

Granskog MA, Stedmon CA, Dodd PA, Amon RMW, Pavlov AK, de Steur L, Hansen E. 2012. Characteristics of colored dissolved organic matter (CDOM) in the Arctic outflow in the Fram Strait: Assessing the changes and fate of terrigenous CDOM in the Arctic Ocean: CDOM DYNAMICS IN ARCTIC OCEAN. *Journal of Geophysical Research: Oceans* **117**(C12): n/a – n/a. doi: 10.1029/2012jc008075

Gruber N, Sarmiento JL. 1997. Global patterns of marine nitrogen fixation and denitrification. *Global Biogeochemical Cycles* **11**(2): 235 – 266. doi: 10.1029/97GB00077

Hölemann JA, Juhls B, Bauch D, Janout M, Koch BP, Heim B. 2021. The impact of the freeze – melt cycle of land-fast ice on the distribution of dissolved organic matter in the Laptev and East Siberian seas (Siberian Arctic). *Biogeosciences* **18**(12): 3637 – 3655. doi: 10.5194/bg-18-3637-2021

Huhn O, Rhein M, Kanzow T, Schaffer J, Sültenfuß J. 2021. Submarine Meltwater From Nioghalvfjerdsbræ (79 North Glacier), Northeast Greenland. *Journal of Geophysical Research: Oceans* **126**(7). doi: 10.1029/2021JC017224

IPCC. 2023. *Climate Change 2021 – The Physical Science Basis: Working Group I Contribution to the Sixth Assessment Report of the Intergovernmental Panel on Climate Change*. 1st ed. Cambridge University Press. doi: 10.1017/9781009157896

Janout MA, Hölemann J, Timokhov L, Gutjahr O, Heinemann G. 2017. Circulation in the northwest Laptev Sea in the eastern Arctic Ocean: Crossroads between Siberian River water, Atlantic water and polynya-formed dense water. *Journal of Geophysical Research: Oceans* **122**(8): 6630 – 6647. doi: 10.1002/2017jc013159

Jeansson E, Jutterström S, Rudels B, Anderson LG, Anders Olsson K, Jones EP, Smethie WM, Swift JH. 2008. Sources to the East Greenland Current and its contribution to the Denmark Strait Overflow. *Progress in Oceanography* **78**(1): 12 – 28. doi: 10.1016/j.pocean.2007.08.031

Johnson MA, Polyakov IV. 2001. The Laptev Sea as a source for recent Arctic Ocean salinity changes. *Geophysical Research Letters* **28**(10): 2017 – 2020. doi: 10.1029/2000GL012740

Jones EP, Anderson LG, Swift JH. 1998. Distribution of Atlantic and Pacific waters in the upper Arctic Ocean: Implications for circulation. *Geophysical Research Letters* **25**(6): 765 – 768. doi: 10.1029/98gl00464

Jones EP, Anderson LG, Wallace DWR. 1991. Tracers of near-surface, halocline and deep waters in the Arctic ocean: Implications for circulation. *Journal of Marine Systems* **2**(1-2): 241 – 255. doi: 10.1016/0924-7963(91)90027-R

Jones EPeter, Coote AR, Levy EM. 1983. Effect of sea ice meltwater on the

alkalinity of seawater. *Journal of Marine Research* **41**(1): 43 – 52. doi: 10.1357/002224083788223063

Jutterström S, Anderson LG. 2005. The saturation of calcite and aragonite in the Arctic Ocean. *Marine Chemistry* **94**(1-4): 101 – 110. doi: 10.1016/j.marchem.2004.08.010

Kaiser K, Canedo-Oropeza M, McMahon R, Amon RMW. 2017. Origins and transformations of dissolved organic matter in large Arctic rivers. *Scientific Reports* **7**(1): 13064. doi: 10.1038/s41598-017-12729-1

Kawaguchi Y, Nishioka J, Nishino S, Fujio S, Lee K, Fujiwara A, Yanagimoto D, Mitsudera H, Yasuda I. 2020. Cold Water Upwelling Near the Anadyr Strait: Observations and Simulations. *Journal of Geophysical Research: Oceans* **125**(9): e2020JC016238. doi: 10.1029/2020JC016238

Kerr DE, Brown PJ, Grey A, Kelleher BP. 2021. The influence of organic alkalinity on the carbonate system in coastal waters. *Marine Chemistry* **237**: 104050. doi: 10.1016/j.marchem.2021.104050

Kim H-C, Lee K. 2009. Significant contribution of dissolved organic matter to seawater alkalinity. *Geophysical Research Letters* **36**(20). doi: 10.1029/2009GL040271

Kinney P, Arhelger ME, Burrell DC. 1970. Chemical characteristics of water masses in the Amerasian Basin of the Arctic Ocean. *Journal of Geophysical Research* **75**(21): 4097 – 4104. doi: 10.1029/JC075i021p04097

Kolås EH, Fer I, Baumann TM. 2024. The Polar Front in the northwestern Barents Sea: Structure, variability and mixing. *Ocean Science* **20**(4): 895 – 916. doi: 10.5194/os-20-895-2024

Kubryakov A, Stanichny S, Zatsepin A. 2016. River plume dynamics in the Kara Sea from altimetry-based lagrangian model, satellite salinity and chlorophyll data.

Remote Sensing of Environment **176**: 177 – 187. doi: 10.1016/j.rse.2016.01.020

Laukert G, Grasse P, Novikhin A, Povazhnyi V, Doering K, Hölemann J, Janout M, Bauch D, Kassens H, Frank M. 2022. Nutrient and Silicon Isotope Dynamics in the Laptev Sea and Implications for Nutrient Availability in the Transpolar Drift. *Global Biogeochemical Cycles* **36**(9): e2022GB007316. doi: 10.1029/2022GB007316

Lien VS, Trofimov AG. 2013. Formation of Barents Sea Branch Water in the north-eastern Barents Sea. *Polar Research* **32**(1): 18905. doi: 10.3402/polar.v32i0.18905

Liguori BTP, Ehlert C, Nöthig E-M, van Ooijen JC, Pahnke K. 2021. The Transpolar Drift Influence on the Arctic Ocean Silicon Cycle. *Journal of Geophysical Research: Oceans* **126**(11): e2021JC017352. doi: 10.1029/2021JC017352

Makkaveev PN, Melnikova ZG, Polukhin AA, Stepanova SV, Khlebopashev PV, Chultsova AL. 2015. Hydrochemical characteristics of the waters in the western part of the Kara Sea. *Oceanology* **55**(4): 485 – 496. doi: 10.1134/S0001437015040116

McClelland JW, Holmes RM, Peterson BJ, Amon R, Brabets T, Cooper L, Gibson J, Gordeev VV, Guay C, Milburn D, et al. 2008. Development of a Pan-Arctic Database for River Chemistry. *Eos, Transactions American Geophysical Union* **89**(24): 217 – 218. doi: 10.1029/2008EO240001

McLaughlin FA, Carmack EC, Macdonald RW, Bishop JKB. 1996. Physical and geochemical properties across the Atlantic/Pacific water mass front in the southern Canadian Basin. *Journal of Geophysical Research: Oceans* **101**(C1): 1183 – 1197. doi: 10.1029/95jc02634

McPherson RA, Wekerle C, Kanzow T. 2023. Shifts of the Recirculation Pathways in central Fram Strait drive Atlantic Intermediate Water Variability on Northeast Greenland shelf. Preprints. doi: 10.22541/essoar.168167222.21218611/v1

Mellat M, Brunello CF, Werner M, Bauch D, Damm E, Angelopoulos M, Nomura D, Welker JM, Schneebeli M, Granskog MA, et al. 2024. Isotopic signatures of snow, sea ice, and surface seawater in the central Arctic Ocean during the MOSAiC expedition. *Elem Sci Anth* **12**(1): 00078. doi: 10.1525/elementa.2023.00078

Melling H, Moore RM. 1995. Modification of halocline source waters during freezing on the Beaufort Sea shelf: Evidence from oxygen isotopes and dissolved nutrients. *Continental Shelf Research* **15**(1): 89 – 113. doi: 10.1016/0278-4343(94)P1814-R

Michel C, Hamilton J, Hansen E, Barber D, Reigstad M, Iacozza J, Seuthe L, Niemi A. 2015. Arctic Ocean outflow shelves in the changing Arctic: A review and perspectives. *Progress in Oceanography* **139**: 66 – 88. doi: 10.1016/j.pocean.2015.08.007

Middelburg JJ, Soetaert K, Hagens M. 2020. Ocean Alkalinity, Buffering and Biogeochemical Processes. *Reviews of Geophysics* **58**(3): e2019RG000681. doi: 10.1029/2019RG000681

Millero FJ, Lee K, Roche M. 1998. Distribution of alkalinity in the surface waters of the major oceans. *Marine Chemistry* **60**(1-2): 111 – 130. doi: 10.1016/S0304-4203(97)00084-4

Min C, Yipu H, Mingming J, Yusheng Q. 2003. The sources of the upper and lower halocline water in the Canada Basin derived from isotopic tracers. *Science in China Series D: Earth Sciences* **46**(6): 625 – 639. doi: 10.1007/BF02984540

Moore GWK, Howell SEL, Brady M, Xu X, McNeil K. 2021. Anomalous collapses of Nares Strait ice arches leads to enhanced export of Arctic sea ice. *Nature Communications* **12**(1): 1. doi: 10.1038/s41467-020-20314-w

Morse JW, Arvidson RS, Lüttge A. 2007. Calcium Carbonate Formation and Dissolution. *Chemical Reviews* **107**(2): 342 – 381. doi: 10.1021/cr050358j

Mortensen J, Rysgaard S, Bendtsen J, Lennert K, Kanzow T, Lund H, Meire L. 2020. Subglacial Discharge and Its Down-Fjord Transformation in West Greenland Fjords With an Ice Mélange. *Journal of Geophysical Research: Oceans* **125**(9). doi: 10.1029/2020jc016301

Mucci A. 1983. The solubility of calcite and aragonite in seawater at various salinities, temperatures, and one atmosphere total pressure. *American Journal of Science* **283**(7): 780 – 799. doi: 10.2475/ajs.283.7.780

Namyatov AA. 2021. δO as a tracer of the main regularities of water mass mixing and transformation in the Barents, Kara, and Laptev seas. *Journal of Hydrology* **593**: 125813. doi: 10.1016/j.jhydrol.2020.125813

Nedashkovsky AP, Khvedynich SV, Petrovsky TV. 2009. Alkalinity of sea ice in the high-latitudinal arctic according to the surveys performed at north pole drifting station 34 and characterization of the role of the arctic ice in the CO2 exchange. *Oceanology* **49**(1): 55 – 63. doi: 10.1134/s000143700901007x

Nelson KH, Thompson TO. 1954. Deposition of salts for seawater by frigid concentration. Seattle, Washington: The university of Washington.

Nitishinsky M, Anderson LG, Hölemann JA. 2007. Inorganic carbon and nutrient fluxes on the Arctic Shelf. *Continental Shelf Research* **27**(10-11): 1584 – 1599. doi: 10.1016/j.csr.2007.01.019

Nomura D, Assmy P, Nehrke G, Granskog MA, Fischer M, Dieckmann GS, Fransson A, Hu Y, Schnetger B. 2013. Characterization of ikaite ($CaCO_3 \cdot 6H_2O$) crystals in first-year Arctic sea ice north of Svalbard. *Annals of Glaciology* **54**(62): 125 – 131. doi: 10.3189/2013AoG62A034

Nurser AJG, Bacon S. 2014. The Rossby radius in the Arctic Ocean. *Ocean Science* **10**(6): 967 – 975. doi: 10.5194/os-10-967-2014

O'Neil JR. 1968. Hydrogen and oxygen isotope fractionation between ice and water. *The Journal of Physical Chemistry* **72**(10): 3683 – 3684. doi: 10.1021/j100856a060

Okazaki (岡崎) M(🄵視). 1993. 石灰藻による炭酸カルシウム形成 – その機構と海洋における規模 – . Calcium carbonate formation by calcareous algae – It's mechanisms and productivity in ocean. doi: 10.14934/chikyukagaku.27.29

Osadchiev AA, Pisareva MN, Spivak EA, Shchuka SA, Semiletov IP. 2020. Freshwater transport between the Kara, Laptev, and East-Siberian seas. *Scientific Reports* **10**(1): 13041. doi: 10.1038/s41598-020-70096-w

Osadchiev A, Sedakov R, Frey D, Gordey A, Rogozhin V, Zabudkina Z, Spivak E, Kuskova E, Sazhin A, Semiletov I. 2023. Intense zonal freshwater transport in the Eurasian Arctic during ice-covered season revealed by in situ measurements. *Scientific Reports* **13**(1): 16508. doi: 10.1038/s41598-023-43524-w

Östlund G. 1994. Isotope tracing of Siberian river water in the Arctic Ocean. *Journal of Environmental Radioactivity* **25**(1-2): 57 – 63. doi: 10.1016/0265-931x(94)90007-8

Östlund HG, Hut G. 1984. Arctic Ocean water mass balance from isotope data. *Journal of Geophysical Research* **89**(C4): 6373. doi: 10.1029/jc089ic04p06373

Ouyang Z, Collins A, Li Y, Qi D, Arrigo KR, Zhuang Y, Nishino S, Humphreys MP, Kosugi N, Murata A, et al. 2022. Seasonal Water Mass Evolution and Non-Redfield Dynamics Enhance CO_2 Uptake in the Chukchi Sea. *Journal of Geophysical Research: Oceans* **127**(8). doi: 10.1029/2021JC018326

Paffrath R, Laukert G, Bauch D, Rutgers van der Loeff M, Pahnke K. 2021. Separating individual contributions of major Siberian rivers in the Transpolar Drift of the Arctic Ocean. *Scientific Reports* **11**(1): 8216. doi: 10.1038/s41598-021-86948-y

Papadimitriou S, Kennedy H, Kennedy P, Thomas DN. 2013. Ikaite solubility in seawater-derived brines at 1atm and sub-zero temperatures to 265K. *Geochimica et Cosmochimica Acta* **109**: 241 – 253. doi: 10.1016/j.gca.2013.01.044

Paquette RG, Bourke RH, Newton JF, Perdue WF. 1985. The East Greenland Polar Front in autumn. *Journal of Geophysical Research* **90**(c3): 4866 – 4882. doi: 10.1029/JC090iC03p04866

Pauly H. 1963. "Ikaite", a New Mineral from Greenland. *ARCTIC* **16**(4): 263. doi: 10.14430/arctic3545

Payne CM, Arrigo KR. 2022. Increases in Benthic Particulate Export and Sedimentary Denitrification in the Northern Chukchi Sea Tied to Under-Ice Primary Production. *Journal of Geophysical Research: Oceans* **127**(2): e2021JC018110. doi: 10.1029/2021JC018110

Penman DE, Caves Rugenstein JK, Ibarra DE, Winnick MJ. 2020. Silicate weathering as a feedback and forcing in Earth's climate and carbon cycle. *Earth-Science Reviews* **209**: 103298. doi: 10.1016/j.earscirev.2020.103298

Quéguiner B. 2016. *The Biogeochemical Cycle of Silicon in the Ocean*. 1st ed. Wiley. doi: 10.1002/9781119136880

Rawlins M, Yang D, Ge S. 2021. Regional and Basin Streamflow Regimes and Changes: Climate Impact and Human Effect. In: Yang D, Kane DL, editors. *Arctic Hydrology, Permafrost and Ecosystems*. Cham: Springer International Publishing. p. 159 – 186. doi: 10.1007/978-3-030-50930-9_6

Raymond PA, McClelland JW, Holmes RM, Zhulidov AV, Mull K, Peterson BJ, Striegl RG, Aiken GR, Gurtovaya TY. 2007. Flux and age of dissolved organic carbon exported to the Arctic Ocean: A carbon isotopic study of the five largest arctic rivers. *Global Biogeochemical Cycles* **21**(4): 2007GB002934. doi: 10.1029/2007GB002934

Redfield AC. 1934. *On the Proportions of Organic Derivatives in Sea Water and Their Relation to the Composition of Plankton*. university press of liverpool Liverpool. (Vol. 1).

Rudels B. 2022. The circulation and transformations of Atlantic water in the Arctic Mediterranean Sea. In: *The Physical Oceanography of the Arctic Mediterranean Sea*. Elsevier. p. 211 – 276. doi: 10.1016/B978-0-12-816930-8.00010-4

Rudels B, Anderson LG, Jones EP. 1996. Formation and evolution of the surface mixed layer and halocline of the Arctic Ocean. *Journal of Geophysical Research: Oceans* **101**(C4): 8807 – 8821. doi: 10/fb5ps5

Rudels B, Björk G, Nilsson J, Winsor P, Lake I, Nohr C. 2005. The interaction between waters from the Arctic Ocean and the Nordic Seas north of Fram Strait and along the East Greenland Current: Results from the Arctic Ocean-02 Oden expedition. *Journal of Marine Systems* **55**(1-2): 1 – 30. doi: 10.1016/j.jmarsys.2004.06.008

Rudels B, Friedrich HJ, Hainbucher D, Lohmann G. 1999. On the parameterisation of oceanic sensible heat loss to the atmosphere and to ice in an ice-covered mixed layer in winter. *Deep Sea Research Part II: Topical Studies in Oceanography* **46**(6-7): 1385 – 1425. doi: 10.1016/S0967-0645(99)00028-4

Rysgaard S, Glud RN, Lennert K, Cooper M, Halden N, Leakey RJG, Hawthorne FC, Barber D. 2012. Ikaite crystals in melting sea ice – implications for pCO_2 and pH levels in Arctic surface waters. *The Cryosphere* **6**(4): 901 – 908. doi: 10.5194/tc-6-901-2012

Rysgaard S, Mortensen J, Haxen M, Gillard LC, Risgaard-Petersen N. 2024. Summer Hydrography Conditions at Proglacial Fjord Entrances Along East Greenland. *Journal of Geophysical Research: Oceans* **129**(7): e2023JC020665. doi: 10.1029/2023JC020665

Schaffer J, Mayer C, de Steur L, Kanzow T. 2017. Warm water pathways toward

Nioghalvfjerdsfjorden Glacier, Northeast Greenland. *Journal of Geophysical Research*: 17. doi: 10.1002/2016JC012462

Sharp JD, Byrne RH. 2021. Technical note: Excess alkalinity in carbonate system reference materials. *Marine Chemistry* **233**: 103965. doi: 10.1016/j.marchem.2021.103965

Shimada K. 2005. Halocline structure in the Canada Basin of the Arctic Ocean. *Geophysical Research Letters* **32**(3): L03605. doi: 10.1029/2004GL021358

Smith WO, Barber DG, editors. 2007. *Polynyas: Windows to the World*. Amsterdam ; Boston: Elsevier. (Elsevier oceanography series; Vol. 74).

Song W, Liu Z, Lan H, Huan X. 2023. Influence of seasonal sea-ice loss on Arctic precipitation δ18O: A GCM-based analysis of monthly data. *Polar Research* **42**. doi: 10.33265/polar.v42.9751

Souchez R, Jouzel J, Lorrain R, Sleewaegen S, Stiévenard M, Verbeke V. 2000. A kinetic isotope effect during ice formation by water freezing. *Geophysical Research Letters* **27**(13): 1923 – 1926. doi: 10.1029/2000GL006103

Speetjens NJ, Hugelius G, Gumbricht T, Lantuit H, Berghuijs WR, Pika PA, Poste A, Vonk JE. 2023. The pan-Arctic catchment database (ARCADE). *Earth System Science Data* **15**(2): 541 – 554. doi: 10.5194/essd-15-541-2023

Stedmon CA, Amon RMW, Bauch D, Bracher A, Gonçalves-Araujo R, Hoppmann M, Krishfield R, Laney S, Rabe B, Reader H, et al. 2021. Insights Into Water Mass Origins in the Central Arctic Ocean From In-Situ Dissolved Organic Matter Fluorescence. *Journal of Geophysical Research: Oceans* **126**(7). doi: 10.1029/2021JC017407

Stedmon CA, Markager S. 2001. The optics of chromophoric dissolved organic matter (CDOM) in the Greenland Sea: An algorithm for differentiation between

marine and terrestrially derived organic matter. *Limnology and Oceanography* **46**(8): 2087 – 2093. doi: 10.4319/lo.2001.46.8.2087

Steele M, Boyd T. 1998. Retreat of the cold halocline layer in the Arctic Ocean. *Journal of Geophysical Research: Oceans* **103**(C5): 10419 – 10435. doi: 10.1029/98JC00580

Steele M, Morison JH, Curtin TB. 1995. Halocline water formation in the Barents Sea. *Journal of Geophysical Research: Oceans* **100**(C1): 881 – 894. doi: 10.1029/94JC02310

Stigebrandt A. 1981 b. A mechanism governing the estuarine circulation in deep, strongly stratified fjords. *Estuarine, Coastal and Shelf Science* **13**(2): 197 – 211. doi: 10.1016/S0302-3524(81)80076-X

Stigebrandt A. 1981 a. A Model for the Thickness and Salinity of the Upper Layer in the Arctic Ocean and the Relationship between the Ice Thickness and Some External Parameters. *Journal of Physical Oceanography* **11**(10): 1407 – 1422. doi: 10.1175/1520-0485(1981)011<1407:AMFTTA>2.0.CO;2

Straneo F, Cenedese C. 2015. The Dynamics of Greenland's Glacial Fjords and Their Role in Climate. *Annual Review of Marine Science* **7**(1): 89 – 112. doi: 10.1146/annurev-marine-010213-135133

Straneo F, Hamilton GS, Sutherland DA, Stearns LA, Davidson F, Hammill MO, Stenson GB, Rosing-Asvid A. 2010. Rapid circulation of warm subtropical waters in a major glacial fjord in East Greenland. *Nature Geoscience* **3**(3): 182 – 186. doi: 10.1038/ngeo764

Sun X, Anderson LG, Dessirier B, Geibel M, Mörth C-M, Humborg C. 2024. Large-Scale Summertime Variability of Carbonate Chemistry Across the East Siberian Sea: Primary Production Versus Ikaite Dissolution. *Journal of Geophysical Research: Oceans* **129**(1): e2023JC020600. doi: 10.1029/2023JC020600

Sun X, Humborg C, Mörth C-M, Brüchert V. 2021. The Importance of Benthic Nutrient Fluxes in Supporting Primary Production in the Laptev and East Siberian Shelf Seas. *Global Biogeochemical Cycles* **35**(7). doi: 10.1029/2020GB006849

Sutherland DA, Pickart RS. 2008. The East Greenland Coastal Current: Structure, variability, and forcing. *Progress in Oceanography* **78**(1): 58 – 77. doi: 10.1016/j.pocean.2007.09.006

Sutherland DA, Straneo F. 2012. Estimating ocean heat transports and submarine melt rates in Sermilik Fjord, Greenland, using lowered acoustic Doppler current profiler (LADCP) velocity profiles. *Annals of Glaciology* **53**(60): 50 – 58. doi: 10.3189/2012AoG60A050

Takeuchi M, Doubell MJ, Jackson GA, Yukawa M, Sagara Y, Yamazaki H. 2019. Turbulence mediates marine aggregate formation and destruction in the upper ocean. *Scientific Reports* **9**(1): 16280. doi: 10.1038/s41598-019-52470-5

Tan FC, Dyrssen D, Strain PM. 1983. Sea-ice meltwater and excess alkalinity in the East Greenland Current. *Oceanologica acta* **6**(3).

Tanaka T, Guo L, Deal C, Tanaka N, Whitledge T, Murata A. 2004. N deficiency in a well-oxygenated cold bottom water over the Bering Sea shelf: Influence of sedimentary denitrification. *Continental Shelf Research* **24**(12): 1271 – 1283. doi: 10.1016/j.csr.2004.04.004

Tank SE, McClelland JW, Spencer RGM, Shiklomanov AI, Suslova A, Moatar F, Amon RMW, Cooper LW, Elias G, Gordeev VV, et al. 2023. Recent trends in the chemistry of major northern rivers signal widespread Arctic change. *Nature Geoscience* **16**(9): 789 – 796. doi: 10.1038/s41561-023-01247-7

Thomas DN, Dieckmann GS. 2010. *Sea Ice, Second Edition*. 2nd ed. Wiley-Blackwell.

Tomczak M. 1981. A multi-parameter extension of temperature/salinity diagram

techniques for the analysis of non-isopycnal mixing. *Progress in Oceanography* **10**(3): 147 – 171. doi: 10.1016/0079-6611(81)90010-0

Tréguer PJ, De La Rocha CL. 2013. The World Ocean Silica Cycle. *Annual Review of Marine Science* **5**(1): 477 – 501. doi: 10.1146/annurev-marine-121211-172346

Tréguer P, Nelson DM, Van Bennekom AJ, DeMaster DJ, Leynaert A, Quéguiner B. 1995. The Silica Balance in the World Ocean: A Reestimate. *Science* **268**(5209): 375 – 379. doi: 10.1126/science.268.5209.375

Valle-Levinson A. 2010. *Contemporary Issues in Estuarine Physics*.

Valle-Levinson A, Caceres MA, Pizarro O. 2014. Variations of tidally driven three-layer residual circulation in fjords. *Ocean Dynamics* **64**(3): 459 – 469. doi: 10.1007/s10236-014-0694-9

Vianco SL. 2024. The origins of the East Greenland Coastal Current on the Northeast Greenland Shelf: A comparison of two reanalysis products [PhD thesis]. the Massachusetts Institute of Technology; the Woods Hole Oceanographic Institution. doi: 10.1575/1912/70545

Waldbusser GG, Hales B, Haley BA. 2016. Calcium carbonate saturation state: On myths and this or that stories. *ICES Journal of Marine Science* **73**(3): 563 – 568. doi: 10.1093/icesjms/fsv174

Wallace DWR, Behrens WJ, Hopkins TS, Kinder C, Deming J, Smith WO, Top Z, Walsh ID. 1995. Collaborative research on the Northeast Water Polynya: NEWP92 hydrographic data report. USCGC Polar Sea cruise, July 15 – August 15, 1992. Report No.: BNL – 61923, 102497. doi: 10.2172/102497

Wallace DWR, Minnett PJ, Hopkins TS. 1995. Nutrients, oxygen, and inferred new production in the Northeast Water Polynya, 1992. *Journal of Geophysical Research* **100**(C3): 4323. doi: 10.1029/94JC02203

Wang X, Zhao J, Lobanov VB, Kaplunenko D, Rudykh YN, He Y, Chen X. 2021. Distribution and Transport of Water Masses in the East Siberian Sea and Their Impacts on the Arctic Halocline. *Journal of Geophysical Research: Oceans* **126**(8). doi: 10.1029/2020JC016523

Weeks WF. 2010. *On Sea Ice*. Fairbanks: University of Alaska Press.

Wilson C, Wallace DWR. 1990. Using the nutrient ratio NO/PO as a tracer of continental shelf waters in the central Arctic Ocean. *Journal of Geophysical Research* **95**(C12): 22193. doi: 10.1029/JC095iC12p22193

Yamamoto-Kawai M, Carmack E, McLaughlin F. 2006. Nitrogen balance and Arctic throughflow. *Nature* **443**(7107): 43 – 43. doi: 10/csstkf

Yamamoto-Kawai M, McLaughlin FA, Carmack EC. 2011. Effects of ocean acidification, warming and melting of sea ice on aragonite saturation of the Canada Basin surface water. *Geophysical Research Letters* **38**(3). doi: 10.1029/2010GL045501

Yamamoto-Kawai M, Tanaka N, Pivovarov S. 2005. Freshwater and brine behaviors in the Arctic Ocean deduced from historical data of δ18O and alkalinity (1929 – 2002 A.D.). *Journal of Geophysical Research: Oceans* **110**(C10). doi: 10.1029/2004JC002793

Yi Y, Gibson JJ, Cooper LW, Hélie J-F, Birks SJ, McClelland JW, Holmes RM, Peterson BJ. 2012. Isotopic signals (18O, 2H, 3H) of six major rivers draining the pan-Arctic watershed. *Global Biogeochemical Cycles* **26**(1). doi: 10.1029/2011gb004159

Young ED, Galy A, Nagahara H. 2002. Kinetic and equilibrium mass-dependent isotope fractionation laws in nature and their geochemical and cosmochemical significance. *Geochimica et Cosmochimica Acta* **66**(6): 1095 – 1104. doi: 10.1016/S0016-7037(01)00832-8

Zeebe RE, Wolf-Gladrow DA. 2001. *CO_2 in Seawater: Equilibrium, Kinetics, Isotopes*.

Amsterdam ; New York: Elsevier. (Elsevier oceanography series; Vol. 65).

Zeng J, Chen M, Zheng M, Hu W, Qiu Y. 2017. A potential nitrogen sink discovered in the oxygenated Chukchi Shelf waters of the Arctic. *Geochemical Transactions* **18**(1): 5. doi: 10.1186/s12932-017-0043-2

3 An Updated View of the Water Masses on the Northeast Greenland Shelf and Their Link to the Laptev Sea and Lena River

Co-authors: J. Bendtsen , J. Mortensen, C. Mohn, M. Lemes, T.-J. Pedersen, J. Holding, E. F. Møller, M. K. Sejr, M.-S. Seidenkrantz, and S. Rysgaard

DOI: https://doi.org/10.1029/2022JC019052

3.1 Abstract

The Northeast Greenland shelf is a broad Arctic shelf located between Greenland and Fram Strait. It is the principal gateway for sea ice export and sea ice-associated freshwater from the Arctic Ocean. Sea ice thickness has decreased by 15% per decade since the early 1990s and meteoric freshwater discharge has increased. The consequence of changing sea-ice and freshwater conditions in the region on ocean dynamics and the biological system remains unknown. Determining the source(s) of freshwater is important to be able to understand how the area will react to future upstream change. Here we present a synoptic survey of the Northeast Greenland shelf and slope with observations of hydrography, the nutrients nitrate, phosphate and silicate, and conservative tracers $\delta^{18}O$, $\delta^{2}H$, and total alkalinity during late summer 2017. We compare these to previously published values, including those which identify Pacific and Atlantic water, the Siberian shelf seas, and the six largest Arctic rivers. We show that a major source of freshwater on the Northeast Greenland

shelf during late summer 2017 is the Laptev Sea and find no conclusive evidence of Pacific Water. Our observations indicate a direct link between Northeast Greenland hydrology and processes occurring on Eurasian shelves.

3.2 Plain Language Summary

The Northeast Greenland shelf is a shallow marine environment between Greenland and the adjacent Fram Strait, where a large fraction of the Arctic Ocean freshwater is exported into the North Atlantic. To predict the regional response to climate change, it is important to determine what the remote sources of freshwater on the shelf are and how these influence mixing. We compare the chemistry of the water found at different locations on the shelf with those found in other areas of the Arctic Ocean to determine where it comes from and conclude that most of the water on the Northeast Greenland shelf in late summer of 2017 is from the Laptev Sea, while surface waters have subsequently been modified by sea ice melt.

3.3 Introduction

The Northeast Greenland shelf is a broad Arctic continental shelf located between Greenland and the adjacent Fram Strait. Fram Strait is the main conduit for the flux of warm high-salinity Atlantic water northward and the southward flow of cold, low-salinity water exiting the Arctic Ocean. The waters leaving the Arctic Ocean have different formation regions, pathways and modification histories and form density stratified layers in the water column. A significant fraction of the surface water has a meteoric freshwater source and can be advected onto the Northeast Greenland shelf and subjected to additional modification. Changes in upstream conditions therefore may exert significant influence on regional hydrography and biogeochemistry. Gaining an understanding of the sources of water found on the shelf will benefit our ability to predict the response of this environment to any changes taking place upstream in the Arctic Ocean. Although the determination of freshwater

fractions has been performed several times in Fram Strait and further south on the East Greenland shelf (Falck, 2001; Sutherland et al., 2009; Dodd et al., 2012) upstream freshwater source regions have yet to be identified. Although riverine biogeochemical tracer values have been published (Cooper et al., 2008), the required number of biogeochemical measurements for the identification of individual rivers are frequently not measured from corresponding downstream oceanographic water samples. This study aims to remedy this by presenting a cohesive analysis of the Northeast Greenland shelf based on a suite of hydrographical and biogeochemical measurements to determine the synoptic hydrography on the shelf and the dominant source region of the meteoric freshwater found on the Northeast Greenland shelf during late summer 2017.

3.3.1 Arctic Ocean Circulation

The Fram Strait receives all the water exiting the Arctic Ocean (Figure 3.1) that is not exported through the Canadian Arctic (or evaporated). As a result, waters with very different spatial and temporal histories are superimposed onto one another as they are geographically constrained in Fram Strait, leading to high hydrographic complexity. The Atlantic Ocean is the sole deep water conduit to the Arctic Ocean. Even Pacific Ocean input is constrained by the Bering Shelf which has depths shallower than 100 m (Jakobsson et al., 2020) and is considered a source of upper layer water only. The warm Atlantic current follows two separate pathways into the Arctic. One across the Barents Sea, and the other through eastern Fram Strait which curves eastward north of Svalbard near Yermak Plateau. Both regions form their own halocline water with a slightly different density, as a result of differences in their Atlantic Water temperature (Rudels et al., 2004). North of Svalbard, warm surface water melts sea ice, forming a surface layer. This fresh and cold water inhibits full depth convection during winter and initiates the halocline formation process, which is repeated in subsequent years, creating the Fram Strait Branch Water (FSBW). The Barents Sea forms its own halocline water. This has a sea ice melt component but also has additional freshwater sources, including but not limited to the Norwegian Coastal Current and freshwater from rivers discharging into the

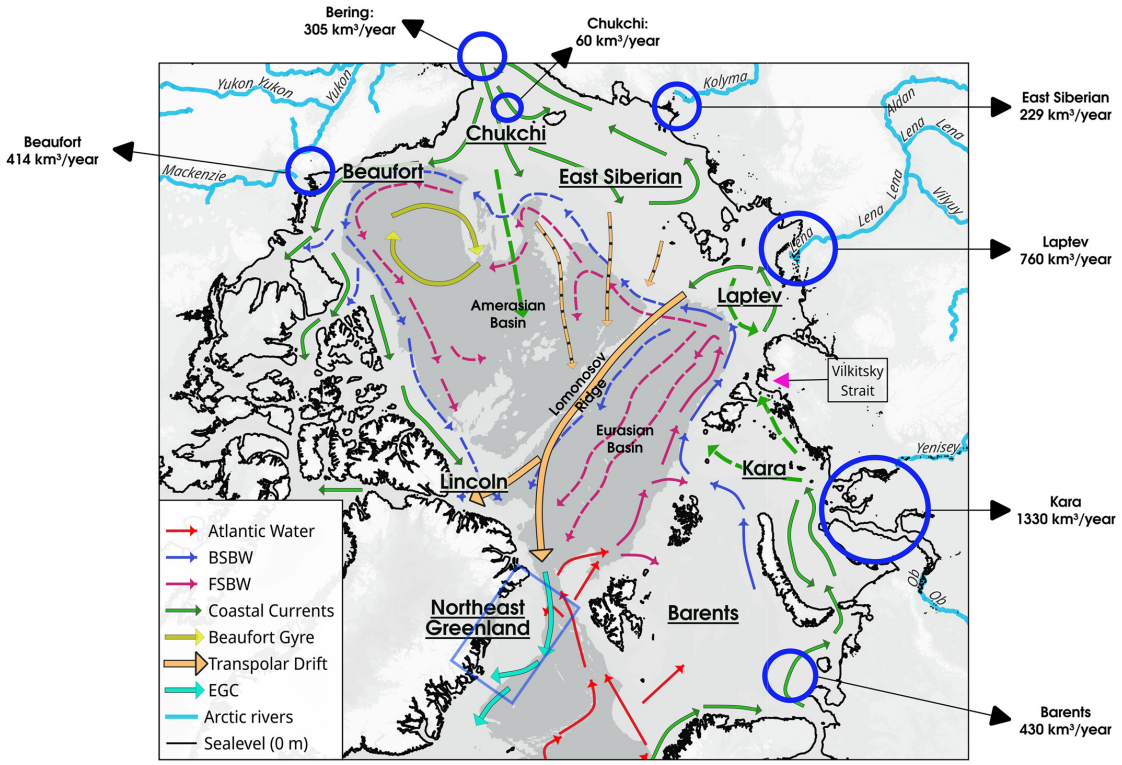

Figure 3.1: Map of the Arctic Ocean and its major surface and boundary currents based on maps in Rudels et al. (2004) and Aksenov et al. (2016). River GIS shapefile was obtained from http://arcticgreatrivers.org. Discharge values are given in the large blue circles as discharge received per shelf sea per annum using values from Shiklomanov et al. (2021). Acronyms FSBW and BSBW are the Fram Strait and Barents Sea branch waters, respectively, and EGC is the East Greenland Current. The Atlantic inflow west of Svalbard is the West Spitsbergen Current. Dashed lines are used where the flow is temporally variable or less information about current specifics is available. The blue rectangle around the Northeast Greenland shelf indicates the study area which is the focus of this paper.

Kara Sea, each of which contribute to limiting the depth of winter convection and the formation of the Barents Sea Branch Water (BSBW). The Nansen Basin is dominated by FSBW while the Amundsen Basin contains a mixture of both branches with BSBW the dominant branch (Figure 3.1) (Schauer et al., 2002; Rudels, 2021).

As Atlantic water is transported around the Arctic Ocean, freshwater is added incrementally by Arctic rivers discharging onto the continental shelves, sea ice melt, and precipitation (Haine et al., 2015). Following Atlantic water in a counter clockwise direction, Barents Sea freshwater is dominated by precipitation and by subpolar coastal freshwater of the Norwegian Coastal Current (Rudels, 2021). This is followed by input from the rivers Ob' and Yenisey which discharge directly into the Kara Sea. Observations of the Ob' -Yenisey plume show that freshwater transport from the Kara to the Laptev Sea through Vilkitsky Strait depends on the persistence of along-shore south-westerly winds and in their absence the water is exported off-shelf (Osadchiev et al., 2020). The Lena river plume direction also depends on atmospheric forcing, with off-shelf transport occurring when winds force anticyclonic circulation which transports freshwater across the shelf and into the Arctic Ocean where, together with underlying Atlantic water, it is entrained in the Transpolar drift (Bauch et al., 2009). Biogeochemical and hydrographic surveys of the Transpolar drift regions show both riverine influence (Charette et al., 2020; Paffrath et al., 2021) and the lower halocline (Kikuchi, 2004; Rabe et al., 2022). The remaining Lena River water is transported by a narrow coastal current to the East Siberian Sea.

The East Siberian Sea shelf receives additional river discharge from the Kolyma river and is advected toward the Chukchi Sea (Osadchiev et al., 2020). The water entering the Arctic from the Pacific Ocean through the Bering Strait and onto the Chukchi shelf is also considered a freshwater source containing a large fraction of meteoric water, including the runoff from the Yukon River. Much of this water is captured by the Beaufort Gyre, as is a portion of the Mackenzie River water on the Beaufort Sea shelf. A small portion of the Pacific Water inflow is captured by a counter current across the East Siberian Sea and potentially entrained into the Transpolar drift, subsequently exiting in Fram Strait. Water transported via this route has an upper halocline with salinities between 33.1 and 34.2, formed by brine

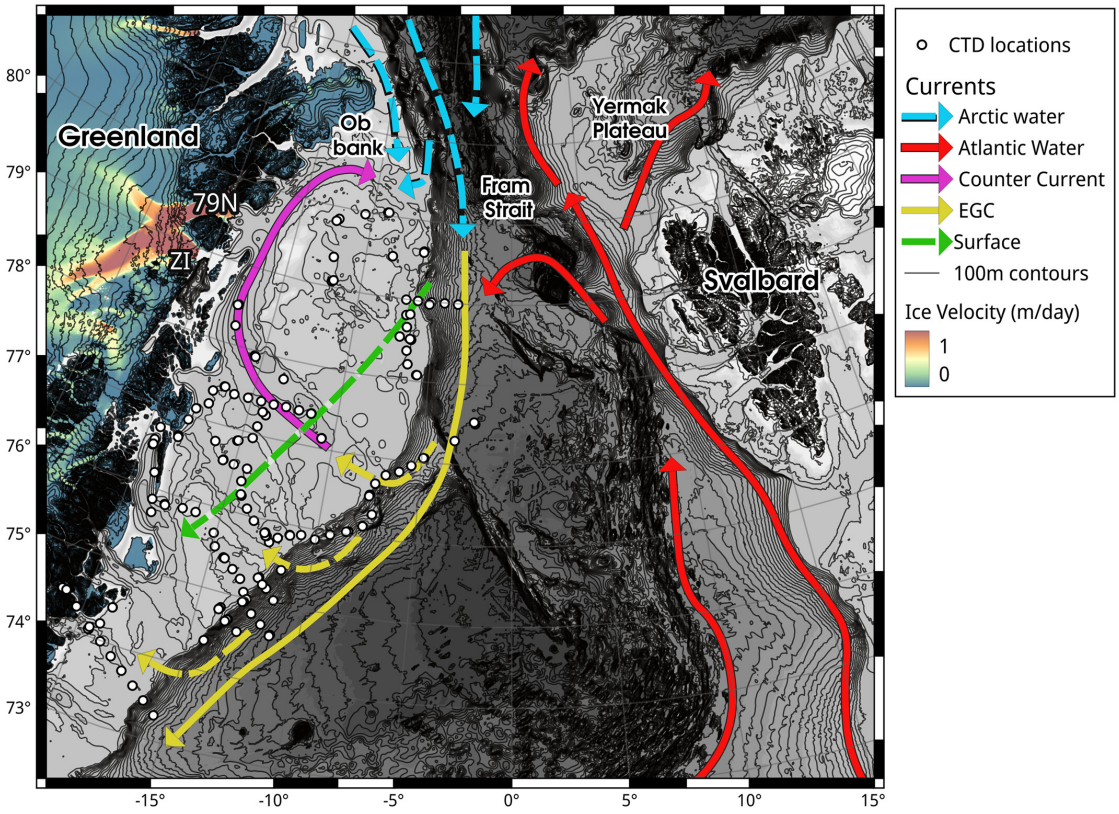

Figure 3.2: Map with the Conductivity Temperature Depth stations that were part of this study and the major known (solid) and hypothesized (dashed) currents. Surface water that is part of the off-shelf currents (including Arctic Water, the East Greenland Current or EGC, and the Atlantic Water) is available for transport onto the Northeast Greenland shelf. On the shelf, the Northeast Greenland Counter Current is relatively well established in literature. Less is known about the cross-shelf surface water. Return Atlantic Water is entrained into the ECG and is known to be available inside Belgica trough, where the counter current is initiated. It is possible that other troughs are also conduits for Atlantic Water though this depends on sill depths. Two outlet glaciers of the Northeast Greenland Ice sheet, Niogerhalfjerdsbrae (79°N) and Zachariae Isstrom (ZI) are identified by their ice velocity.

rejection during sea ice formation on the continental shelf, which is characterized by high nutrient concentrations due to processes taking place in the Chukchi and East Siberian Seas (Jones and Anderson, 1986; Anderson et al., 2013; Alkire et al., 2021). Fram Strait is the ultimate destination for all the Arctic freshwater that is not exported through the Canadian Archipelago. This means that water masses from all these sources with vastly different histories are superimposed here based on their density.

Only water relatively close to the surface compared to the full depth of Fram Strait can be advected onto the Northeast Greenland shelf due to bathymetric constraints. This limits the available water types to those found at depths less than the maximum trough depth at the shelf edge (300 – 370 m) plus any deeper water available for entrainment during upwelling events (Arndt et al., 2015). The top few hundred meters include most of the typically Arctic-associated hydrographic features, such as the summer mixed layer, and the cold halocline layer with temperatures close to freezing and salinities between the Lower Halocline Water (LHW) at S ~ 34.2 (Jones et al., 1991) and those of the (summer or winter) mixed layer. Subsurface Atlantic water can take one of several routes across the Arctic. Canadian Basin Atlantic Water (CBAW) has circulated across the Canadian Basin and is cooler, compared to Eurasian Basin Atlantic Water (EBAW) which has circulated only in the Eurasian Basin (Figure 3.1). Together, the EBAW and CBAW are sometimes referred to as Arctic Atlantic Water when they exit the Arctic Ocean at Fram Strait. The final source of Atlantic water that may be transported onto the Northeast Greenland shelf is Return Atlantic Water (RAW). This is Atlantic Water from the northward inflow current west of Svalbard and is the warmest found on the shelf (Figure 3.2). The local freshwater contributions from Nioghalvfjerdsbrae (79°N) and Zachariae Isstrøm are small compared to those from the Arctic great rivers (Haine et al., 2015) and mix to such an extent to not be distinguishable proximal to the shelf break (Huhn et al., 2021).

The precise residence time of waters on the Northeast Greenland Shelf itself is currently unknown. Although Atlantic Water flow rates are available, they rely on the accurate estimation of the Pacific water fraction (Lin et al., 2022), which may be biased through denitrification in the Laptev Sea (Nitishinsky et al., 2007; Bauch et

al., 2011; Sun et al., 2021). The transport of the off-shelf East Greenland Current has been estimated at ~ 3 Sv, and to be barotropically driven and contain superimposed eddies with widths around 10 km and depths to 400 m (Foldvik et al., 1988).

A subsurface water type referred to as East Greenland Shelf Water by Budéus and Schneider (1995) and as Polynya Intermediate Water by Bignami and Hopkins (1997) was previously identified on the Northeast Greenland shelf. These authors argued for its local formation in the Northeast Water polynya due to its geographical proximity to this feature. This polynya was an open water feature in summer and is thought to contain thinner ice than is expected from atmospheric conditions in winter (Smith IV and Morison, 1998; Smith and Barber, 2007) It used to be established just northeast of the Norske Øer ice barrier and south of the Ob Bank ice barrier, where large icebergs would run aground and restrict the advection of ice into the region, while ice was simultaneously being removed by the anticyclonic surface Northeast Greenland Counter Current (Figure 3.2). The Norske Øer ice barrier has since ceased to be a persistent feature in the region (Sneed and Hamilton, 2016) and is unlikely to play as large a role now. Neither the Norske Øer nor the Ob bank ice barrier were present in the late summer of 2017.

3.4 Tracking Freshwater Source Through Tracers

Source regions of freshwater with different characteristics may be identified using tracers. These are (quasi-) conservative chemical signatures with a known concentration at each source and known to respond primarily to physical mixing processes. They have been used extensively to determine freshwater fractions, specifically meteoric water (precipitation and river discharge), sea ice melt, and Pacific Water fractions (Falck, 2001; Falck et al., 2005; Sutherland et al., 2009; Bauch et al., 2011; Dodd et al., 2012).

The methodology for using tracers to determine the origin of different freshwater fractions relies on knowing accurate and distinguishable tracer concentrations for each end-member and inserting them into a system of linear equations (Jones et al.,

2008). Common tracers in an Arctic Ocean three end-member system to identify fractions of sea ice melt, meteoric water, and Atlantic Water are stable oxygen isotopic composition ($\delta^{18}O$) and total alkalinity (TA). These have end-members which are distinguishable from one another and respond to freezing in a predictable way (O'Neil, 1968; Rysgaard et al., 2007).

The most common tracer for identifying Pacific water, which enters the Arctic Ocean through Bering Strait, is the N:P ratio. Although its constituents are not conservative, their ratio is considered quasi-conservative and can be calculated using either the ratio of total dissolved inorganic nitrogen (Yamamoto-Kawai et al., 2008) or that of dissolved nitrate (Jones et al., 1998; Falck, 2001; Falck et al., 2005) to dissolved phosphate concentration. Water transported into the Arctic via the Bering Strait has a lower nitrogen concentration relative to phosphate compared to Atlantic-sourced water. This difference is further enhanced during advection across Chukchi Sea shelf sediments, where bacterial denitrification takes place (Codispoti et al., 1991; Cooper et al., 1999; Tanaka et al., 2004). More recently denitrification has also been found to occur in Laptev shelf sediments (Nitishinsky et al., 2007; Bauch et al., 2011; Sun et al., 2021) close to the source of the Transpolar drift which could bias fraction attribution to Pacific Water. The Upper Halocline Water (UHW) at its salinity range between 32 and 34, and high nutrient concentrations is also associated with Pacific water inflow (Nguyen et al., 2012; Anderson et al., 2013).

3.5 Materials and Methods

Sampling for the present study was done during two 3-week cruises with RV Dana to NE Greenland during August – September 2017. Leg 1 was carried out in the context of a monitoring project by the Government of Greenland and Leg 2 as a research expedition (NorthGreen2017) organized by the Department of Geoscience and the Arctic Research Center, Aarhus University. The combination of the two cruise legs, made it possible to save significant transit time for both expeditions and low sea-ice cover made it possible to work in a larger area on the Greenland shelf than expected, up to 80°N (Figure 3.2).

In total 115 Conductivity Temperature Depth (CTD) stations were sampled. We used a rosette (12 Niskin bottles) to collect water at 1 m, 5 m, 10 m, 20 m, deep chlorophyll maximum, 30 m, 50 m, 100 m, 200 m, 400 m, and the bottom. A CTD (Seabird 911 system) attached to the rosette measured conductivity, temperature, and pressure. Two oxygen sensors were also mounted on the rosette. The CTD sensors were calibrated yearly by the manufacturer and uncertainty of salinity was typically within the range $0.005 - 0.010$. We use the term salinity (S) for practical salinity (psu, practical salinity scale 1978), the term temperature (T) refers to the potential temperature (Θ). The terms depth and pressure are also considered interchangeable.

At every station, we collected water for TA analysis at all depths in 13 mL glass vials to which we added 50 µL of HgCl (5% solution); 11 water bottles (50 mL in polyethylene vials) for nutrients analyses at all depths and frozen for later analysis (silicate, nitrate + nitrite, and phosphorous); 11 water (glass vials of 2 mL) for water isotope analysis ($\delta^{18}O$; $\delta^{2}H$). Small drifting sea ice pieces were collected with a net from the deck of RV Dana for similar analysis.

Samples for TA were stored at 4°C until analysis. Samples for nutrient analysis were frozen in polyethylene vials until later analysis. The vials were rinsed several times with water from the specific depth before filling and freezing. TA was determined by Gran titration (Gran, 1952) using a TIM 840 titration system (Radiometer Analytical, ATS Scientific), consisting of a Ross sure-flow combination pH glass electrode (Orion 8172BNWP, Thermo Scientific) and a temperature probe (Radiometer Analytical). A 12 mL sample was titrated with a standard 0.05 M HCl solution (Alfa Aesar). Routine analysis of Certified Reference Materials (provided by A. G. Dickson, Scripps Institution of Oceanography; http://andrew.ucsd.edu/co2qc/) verified that the accuracy of TA was ±3 µmol kg -1. The isotopic compositions ($\delta^{18}O$; $\delta^{2}H$) of the samples were analyzed with a Cavity Ringdown Spectrometer, L2130-i Isotopic H20 (Picarro Inc., USA). Nine injections were taken from each sample and vapourized and the first three were excluded to remove any residual results from the previous sample. Vapor content, $\delta^{2}H$ and $\delta^{18}O$ values were calculated relative to certified standards. Four standards were measured at the beginning and end of the sample set. The external standards used to calibrate the results were Vienna Standard

Ocean Water 2 (δ^2HVSMOW, δ^{18}OVSMOW) (VSMOW2), Greenland Ice Sheet Precipitation (δ^2HGISP, δ^{18}OGISP) (GISP), and Standard Light Antarctic Precipitation 2 (δ^2HSLAP2, δ^{18}OSLAP2) (SLAP2). Detection limit for nutrient concentrations were 0.1 µmol kg −1 (NO_3^-), 0.06 µmol kg −1 (PO_4^{3-}), and 0.2 µmol kg^{-1} (Si).

Table 3.1: Datasets and Relationships Used for Comparison With 2017 Northeast Greenland Shelf Data to Determine Possible Source Location(s) for Water Found on the Northeast Greenland Shelf

Tracer relationship	Region	Detail used	Paper
NO_3^-:PO_4^{3-}	Laptev	Supplementary data	Supplement to Thibodeau et al. (2017)
	East Siberian Sea	Surface water average	Table 1 in Semiletov (2005)
	Atlantic & Pacific	Linear fit	eigure 2 in Jones et al. (1998)
TA:S	Atlantic & Pacific	End member values	Table 2 in Sutherland et al. (2009)
	Major rivers	End-member values	Table 1 in Cooper et al. (2008)
δ^{18}O:S	Arctic Deltas	Polynomial fit	Figure 2 in Namyatov (2021)
δ2H:δ^{18}O	Major rivers	Linear fit lines	Table 1 in Yi et al. (2012)
	Global Meteoric Water Line	Linear fit line	Craig (1961)
	Arctic Meteoric Water Line	Linear fit line	Equation 3 in Mellat et al. (2021)
Si:AOU & PO_4^{3-}:AOU	Laptev Sea water column	Linear fit lines	Figure 4 in Sun et al. (2021)
Sea ice melt	Local	Own measurements (5)	TA: 393, 130, 364, 61, 70
			δ^{18}O: −3.02, −2.95, −1.52, −1.56, −2.67

Data from the CTD casts from both cruises were combined into a 1 m (±0.5) binned dataset. A second dataset was created by combining the CTD bottle data with the analyses of δ^{18}O, δ^2H, TA, and nutrients based on cruise, station, and depth. The freezing line, oxygen saturation w.r.t. the atmosphere, and apparent oxygen utilisation (oxygen loss attributed to photosynthetic use, AOU = $[O2]_{s,t,p} - [O2]_{obs}$) were calculated with the Julia programming language (Bezanson et al., 2017) imple-

mentation of the TEOS-10 (Feistel, 2012) library.

To identify potential freshwater source locations, we compared our data to literature (Table 3.1). All maps were produced in QGIS (QGIS Development Team, 2022) with bathymetric data from IBCAO v4 (Jakobsson et al., 2020) and ice velocity from QGreenland (Moon et al., 2020).

3.6 Results and Interpretation

First, we manually assigned each individual CTD cast to one of five groups based on their clearly distinguishable shape in a TS diagram (Figure 3.3) and according to the presence of specific water types (Table 3.1). This was done first to avoid biasing our interpretation by taking geography as a starting point. Average profiles for each group are shown in Figure 3.4 together with the Brunt-Väisälä frequency squared (N^2) and the oxygen saturation w.r.t. that of the atmosphere. Mapping their longitude and latitude did show a geographical relationship with CTD cast group (Figure 3.5).

3.6.1 Geographical Groups

3.6.1.1 North Shelf Group

The North Shelf group stations (Figure 3.3a, Figure 3.4a – Figure 3.4d, and Figure 3.5) are found in the area formerly associated with the Northeast Water Polynya. This group has a summer halocline identifiable from temperature and salinity (Figure 3.4a and Figure 3.4b) with a Brunt-Väisälä frequency squared maximum (N^2, Figure 3.4 c) at around 10 m depth. Below the summer halocline there is a relatively more homogeneous layer down to a depth of 50 m which is associated with the Northeast Greenland Winter Water (NGWW). This is interpreted as the remnant of the winter mixed layer. In the upper part, between 20 and 30 m a dissolved oxygen maximum occurs which reaches almost 100% of atmospheric saturation (Figure 3.4

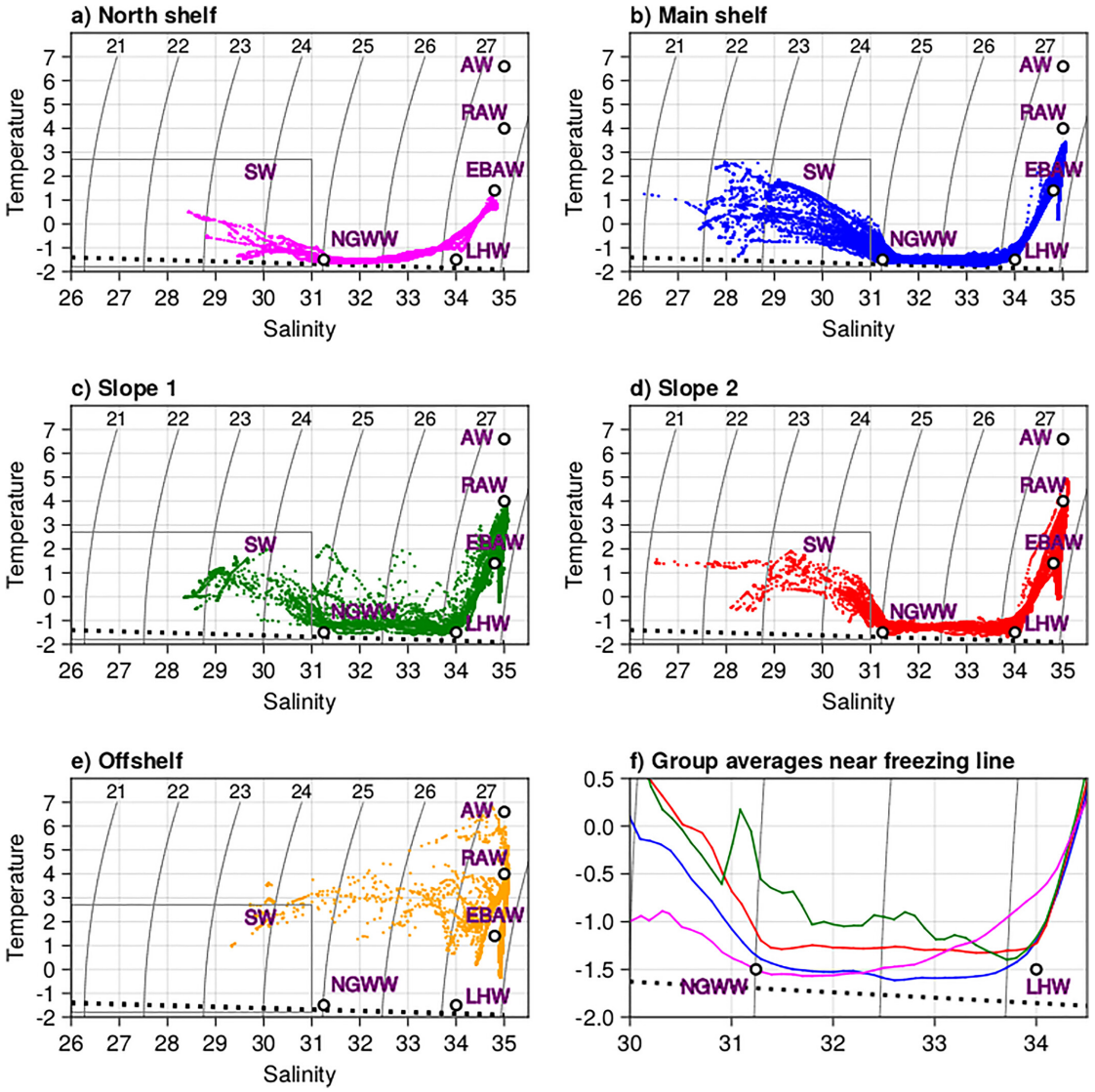

Figure 3.3: Hydrography on the Northeast Greenland shelf from Conductivity Temperature Depth casts. These are the five (a – e) groups which were identified by their shape in the TS diagram per the water types that were present (Table 3.2). Their names were subsequently chosen after they were mapped (Figure 3.5). (f) Closeup of the cold halocline layer where present, for example, all groups except the Offshelf group

d). This group is marked by the absence of AW, RAW, and LHW (Figure 3.3 a), rather showing direct diapycnal mixing between EBAW to the freezing line with which it intersects at a salinity of ~32.5 and at a depth of ~80 m (Figure 3.4 b).

3.6.1.2 Main Shelf Group

Stations in the main shelf group (Figure 3.3b, Figure 3.4a – Figure 3.4d, and Figure 3.5) show both a subsurface halocline and remnant winter mixed layer with an oxygen maximum depth similar to the North shelf group (Figure 3.4 a – Figure 3.4 e). This group is both fresher and warmer than the North shelf group at densities $\sigma T < 25$ above the NGWW. This group contains both LHW and NGWW and the TS data connecting these two water mases follows the freezing point line closely, indicating a well-established cold halocline layer (Figure 3.3b). This is the dominant group in and south of Belgica Trough away from the slope (Figure 3.5).

3.6.1.3 Slope 1 Group

The stations selected to be part of this group (Figure 3.3 c, Figure 3.4 e – Figure 3.4 h, and Figure 3.5) were those which deviated greatly from the freezing line at salinities associated with the cold halocline layer (Figure 3.3c). This is interpreted as evidence of mixing with the warmer Offshelf group. This group contains all defined water types except for AW but it lacks a remnant of the winter mixed layer which differentiates it from North and Main shelf, and Slope 2 groups. Instead, it has a summer halocline which is deeper than that of any other group. The dissolved oxygen saturation relative to the atmosphere is lowest compared to that of the other groups although it is present at the same depths.

3.6.1.4 Slope 2 Group

The profiles in this group (Figure 3.3c, Figure 3.4e – Figure 3.4h, and Figure 3.5) are similar to the Main shelf group profiles, their main difference being that the

Slope 2 TS plot (Figure 3.3c) does not follow the freezing line as closely, being around 0.5°C warmer than main shelf stations on average (Figure 3.3f). This group does have a remnant winter mixed layer, but it is less homogeneous or well-defined than that of the shelf groups, being both deeper and across a larger salinity range.

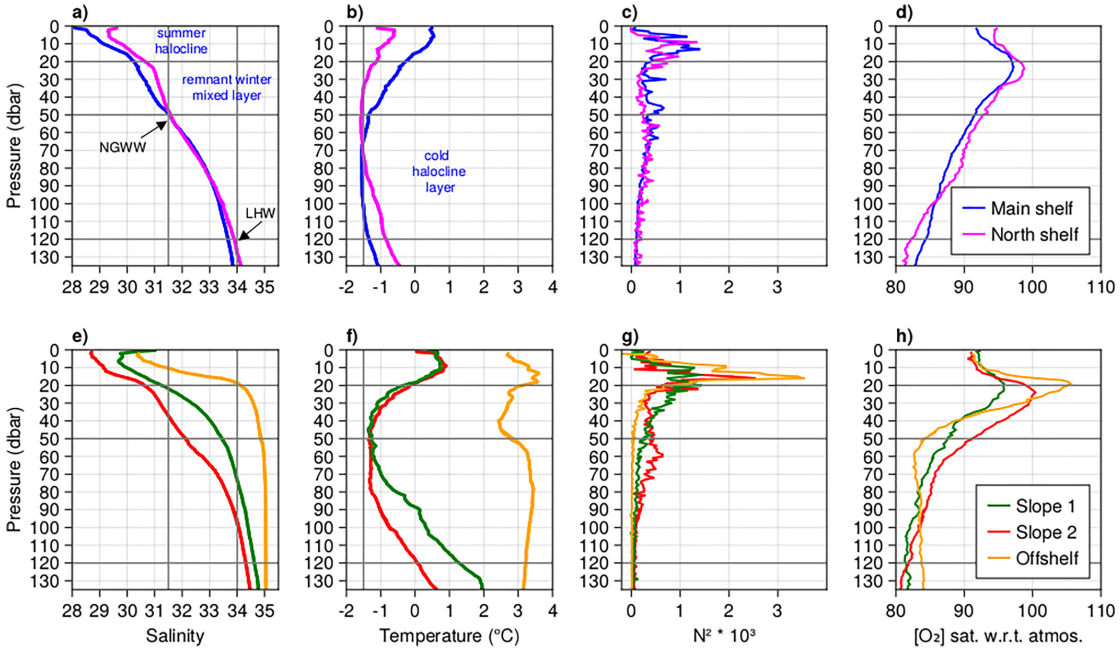

Figure 3.4: Hydrography on the Northeast Greenland shelf from Conductivity Temperature Depth casts. These are the five (a – e) groups which were identified by their shape in the TS diagram per the water types that were present (Table 3.2). Their names were subsequently chosen after they were mapped (Figure 3.5). (f) Closeup of the cold halocline layer where present, for example, all groups except the Offshelf group.

3.6.1.5 Offshelf Group

The Offshelf group (Figure 3.3 – Figure 3.5) is the only group entirely lacking a cold halocline layer that is, the layer between the NGWW and the LHW which follows the freezing point line. Mixing occurs directly between the Atlantic source water (AW, RAW, EBAW) and SW. Average profiles (Figure 3.4e – Figure 3.4h) for this group show a summer halocline with a maximum N^2 at 16 m. The difference in depth between the maximum N^2 and the maximum oxygen saturation is only 3 m for this group, the smallest of all groups and it is the only group with a supersaturation

in dissolved oxygen with respect to the atmosphere. Cooling of up to 1°C occurs between 20 and 50 m (Figure 3.4f). At depths below 50 m temperatures remain just over 3°C while the salinity remains at 35.

3.6.2 Freshwater Sources

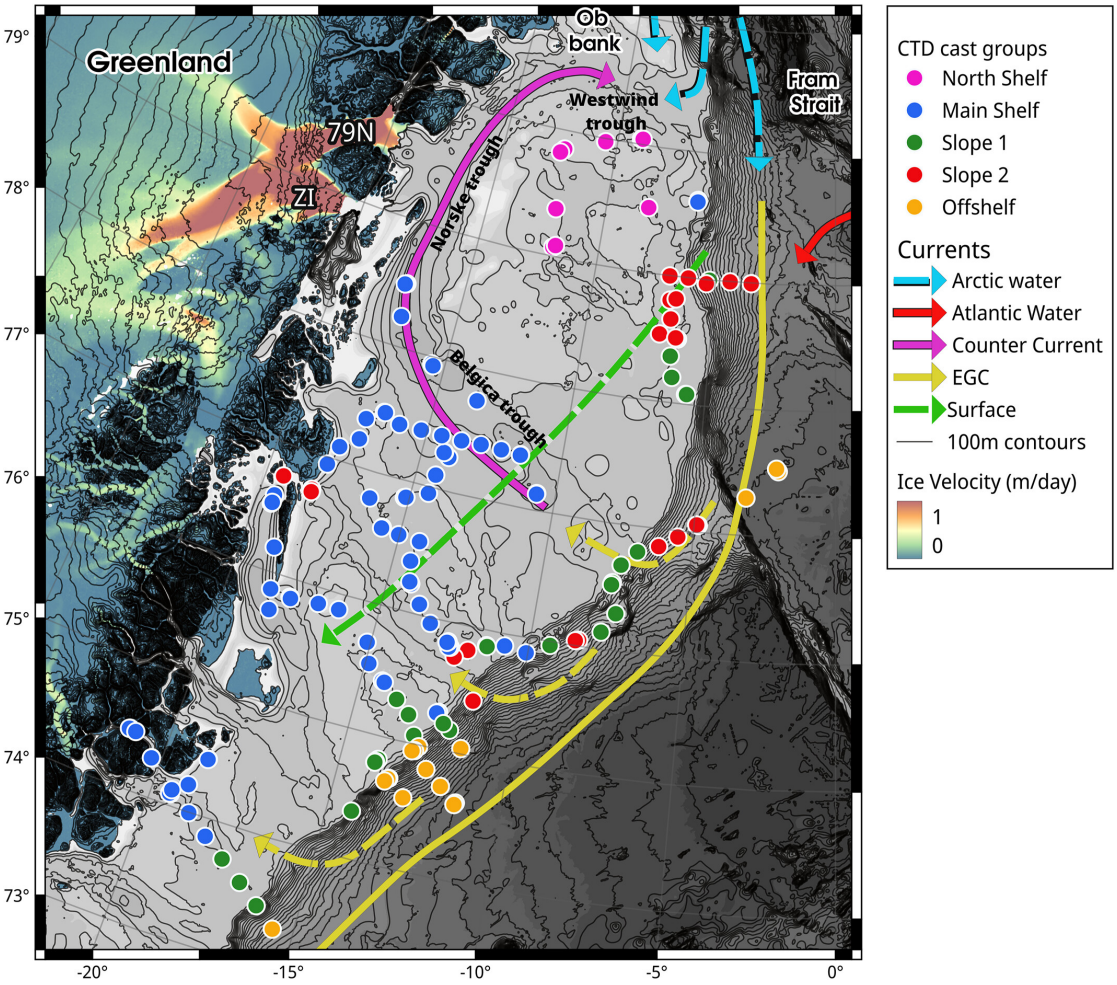

Figure 3.5: Conductivity Temperature Depth group locations plotted in their geographical setting with known and hypothesized currents (currents as described in Figure 3.2. Solid currents are those which have been described in the literature, and dashed currents are hypothesized.

To determine the difference between meteoric and sea ice melt freshwater sources, an assessment was made of the TA and stable water oxygen isotopic ($\delta^{18}O$) composi-

tion variation with salinity (Figure 3.6a and Figure 3.6b). The sea ice melt water lines were obtained from local measurements (Table 3.2). The data is characterized in both plots by two slopes which diverge at a salinity of 31.4, that is, the NGWW. This salinity is also associated with the highest dissolved oxygen saturation with respect to the atmosphere. The presence of this divergence for both tracers in the direction of the sea ice melt end-member indicates a clear increasing sea ice melt influence with decreasing salinity above the NGWW.

In the cold halocline layer between NGWW and LHW, δ^{18}O-S values are found at higher salinities than the regression lines obtained from Cooper et al. (2008) and Namyatov (2021) (Figure 3.6b). This is interpreted as the influence of brine on river discharge modified Atlantic water (Bauch et al., 2011). Distinguishing between different riverine or shelf sources is difficult using these tracers since each of the lines are increasingly close together as they approach the Atlantic water end-member. Although these may be good tracers at lower salinities, closer to their discharge source, they are inappropriate for identifying remote source water on the Northeast Greenland shelf, especially where additional deviation from the mixing line is introduced by brine drainage and sea ice melt. The same is true for the Pacific water end-member, which clearly falls close to several of the mixing lines.

Table 3.2: Water Types and Conductivity Temperature Depth Group Assignment

	Properties		Group characteristics				
			Off-	Main	North	Slope	Slope
	S	θ (°C)	shelf	shelf	shelf	1	2
Atlantic Water (AW)	35						
Return Atlantic Water (RAW)	35			X		X	X
Eurasian Basin Atlantic Water (EBAW)	34.8			X	X	X	X
Lower Halocline Water (LHW)	34.0			X		X	X
Northeast Greenland Winter Water (NGWW)	31.4			X	X		X
Surface Water (SW)	<31.4			X	X	X	X

To distinguish between Pacific and Atlantic source water, we assessed the nitrate

to phosphate ratio (N:P, Figure 3.7a) and the presence of UHW (Figure 3.7b and Figure 3.7c). The N:P for our data follows the Atlantic water regression line (Jones et al., 1998) down to ~6 µmol/kg nitrate. At nitrate concentrations below this, the corresponding phosphate concentrations are relatively constant at around 0.5 µmol/kg, a signal commonly associated with a denitrification signal. This is generally interpreted as denitrification from Pacific water crossing the Chukchi shelf. This interpretation is likely erroneous for our dataset since it compares well to data from the Laptev Sea which expresses a similar pattern (Thibodeau et al., 2017) even though this region does not contain Pacific water. Values of nitrate versus phosphate observed in the eastern versus western East Siberian Sea (Semiletov, 2005) also indicate that Pacific water may not necessarily have the highest influence on this signal in the Siberian Arctic shelf areas. At the lowest and most sea ice melt influenced layers the nitrate is almost entirely depleted with a median dissolved nitrate concentration of 0.0 µmol/kg which limits the usability of this quasi-conservative tracer. Phosphate concentrations are not similarly depleted.

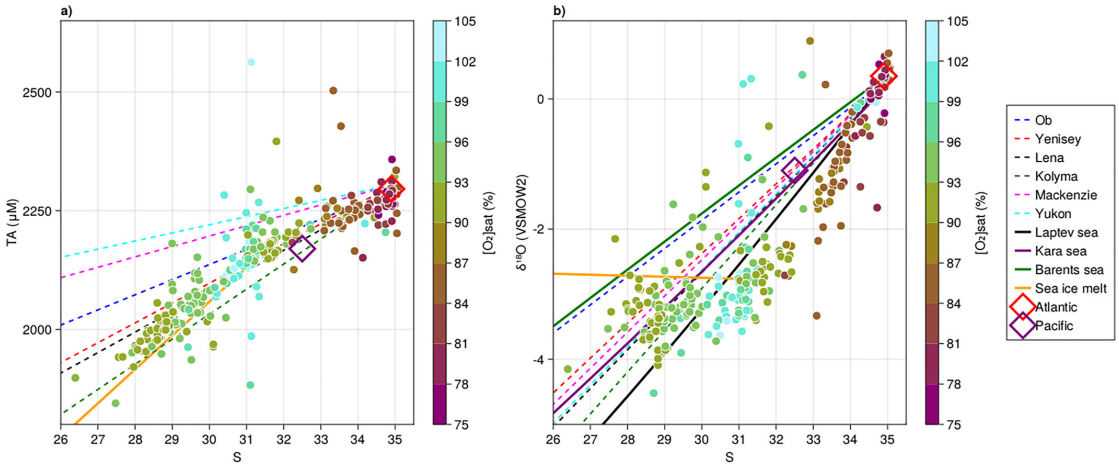

Figure 3.6: Conductivity Temperature Depth bottle data for all depths and geochemical tracers. (a) Total alkalinity (TA) with best fit line sources shown in Table 3.2: For individual rivers from Cooper et al. (2008) and Atlantic and Pacific end members from Sutherland et al. (2009). (b) $\delta^{18}O$ plotted against practical salinity with Eurasian shelf polynomials from Namyatov (2021) and river lines from Yi et al. (2012). Sea ice melt lines were calculated using the average of our measurements (Table 3.2) against a nominal salinity of 4 which was not measured. Note that this is a high salinity value for multiyear ice.

The UHW (Figure 3.7b and Figure 3.7c) is generally associated with a sharp increase in nutrient concentrations, low oxygen concentrations and is present in the Canadian Basin at salinities between 32 and 34 (Nguyen et al., 2012; Anderson et al., 2013). We see no sharp increase in nutrient concentrations at these salinities. We interpret this as the absence of UHW on the Northeast Greenland shelf in late summer 2017.

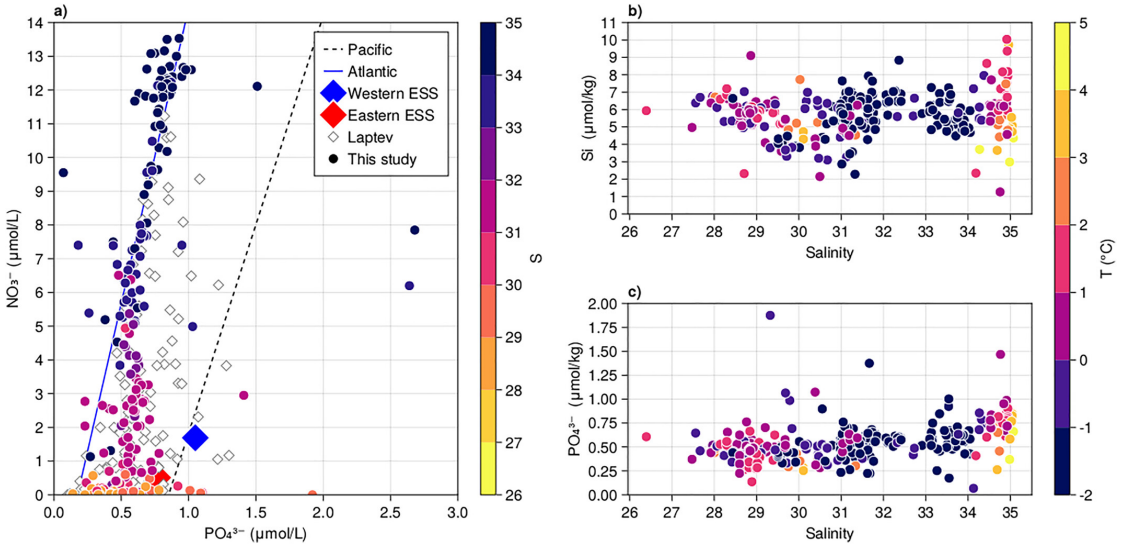

Figure 3.7: Conductivity Temperature Depth bottle data for all depths and geochemical tracers of (a) N:P superimposed on Laptev Sea data from Thibodeau et al. (2017). Pacific (black dashed) and Atlantic (blue solid) regression lines obtained from Jones et al. (1998). Two nutrients which should indicate Upper Halocline Water (UHW) presence as a dramatic increase in concentration at salinities between 32 and 33 (b) Si:S and (c) PO_4^{3-}:S. Neither of these tracers shows this clear.

Values for hydrogen and oxygen stable water isotopes (δ^2H:$\delta^{18}O$) fall between the Arctic Meteoric Water Line (Mellat et al., 2021) and the best fit line for the Lena River (Yi et al., 2012). The AMWL was calculated using terrestrial summer measurements across the Arctic and so does not provide a single source location, rather it is taken as an average across the entire Arctic. Contrary to these, (Yi et al., 2012) created flux weighted average regression lines for each of the 6 major Arctic rivers (Figure 3.8). Due to the proximity of the data to the Lena River line and the distance between the data and any other river we interpret these data as containing a significant volume of Lena River water. At the lowest values of both δ^2H and $\delta^{18}O$ some datapoints approach the GMWL. This may reflect the influence of precipitation. The usability

of this tracer for the purpose of identifying individual rivers will require future verification.

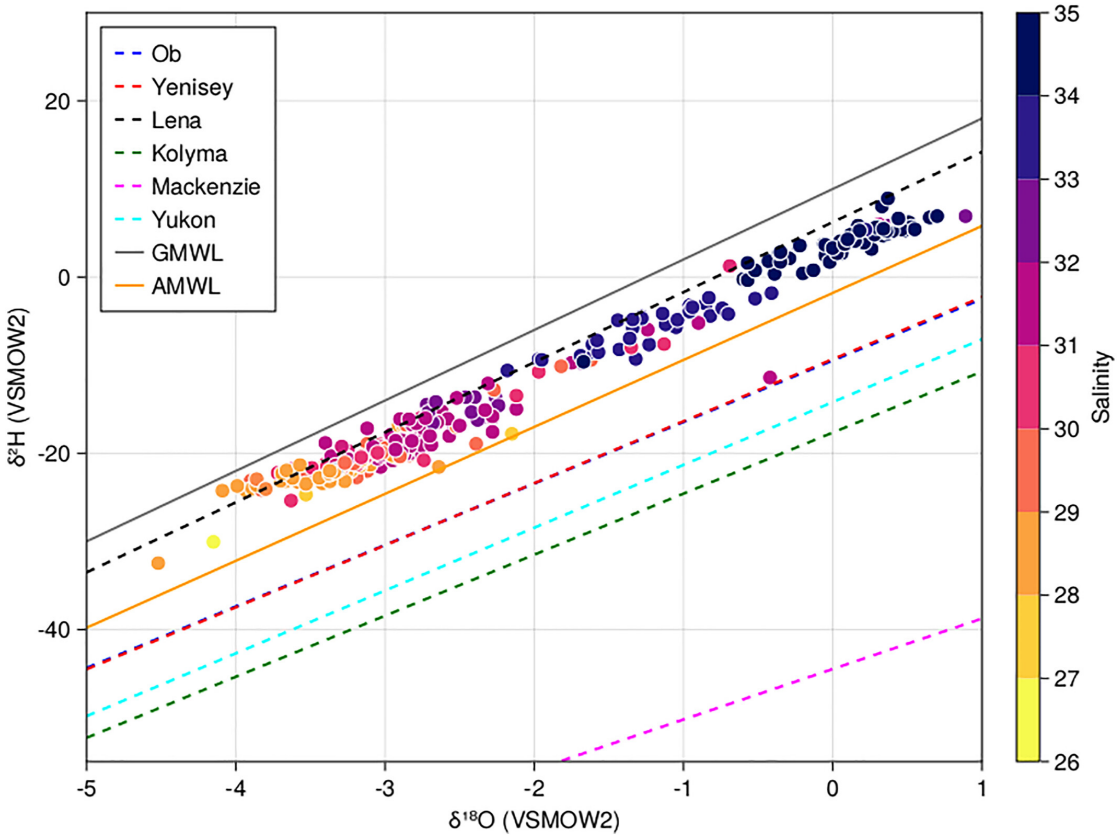

Figure 3.8: Conductivity Temperature Depth bottle data stable water isotopic ratio of deuterium (δ2H) against oxygen (δ^{18}O) from the Northeast Greenland shelf together with meteoric regression lines for each river from Yi et al. (2012) and global (GMWL, Craig, 1961) and Arctic meteoric water lines (AMWL, Mellat et al., 2021). Note that rivers Yenisey and Ob' are indistinguishable from one another in this figure due to overlap.

Neither silicate nor phosphate are conservative tracers as both are utilized by organisms in the water column. It was therefore surprising to find that when these are plotted against apparent oxygen utilization (Figure 3.9), the difference between the oxygen solubility and the dissolved oxygen measured, our data follows the relationship found by Sun et al. (2021) for the Laptev Sea closely. This observation might be produced by two processes: The first is repeated production and remineralization cycles occurring in such a way that this relationship is exactly maintained

during successive seasonal cycles. The second that there is too little water column biological activity during the time taken for water to be advected across the Arctic Ocean to result in an observable change, and the layer is created and maintained solely by seasonal physical processes. The latter is plausible only if either the sea ice cover is extensive and limits photosynthetically active radiation during water transport across the Arctic Ocean or if the nitrate concentrations are limited to a point where primary production is inhibited.

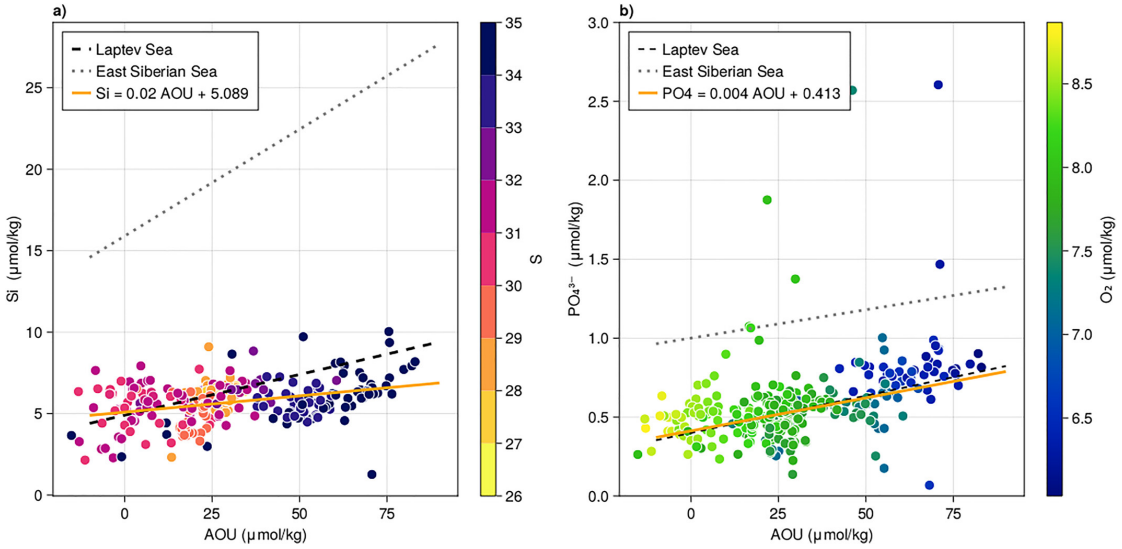

Figure 3.9: Conductivity Temperature Depth bottle data from this study (points) for all depths of non-conservative nutrient (a: silicate; b: phosphate) to apparent oxygen utilization (AOU) with the regression lines for the Laptev and East Siberian Sea (Sun et al., 2021).

3.7 Discussion

The most remarkable hydrographic feature on the Northeast Greenland shelf is the extensive cold halocline layer, which occupies the TS-space along the freezing point line (Figures 3.3, 3.4) between the NGWW and the LHW. The presence or absence of these two water types is geographically correlated (Figure 3.5). This contrasts with the relationship between geochemical tracers and salinity which show a clear change in slope with salinity at the NGWW but has a much smaller or absent signal

for the LHW. Our data best support the hypothesis that the layers above the NGWW, for example, the remnant winter mixed layer, summer halocline and surface water are strongly sea ice melt influenced, where the cold halocline layer is both brine and Lena river discharge influenced.

Although the NGWW is the most prominent feature on the shelf and is interpreted as the maximum depth of winter mixing on the Northeast Greenland shelf, not much can be definitively concluded about its formation. Since the residence time of waters on the shelf is currently unknown, it is difficult to determine whether this water type is solely a product of a local process as suggested in the past (Budéus and Schneider, 1995; Bignami and Hopkins, 1997; Budéus et al., 1997), for example, from multi-annual winter mixing of water trapped in the Northeast Water polynya, or whether it is advected. A significant difference between older studies and ours is that the NGWW is at least 1 salinity unit fresher than it was in the 1990s, while temperatures remain in the same range (our Figures 3.3, 3.4; Bignami and Hopkins (1997) Figure 2). This implies a large increase in freshwater input, which influences the energy requirement for winter mixing to the same depths as during winters with lower volumes of freshwater.

In other parts of the Arctic Ocean, similar remnant winter mixed layers and/or types have been identified such as the Polar Mixed Layer (PML), defined as the depth of the temperature minimum remaining after winter convection in the Canadian Arctic (Peralta-Ferriz and Woodgate, 2015). In the Beaufort Sea, the PML has been identified by its S, TA, and $\delta^{18}O$ properties (Lansard et al., 2012). There, the PML mixes down to the UHW which is not present in our dataset (Figure 3.7) although it may be present north of Ob bank where we have no data as was found by (Budéus et al., 1997). On the Northeast Greenland shelf, the NGWW mixes with the LHW instead. Similar to findings in the Beaufort Sea, the sharp inflection in the TA:S and $\delta^{18}O$:S toward the sea ice melt regression line (Figure 3.6a and Figure 3.6b) imply that water with densities of $\sigma T < 25$ and above the NGWW is strongly influenced by sea ice melt, where water found at $\sigma T > 25$ and below the NGWW, consist primarily of brine-modified river water. This influence by sea ice melt in the surface layer may also be the reason for the dissolved oxygen sub-saturation in the surface mixed layer where atmospheric saturation is otherwise expected. Winter water of this

type is not seen in profiles from the Siberian Arctic (Bourgain and Gascard, 2011; Janout et al., 2017) or in the Eurasian Basin of the Arctic Ocean, including along the Transpolar Drift (Rabe et al., 2022) which means that these are an unlikely source. A similar water type is observed in the Wandel Sea at the deeper depth of 80 m (Dmitrenko et al., 2017). Ob bank is shallow (50 m) and, although absent in 2017, frequently obstructed by an ice barrier which would modify any water advected via this route. We subsequently conclude the water must therefore be advected from the east or be formed locally.

The NGWW is absent only in the Offshelf group where mixing occurs directly between the sea ice influenced surface and the Atlantic influenced water types. This implies that sea ice is melting directly into RAW and there is low to no remote riverine contribution at these CTD station locations. Additionally, the LHW is absent for these stations indicating that this water has not experienced the required conditions for it to be formed, for example, the entrainment of Atlantic water into a low salinity mixed layer and subsequent cooling (Rudels, 2021). This suggests that this is unmodified RAW.

The UHW is absent from our data and based on the N:P ratio the presence of Pacific water is unlikely. Rather, the geochemical tracers indicate that the entire cold halocline layer is composed of Atlantic water which is both diluted by river discharge and influenced by brine extrusion due to sea ice freezing. The TA:S (Figure 3.6a) and δ^{18}O:S (Figure 3.6b) show that the Pacific end-member falls on the mixing lines for the Kolyma (TA:S) and the Yenisey/Mackenzie (δ^{18}O:S) rivers and therefore cannot be used to identify Pacific water or even the primary meteoric river source. This has previously been observed and commented on (Forryan et al., 2019). Care must be taken in the use of non-conservative tracers as is apparent from our N:P analysis. Be that as it may, the nutrients plotted against AOU (Figure 3.9) are surprisingly similar to the regression relationship found for the Laptev Sea, especially near the surface. Far more similar in fact than they are to these ratios for the East Siberian Sea, which is geographically closer to and downstream of the Laptev Sea, does contain Pacific water and may be entrained into the Transpolar drift. We therefore consider AOU plotted against nutrient ratios as tentative but

weak additional evidence against Pacific water presence on the Northeast Greenland shelf in late summer 2017.

The slope of the δ^2H:$\delta^{18}O$ relationships of the six major Arctic rivers are known to be unique to each river (Yi et al., 2012; Table 1). They provide a clue to the provenance of the meteoric water found on the Northeast Greenland shelf (Figure 3.8). The bulk of these data fall between the Lena River regression and the summer Arctic Meteoric Water Line (Mellat et al., 2021) for all salinities. We interpret the proximity of our data to the Lena River line from Yi et al. (2012) on the δ^2H:$\delta^{18}O$ diagram as evidence of the presence of a detectable volume of Lena river water on the Northeast Greenland shelf. Some of the lowest isotopic values δ-values tend more toward the Global Meteoric Water Line. These datapoints have the lowest salinities. Discussing the deuterium excess is beyond the scope of this paper, however we tentatively suggest this is due to the increased influence of precipitation in the fresher water on the shelf.

Although more data is required to verify the connection, our data imply that a large fraction of the meteoric water on the Northeast Greenland shelf during August – September 2017 has its origin in the Laptev Sea and ultimately in the Lena River catchment area. This is in line with previous suggestions of a connection between Siberian rivers and freshwater provenance in Fram Strait (Dodd et al., 2012; Granskog et al., 2012) shown by isotopic and organic matter fluorescence tracing. Furthermore, the layer above the maximum winter mixed layer depth, the NGWW, is significantly influenced by sea ice melt and much fresher than it was in previous decades.

3.8 Conclusions

Our data suggest a complex hydrography for the Northeast Greenland shelf, with much of the freshwater contained at depths below the maximum winter mixed layer depth (NGWW) having its source in the Laptev Sea region of the Siberian

Arctic. From there it is transported to Fram Strait by the Transpolar Drift and subsequentially advected onto the shelf. The freshwater shows a geochemical signature typical of that area, mixing along a line from brine-enhanced river discharge to Atlantic water. The Northeast Greenland Shelf lacks both Pacific water and UHW biogeochemical signatures in late summer 2017.

The NGWW is interpreted as the remnant of the previous seasons maximum winter mixed layer depth due to similarities with such winter mixed layer remnants elsewhere in the Arctic. The unique high oxygen saturation in the upper part of the remnant winter mixed layer may be partially associated with export during freezing but more data is required to verify this since it may also result from primary productivity. This layer is much fresher now than it was two decades ago, which is evidence of climate-change induced Arctic freshening. The SW above the NGWW is strongly influenced by sea ice melt, which imposes its geochemical signature in TA and $\delta^{18}O$ and possibly in the relatively low surface dissolved oxygen saturation.

The supply of freshwater to the Northeast Greenland shelf will likely increase in the following decades due to increases in discharge from the Siberian rivers and the Greenland Ice Sheet, and sea ice melt. If the Atlantic inflow continues to warm and return Atlantic flow remains available along the slope, the difference between on- and off-shelf water masses will increase. Mixing processes along the slope and LHW erosion may be enhanced consequently.

References

Alkire MB, Rember R, Polyakov I. 2021. The Pacific-Atlantic Front in the East Siberian Sea of the Arctic Ocean. In: Belkin IM, editor. *Chemical Oceanography of Frontal Zones*. Berlin, Heidelberg: Springer Berlin Heidelberg. p. 63 – 94. doi: 10.1007/698_2021_795

Anderson LG, Andersson PS, Björk G, Peter Jones E, Jutterström S, Wåhlström I. 2013. Source and formation of the upper halocline of the Arctic Ocean. *Journal of*

Geophysical Research: Oceans **118**(1): 410 – 421. doi: 10.1029/2012JC008291

Arndt JE, Jokat W, Dorschel B, Myklebust R, Dowdeswell JA, Evans J. 2015. A new bathymetry of the Northeast Greenland continental shelf: Constraints on glacial and other processes. *Geochemistry, Geophysics, Geosystems* **16**(10): 3733 – 3753. doi: 10.1002/2015gc005931

Bauch D, Dmitrenko IA, Wegner C, Hölemann J, Kirillov SA, Timokhov LA, Kassens H. 2009. Exchange of Laptev Sea and Arctic Ocean halocline waters in response to atmospheric forcing. *Journal of Geophysical Research* **114**(C5): C05008. doi: 10.1029/2008jc005062

Bauch D, van der Loeff MR, Andersen N, Torres-Valdes S, Bakker K, Abrahamsen EP. 2011. Origin of freshwater and polynya water in the Arctic Ocean halocline in summer 2007. *Progress in Oceanography* **91**(4): 482 – 495. doi: 10.1016/j.pocean.2011.07.017

Bezanson J, Edelman A, Karpinski S, Shah VB. 2017. Julia: A Fresh Approach to Numerical Computing. *SIAM Review* **59**(1): 65 – 98. doi: 10.1137/141000671

Bignami F, Hopkins TS. 1997. The water mass characteristics of the Northeast Water Polynya: Polar Sea data 1992 – 1993. *Journal of Marine Systems* **10**(1-4): 139 – 156. doi: 10.1016/S0924-7963(96)00079-6

Bourgain P, Gascard JC. 2011. The Arctic Ocean halocline and its interannual variability from 1997 to 2008. *Deep Sea Research Part I: Oceanographic Research Papers* **58**(7): 745 – 756. doi: 10.1016/j.dsr.2011.05.001

Budéus G, Schneider W. 1995. On the hydrography of the Northeast Water Polynya. *Journal of Geophysical Research* **100**(C3): 4287. doi: 10.1029/94jc02024

Budéus G, Schneider W, Kattner G. 1997. Distribution and exchange of water masses in the Northeast Water polynya (Greenland Sea). *Journal of Marine Systems*

10(1): 123 – 138. doi: 10.1016/s0924-7963(96)00074-7

Charette MA, Kipp LE, Jensen LT, Dabrowski JS, Whitmore LM, Fitzsimmons JN, Williford T, Ulfsbo A, Jones E, Bundy RM, et al. 2020. The Transpolar Drift as a Source of Riverine and Shelf-Derived Trace Elements to the Central Arctic Ocean. *Journal of Geophysical Research: Oceans* **125**(5). doi: 10.1029/2019JC015920

Codispoti LA, Friederich GE, Sakamoto CM, Gordon LI. 1991. Nutrient cycling and primary production in the marine systems of the Arctic and Antarctic. *Journal of Marine Systems* **2**(3-4): 359 – 384. doi: 10.1016/0924-7963(91)90042-S

Cooper LW, Cota GF, Pomeroy LR, Grebmeier JM, Whitledge TE. 1999. Modification of NO, PO, and NO/PO during flow across the Bering and Chukchi shelves: Implications for use as Arctic water mass tracers. *Journal of Geophysical Research: Oceans* **104**(C4): 7827 – 7836. doi: 10.1029/1999JC900010

Cooper LW, McClelland JW, Holmes RM, Raymond PA, Gibson JJ, Guay CK, Peterson BJ. 2008. Flow-weighted values of runoff tracers (d18O, DOC, Ba, alkalinity) from the six largest Arctic rivers. *Geophysical Research Letters* **35**(18): L18606. doi: 10.1029/2008gl035007

Craig H. 1961. Isotopic Variations in Meteoric Waters. *Science* **133**(3465): 1702 – 1703. American Association for the Advancement of Science. doi: 10.1126/science.133.3465.1702

Dmitrenko IA, Kirillov SA, Rudels B, Babb DG, Pedersen LT, Rysgaard S, Kristoffersen Y, Barber DG. 2017. Arctic Ocean outflow and glacier – ocean interactions modify water over the Wandel Sea shelf (northeastern Greenland). *Ocean Science* **13**(6): 1045 – 1060. doi: 10.5194/os-13-1045-2017

Dodd PA, Rabe B, Hansen E, Falck E, Mackensen A, Rohling E, Stedmon C, Kristiansen S. 2012. The freshwater composition of the Fram Strait outflow derived from a decade of tracer measurements: COMPOSITION OF THE FRAM STRAIT

OUTFLOW. *Journal of Geophysical Research: Oceans* **117**(C11): n/a – n/a. doi: 10.1029/2012JC008011

Falck E. 2001. Contribution of waters of Atlantic and Pacific origin in the Northeast Water Polynya. *Polar Research* **20**(2): 193 – 200. doi: 10.3402/polar.v20i2.6517

Falck E, Kattner G, Budéus G. 2005. Disappearance of Pacific Water in the northwestern Fram Strait: DISAPPEARANCE OF PACIFIC WATER. *Geophysical Research Letters* **32**(14). doi: 10.1029/2005gl023400

Feistel R. 2012. TEOS-10: A New International Oceanographic Standard for Seawater, Ice, Fluid Water, and Humid Air. *International Journal of Thermophysics* **33**(8-9): 1335 – 1351. doi: 10.1007/s10765-010-0901-y

Foldvik A, Aagaard K, Tørresen T. 1988. On the velocity field of the East Greenland Current. *Deep Sea Research Part A Oceanographic Research Papers* **35**(8): 1335 – 1354. doi: 10.1016/0198-0149(88)90086-6

Forryan A, Bacon S, Tsubouchi T, Torres-Valdés S, Naveira Garabato AC. 2019. Arctic freshwater fluxes: Sources, tracer budgets and inconsistencies. *The Cryosphere* **13**(8): 2111 – 2131. doi: 10.5194/tc-13-2111-2019

Gran G. 1952. Determination of the Equivalence Point in Potentiometric Titrations. Part 11. *Analyst* **77**: 11. doi: 10.1039/an9527700661

Granskog MA, Stedmon CA, Dodd PA, Amon RMW, Pavlov AK, de Steur L, Hansen E. 2012. Characteristics of colored dissolved organic matter (CDOM) in the Arctic outflow in the Fram Strait: Assessing the changes and fate of terrigenous CDOM in the Arctic Ocean: CDOM DYNAMICS IN ARCTIC OCEAN. *Journal of Geophysical Research: Oceans* **117**(C12): n/a – n/a. doi: 10.1029/2012jc008075

Haine TWN, Curry B, Gerdes R, Hansen E, Karcher M, Lee C, Rudels B, Spreen G, de Steur L, Stewart KD, et al. 2015. Arctic freshwater export: Status, mechanisms,

and prospects. *Global and Planetary Change* **125**: 13 – 35. doi: 10.1016/j.gloplacha.2014.11.013

Huhn O, Rhein M, Kanzow T, Schaffer J, Sültenfuß J. 2021. Submarine Meltwater From Nioghalvfjerdsbræ (79 North Glacier), Northeast Greenland. *Journal of Geophysical Research: Oceans* **126**(7). doi: 10.1029/2021JC017224

Jakobsson M, Mayer LA, Bringensparr C, Castro CF, Mohammad R, Johnson P, Ketter T, Accettella D, Amblas D, An L, et al. 2020. The International Bathymetric Chart of the Arctic Ocean Version 4.0. *Scientific Data* **7**(1): 176. doi: 10.1038/s41597-020-0520-9

Janout MA, Hölemann J, Timokhov L, Gutjahr O, Heinemann G. 2017. Circulation in the northwest Laptev Sea in the eastern Arctic Ocean: Crossroads between Siberian River water, Atlantic water and polynya-formed dense water. *Journal of Geophysical Research: Oceans* **122**(8): 6630 – 6647. doi: 10.1002/2017jc013159

Jones EP, Anderson LG. 1986. On the origin of the chemical properties of the Arctic Ocean halocline. *Journal of Geophysical Research: Oceans* **91**(C9): 10759 – 10767. doi: 10.1029/JC091iC09p10759

Jones EP, Anderson LG, Jutterström S, Swift JH. 2008. Sources and distribution of fresh water in the East Greenland Current. *Progress in Oceanography* **78**(1): 37 – 44. doi: 10.1016/j.pocean.2007.06.003

Jones EP, Anderson LG, Swift JH. 1998. Distribution of Atlantic and Pacific waters in the upper Arctic Ocean: Implications for circulation. *Geophysical Research Letters* **25**(6): 765 – 768. doi: 10.1029/98gl00464

Jones EP, Anderson LG, Wallace DWR. 1991. Tracers of near-surface, halocline and deep waters in the Arctic ocean: Implications for circulation. *Journal of Marine Systems* **2**(1-2): 241 – 255. doi: 10.1016/0924-7963(91)90027-R

Kikuchi T. 2004. Distribution of convective Lower Halocline Water in the eastern Arctic Ocean. *Journal of Geophysical Research* **109**(C12): C12030. doi: 10.1029/2003JC002223

Lansard B, Mucci A, Miller LA, Macdonald RW, Gratton Y. 2012. Seasonal variability of water mass distribution in the southeastern Beaufort Sea determined by total alkalinity and δ ^{18} O: WATER MASSES IN THE BEAUFORT SEA. *Journal of Geophysical Research: Oceans* **117**(C3): n/a – n/a. doi: 10.1029/2011JC007299

Lin G, Lin M, Qiao J, Sejr MK, Steier P, Meire L, Stedmon CA. 2022. Estimation of Atlantic Water transit times in East Greenland fjords using a 233U-236U tracer approach. *Chemical Geology* **607**: 121007. doi: 10.1016/j.chemgeo.2022.121007

Mellat M, Bailey H, Mustonen K-R, Marttila H, Klein ES, Gribanov K, Bret-Harte MS, Chupakov AV, Divine DV, Else B, et al. 2021. Hydroclimatic Controls on the Isotopic (δ18 O, δ2 H, d-excess) Traits of Pan-Arctic Summer Rainfall Events. *Frontiers in Earth Science* **9**: 651731. doi: 10.3389/feart.2021.651731

Moon TA, Gardner AS, Csatho B, Parmuzin I, Fahnestock MA. 2020. Rapid Reconfiguration of the Greenland Ice Sheet Coastal Margin. *Journal of Geophysical Research: Earth Surface* **125**(11). doi: 10.1029/2020jf005585

Namyatov AA. 2021. δO as a tracer of the main regularities of water mass mixing and transformation in the Barents, Kara, and Laptev seas. *Journal of Hydrology* **593**: 125813. doi: 10.1016/j.jhydrol.2020.125813

Nguyen AT, Kwok R, Menemenlis D. 2012. Source and Pathway of the Western Arctic Upper Halocline in a Data-Constrained Coupled Ocean and Sea Ice Model. *Journal of Physical Oceanography* **42**(5): 802 – 823. doi: 10.1175/JPO-D-11-040.1

Nitishinsky M, Anderson LG, Hölemann JA. 2007. Inorganic carbon and nutrient fluxes on the Arctic Shelf. *Continental Shelf Research* **27**(10-11): 1584 – 1599. doi: 10.1016/j.csr.2007.01.019

O' Neil JR. 1968. Hydrogen and oxygen isotope fractionation between ice and water. *The Journal of Physical Chemistry* **72**(10): 3683 – 3684. doi: 10.1021/j100856a060

Osadchiev AA, Pisareva MN, Spivak EA, Shchuka SA, Semiletov IP. 2020. Freshwater transport between the Kara, Laptev, and East-Siberian seas. *Scientific Reports* **10**(1): 13041. doi: 10.1038/s41598-020-70096-w

Paffrath R, Laukert G, Bauch D, Rutgers van der Loeff M, Pahnke K. 2021. Separating individual contributions of major Siberian rivers in the Transpolar Drift of the Arctic Ocean. *Scientific Reports* **11**(1): 8216. doi: 10.1038/s41598-021-86948-y

Peralta-Ferriz C, Woodgate RA. 2015. Seasonal and interannual variability of pan-Arctic surface mixed layer properties from 1979 to 2012 from hydrographic data, and the dominance of stratification for multiyear mixed layer depth shoaling. *Progress in Oceanography* **134**: 19 – 53. doi: 10.1016/j.pocean.2014.12.005

QGIS Development Team. 2022. *QGIS Geographic Information System*. QGIS Association.

Rabe B, Heuzé C, Regnery J, Aksenov Y, Allerholt J, Athanase M, Bai Y, Basque C, Bauch D, Baumann TM, et al. 2022. Overview of the MOSAiC expedition: Physical oceanography. *Elementa: Science of the Anthropocene* **10**(1): 00062. doi: 10.1525/elementa.2021.00062

Rudels B. 2021. *The Physical Oceanography of the Arctic Mediterranean Sea: Explorations, Observations, Interpretations*. Amsterdam, Netherlands: Elsevier.

Rudels B, Jones EP, Schauer U, Eriksson P. 2004. Atlantic sources of the Arctic Ocean surface and halocline waters. *Polar Research* **23**(2): 181 – 208. doi: 10.3402/polar.v23i2.6278

Rysgaard S, Glud RN, Sejr MK, Bendtsen J, Christensen PB. 2007. Inorganic carbon

transport during sea ice growth and decay: A carbon pump in polar seas. *Journal of Geophysical Research* **112**(C3): C03016. doi: 10.1029/2006JC003572

Schauer U, Rudels B, Jones EP, Anderson LG, Muench RD, Björk G, Swift JH, Ivanov V, Larsson A-M. 2002. Confluence and redistribution of Atlantic water in the Nansen, Amundsen and Makarov basins. *Annales Geophysicae* **20**(2): 257 – 273. Copernicus GmbH. doi: 10.5194/angeo-20-257-2002

Semiletov I. 2005. The East Siberian Sea as a transition zone between Pacific-derived waters and Arctic shelf waters. *Geophysical Research Letters* **32**(10): L10614. doi: 10.1029/2005GL022490

Smith IV DC, Morison JH. 1998. Nonhydrostatic haline convection under leads in sea ice. *Journal of Geophysical Research: Oceans* **103**(C2): 3233 – 3247. doi: 10.1029/97JC02262

Smith WO, Barber DG, editors. 2007. *Polynyas: Windows to the World*. Amsterdam ; Boston: Elsevier. (Elsevier oceanography series; Vol. 74).

Sneed WA, Hamilton GS. 2016. Recent changes in the Norske Øer Ice Barrier, coastal Northeast Greenland. *Annals of Glaciology* **57**(73): 47 – 55. doi: 10.1017/aog.2016.21

Sun X, Humborg C, Mörth C-M, Brüchert V. 2021. The Importance of Benthic Nutrient Fluxes in Supporting Primary Production in the Laptev and East Siberian Shelf Seas. *Global Biogeochemical Cycles* **35**(7). doi: 10.1029/2020GB006849

Sutherland DA, Pickart RS, Peter Jones E, Azetsu-Scott K, Jane Eert A, Ólafsson J. 2009. Freshwater composition of the waters off southeast Greenland and their link to the Arctic Ocean. *Journal of Geophysical Research* **114**(C5): C05020. doi: 10.1029/2008JC004808

Tanaka T, Guo L, Deal C, Tanaka N, Whitledge T, Murata A. 2004. N deficiency in

a well-oxygenated cold bottom water over the Bering Sea shelf: Influence of sedimentary denitrification. *Continental Shelf Research* **24**(12): 1271 – 1283. doi: 10.1016/j.csr.2004.04.004

Thibodeau B, Bauch D, Voss M. 2017. Nitrogen dynamic in Eurasian coastal Arctic ecosystem: Insight from nitrogen isotope: Nitrogen Cycle Over Arctic Shelves. *Global Biogeochemical Cycles* **31**(5): 836 – 849. doi: 10.1002/2016gb005593

Yamamoto-Kawai M, McLaughlin FA, Carmack EC, Nishino S, Shimada K. 2008. Freshwater budget of the Canada Basin, Arctic Ocean, from salinity, δ^{18}O, and nutrients. *Journal of Geophysical Research* **113**(C1): C01007. doi: 10.1029/2006jc003858

Yi Y, Gibson JJ, Cooper LW, Hélie J-F, Birks SJ, McClelland JW, Holmes RM, Peterson BJ. 2012. Isotopic signals (18O, 2H, 3H) of six major rivers draining the pan-Arctic watershed. *Global Biogeochemical Cycles* **26**(1). doi: 10.1029/2011gb004159

4 The Northeast Greenland Shelf as a potential late-summer CO_2 source to the atmosphere

Co-authors: Marcos Lemes, Thomas Juul-Pedersen, Mikael Kristian Sejr, Johnna Marchiano Holding, and Søren Rysgaard

DOI: https://doi.org/10.5194/bg-21-4037-2024

4.1 Abstract

The Northeast Greenland shelf is a region currently considered to be an annual net sink of carbon dioxide (CO_2) from the atmosphere. Water from the Northeast Greenland shelf is advected to the formation regions of North Atlantic Deep Water and therefore any carbon uptake may be stored for ocean thermohaline circulation timescales. We present the most extensive study of carbon chemistry on the Northeast Greenland shelf to date made possible by opportunistic sampling due to a sudden decrease in sea ice concentration in late August and September 2017. These are the first full-depth measurements of total alkalinity and dissolved inorganic carbon at latitudes between 75 and 79°N with additional data collected in the region of the Northeast Water Polynya and outside Young Sund. We find that surface mixed layer concentrations are variable and for many stations higher than the interpolated atmospheric concentration for the region during the sampling period. Below the

surface mixed layer, CO_2 concentrations increase linearly with decreasing apparent oxygen utilisation. The mixed layer deepens during the study period which is associated with apparent changes in CO_2 uptake. The Northeast Greenland shelf is a hydrologically complex region with many processes influencing the carbonate system at smaller scales than our sampling density. The scatter in the dataset are more than mere outliers and their lack of relationship to any measured variable indicates a strong influence of currently undescribed process(es) or variable(s) at the sampled scales. These data were collected during a time of radically low sea ice concentrations for the region and may be an indication of future conditions. Since they indicate the potential of the region to act as a seasonal source of CO_2 to the atmosphere this may modify our current estimate of the region as a strong annual net sink relatively protected from the immediate influence of atmospheric warming and climate change.

4.2 Introduction

The Arctic Ocean and adjecent continental shelves are changing rapidly under the influence of climate change (Serreze and Barry, 2011; Richter-Menge et al., 2017; Overland et al., 2019; Stroh et al., 2019). The Northeast Greenland shelf is an Arctic outflow shelf (Carmack and Wassmann, 2006; Michel et al., 2015) and one of the two gateways (the other the Canadian Arctic Archipelago) through which water from the Arctic Ocean is transported southward into the North Atlantic Ocean (Hunt et al., 2016). Together with the along-slope East Greenland Current (EGC), the shelf acts as a gateway through which water from the Arctic Ocean can be advected to the Greenland Sea, the Irminger Sea, and the Labrador Sea, regions that are crucial to the Atlantic Meridional Overturning Circulation through the formation of intermediate and deep water masses (Smethie and Fine, 2001) This means that any carbon stored in the region may be retained in the global oceans on the timescales of the thermohaline circulation (Broecker, 1997; Farmer et al., 2019). The consensus is that the Northeast Greenland shelf has been a net annual carbon sink like other Arctic shelf regions, though this appears to be changing in response to changing conditions. The initial determination of the region as a sink was made through

interpolation studies (Takahashi et al., 2014), Self Organising Maps (SOM, Yasunaka et al. (2018)), and temporally and/or spatially limited observations using various methods, most focused on the Northeast Water Polynya or the near-coastal regions and fjords (Yager et al., 1995; Nakaoka et al., 2006; Sejr et al., 2011; Bakker et al., 2023). Recent studies have indicated the potential for the region to become corrosive in terms of aragonite saturation (Fransson et al., 2023) and highlight the difference between the carbon system on the eastern side of Greenland versus the west in terms of the relationship between carbon chemistry and depth (Henson et al., 2023; Henson et al., 2024). The latter is far more pronounced in western than eastern shelf areas and may be related to differences in their respective hydrography. Higher benthic production nearer to the shelf edge may be indicative of stronger primary productivity in this area, though the shelf is considered to be oligotrophic and the previously strong benthic-pelagic coupling in the region may be weakening (Bodur et al., 2024). Due to high sea ice cover during all seasons the shelf is challenging to access, making it difficult to consistently measure all the parameters required to determine the conditions and processes influencing dissolved CO_2 concentrations. The northern North Atlantic and the Greenland Sea are more accessible and studies in these regions receiving water from the Northeast Greenland shelf and EGC (e.g. Olsen et al. (2008), Olafsson et al. (2021)) show that waters sourced from the Arctic remain undersaturated in dissolved CO_2 while Atlantic waters can act as a weak seasonal source. Water from the North Atlantic that might be entrained into the EGC also tends to be undersaturated (Jones et al., 2021; Ericson et al., 2023), but has rapidly increasing concentrations, particularly in Autumn below latitudes of 78 °N when concentrations are at or near that of the atmosphere.

The uptake of CO_2 gas from the atmosphere in the northern North Atlantic (>50 °N) is partially driven by the cooling of warm water at the surface during northward transport which increases gas solubility, including CO_2. High stratification and primary productivity in summer combined with deep convective mixing in winter enable the exposure of a more water to the atmosphere which further facilitates uptake. The Arctic Ocean carbon system is less well understood due to low (spatial and temporal) sampling densities though the Eurasian Basin uptake of anthropogenic CO_2 is thought to be increasing (Rajasakaren et al., 2019). There are also additional

processes at play in northern latitudes that influence CO_2 gas exchange, affecting both the solubility and biological pumps in the region such as the sea ice related processes of brine expulsion and sea ice melting, and the input of 10-11% of global meteoric river water (Shiklomanov et al., 2021). Each of these is characterised by their seasonality (Bates et al., 2009; von Appen et al., 2021). The Atlantic Water being transported north into the Arctic (and into the EGC as part of the return Atlantic Current) is much warmer than it was in previous decades (Polyakov et al., 2017). This increase in heat has been associated with changes in the Arctic halocline which shields sea ice from melting from below (Polyakov et al., 2020) and is likely to also stimulate heating in the EGC and potentially the Northeast Greenland shelf where the warm surface water from the return Atlantic Current (RAC) comes in direct contact with sea ice advected from the Arctic Ocean. Since the RAC is a surface current this energy is directly available for the melting of ice (icebergs, melange, and sea ice). While the melting of melange and icebergs merely reduces the temperature and freshen the surface water, changing the gas solubility, melting sea ice can release ikaite ($CaCO_3 \cdot 6H_2O$) which facilitates additional CO_2 gas dissolution (Rysgaard et al., 2009). Reduced sea ice cover is thought to facilitate primary productivity through enhanced availability of light, providing nutrients are also available (Bates et al., 2009) and rates of net primary productivity are thought to be increasing (Arrigo and van Dijken, 2015) even in the face of increasing stratification and the associated nutrient limitation von Appen et al. (2021). The Arctic Ocean surface waters are nutrient limited (Tuerena et al., 2022) and the regions of extreme nitrate limitation are expanding, though primarily in the Western Arctic (Zhuang et al., 2021; Zhuang et al., 2022). As a result of surface water nutrient limitation primary producers are generally found under sea ice (Ardyna et al., 2020), in the sea ice marginal zone, particular where there is upwelling (Mundy et al., 2009), or as a 'deep chlorophyll maximum' (DCM) below the nitrogen depleted surface layer ((Martin et al., 2013) and references therein). Since the DCM is not directly in contact with the atmosphere the uptake by primary producers is not directly associated with drawdown from the atmosphere unless the strong stratification is broken and has a chance to equilibrate prior to sea ice freeze up. This equilibration needs to occur before the produced organic carbon is remineralised and before sea ice cover is extensive enough to form a barrier between ocean and atmosphere.

This dominance of DCM may be a recent development. During the 1990s, primary productivity on the northern Northeast Greenland shelf was found near the surface in the Northeast Water Polynya and the required nutrients were associated with water from beneath the landfast and glacial ice (Wallace, Behrens, et al., 1995). This led to the development of the 'seasonal rectification hypothesis' which describes strong uptake of atmospheric CO_2 during the sea ice melt season by primary producers followed by a season of inhibited autumn CO_2 release to the atmosphere by the development of an extensive sea ice cover (Yager et al., 1995). Since then, the open water fraction in the region has changed dramatically as has the temperature of the Arctic river influenced Polar Water layer (De Steur et al., 2023). In the summer of 2017 the Northeast Greenland shelf experienced a sudden drop in sea ice cover starting in August 2017 initiating a previously unseen decline in Arctic Ocean sea ice export which persisted throughout 2018 (Sumata et al., 2022). These ice-free conditions allowed unprecedented access to previously unstudied parts of the Northeast Greenland shelf (Figure 4.1 a). The observations for this study were made opportunistically in these suddenly ice-free waters and may offer some insight into the response of the CO_2 system on the Northeast Greenland shelf to an increasingly warm and ice-free Arctic.

4.3 Materials & methods

4.3.1 Cruise & hydrographical setting

Data for this study was collected during two cruises (DANA2017 and NEGREEN2017). The hydrography of the Northeast Greenland shelf during these cruises was described in our previous paper (Willcox et al., 2023). To summarize briefly, several water types were found to be superimposed on much of the shelf albeit in different ways in different geographical areas. The hydrography is dominated by freshwater from various Arctic Ocean sources with different total alkalinity (Figure 4.1 a) down to the depths of the Eurasian Basin Atlantic Water (EBAW) and Return Atlantic Water (RAW) which have similar practical salinities of respectively 34.8 and 35. The

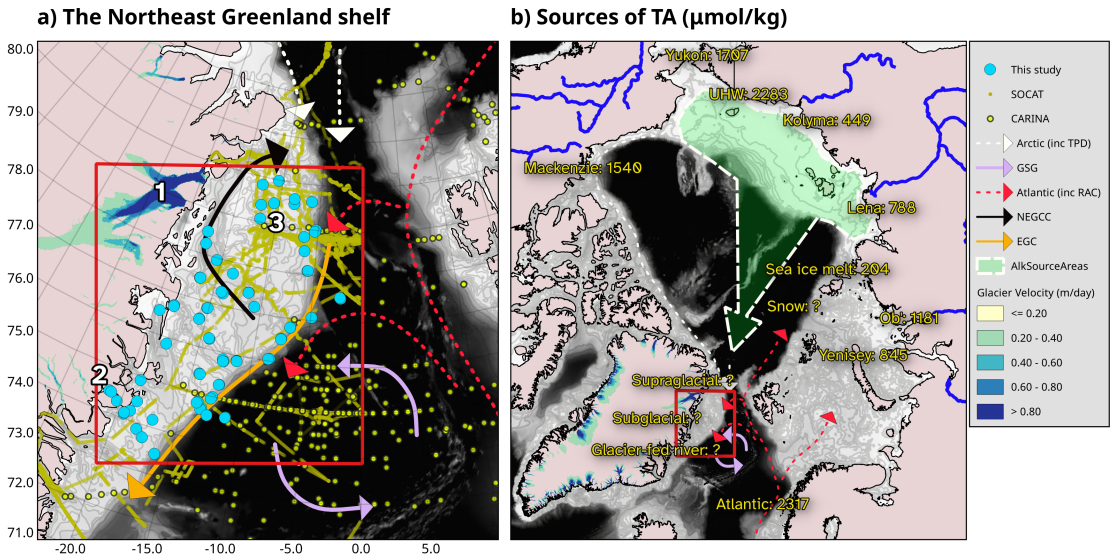

Figure 4.1: (a) Overview of carbon system chemistry and CO_2 fugacity (fCO_2) samples on the Northeast Greenland shelf. Arrows indicate known major currents. White indicates the advection of Arctic sourced water including Polar Surface Water (PSW) and Eurasian Basin or Arctic Atlantic Water (EBAW/AAW). Red arrows indicate Atlantic sourced water, including Return Atlantic Water (RAW) which is transported by the Return Atlantic Current (RAC) from the east side of Fram Strait towards Northeast Greenland. Black is the Northeast Greenland Counter current (NEGCC) which transports water west then northward in a counterclockwise direction directly past the coast, purple is the Greenland Gyre, and orange is the East Greenland Current (EGC) which roughly follows the continental slope. SOCAT surface water fCO_2 measurement coordinates from Bakker et al. (2023), CARINA full depth carbon chemistry stations from Olsen (2009). Numbers 1, 2, and 3 refer to the Northeast Greenland Ice Stream (culminating in 79N glacier or Nioghalvfjerdsbrae and Zachariae Isstrom), Young Sund, and the Northeast Water Polynya region respectively. (b) Known sources of total alkalinity to the Arctic Ocean highlighting the source regions (green area with dashed white outline) of the Transpolar drift (TPD) and the location of the study area (red rectangle). Sources to the Arctic Ocean include Arctic rivers with variable catchment geology, sea ice and snow melt, and the Pacific Water coming in through the Bering Strait. River TA values from Cooper et al. (2008), Pacific from Anderson et al. (2013), and Atlantic from Jones et al. (2021). Sea ice TA is from own measurements during these cruises Willcox et al. (2023). Locally, there is an unknown contribution of both sub- and supraglacial sources as well as glacier-fed rivers. Bathymetry was sourced from IBCAO (Jakobsson et al., 2020), and ice velocity from QGreenland v2 (Moon et al., 2022)

freshwater is primarily sourced from the Russian Shelf (particularly the Laptev Sea) where vast amounts of riverine freshwater are introduced changing the salinity and surface water geochemical properties. This water is further geochemically modified in the Siberian shelf seas prior to cross-Arctic transport as a result of shallow bathymetry combined with high winds and extensive polynyas adding a measurable denitrification signal (Nitishinsky et al., 2007; Chang and Devol, 2009; Anderson et al., 2013) and changing the isotopic fractionation (Bauch et al., 2010). Finally the surface water masses are advected off of the Siberian continental shelves and entrained into the Transpolar Drift (TPD). Once entrained into the TPD the annual sea ice freeze-melt cycle will continue to freshen the surface layer by the export of brine and dilution with meltwater. This process diverts the slope of the surface water from that between Atlantic Water and meteoric freshwater toward the sea ice melt end-member in both TA-S and $\delta^{18}O$-S diagrams. A comparison between the Laptev Sea and Northeast Greenland shelf in terms of apparent oxygen utilisation (AOU) against the nutrients phosphate and silicate, and nitrate to phosphate ratio, confirm the strong link between the Laptev Sea and the Northeast Greenland Shelf via the TPD. The surface water, located above the maximum Brunt-Väisälä frequency squared (N^2), and above the remnant of the winter mixed layer, is almost entirely depleted in nitrogen (median NO_3^- = 0 µmol/kg). Directly below this is a remnant of the winter mixed layer which exists at freezing temperatures and a practical salinity of ~ 31.4 psu (σT ~ 25). This is fresher than this inflection point was in previous decades (Budéus and Schneider, 1995; Bignami and Hopkins, 1997; Budéus et al., 1997). This layer contains, and apparently traps, the oxygen maximum indicating that it is not actively ventilated during the time when sampling occurred. From the salinity at the inflection point (and the oxygen maximum), there is a cold halocline layer which follows the freezing line up to a salinity of 34.0, the Lower Halocline Water. At this point we find another inflection away from the freezing line with a sharp temperature increase in temperature to EBAW at 4 °C (S = 34.8) and AW at 6 °C (S = 35). The saltiest and warmest Atlantic Water found is likely sourced from the West-Spitsbergen Current. This water can be found at the surface just off the continental shelf and can make incursions onto the continental shelf, particularly further south. Surface conditions in terms of sea ice cover and surface temperature during the three weeks of the two cruises were variable (Figure 4.2) with warm

surface temperatures and patchy sea ice dominating the first part, after which the sea ice fraction increased, particularly toward the north and north-west part of the shelf.

4.3.2 Sample Analysis

A full description of the hydrography based on the Conductivity, Temperature, and Depth (CTD) instrument data, nutrients, and total alkalinity are included in the methods section of Willcox et al. (2023). To analyse DIC, seawater samples were transferred from the CTD Rosette to gas-tight vials (12 mL Exetainer, Labco High Wycombe,UK), poisoned with 12 µL solution of saturated $HgCl_2$, and stored in the dark at room temperature until analysis. DIC was measured on a DIC analyzer (Apollo SciTech, Newark, DE, USA) by acidification of a 0.75 mL subsample with 1 mL 10% H_3PO_4 (Sigma-Aldrich, Saint-Louis, MO, USA), and quantification of the released CO_2 with a nondispersive infrared CO_2 analyzer (LI-COR, LI-7000, Lincoln, NE, USA). Results were then converted from µmol L^{-1} to µmol kg^{-1} based on sample density, which was estimated from salinity and temperature. An accuracy of ± 2 µmol kg^{-1} was determined for DIC from routine analysis of certified reference material (A.G. Dickson, Scripps Institution of Oceanography, San Diego, CA, USA). CTD measurements of temperature and salinity were combined with the TA and DIC bottle data to calculate the pCO_2 using the program CO2SYS (van Heuven et al., 2011) with the dissociation constants k1 and k2 of Mehrbach et al. (1973) refitted by Dickson and Millero (1987) and the hydrogen sulfite dissociation constant from (Dickson, 1990).

4.3.3 Mixed layer depth determination

We estimate the depth of the mixed layer by estimating the pycnocline from the determination of the maximum Brunt-Väisälä frequency (N^2) (Jones et al., 2021) for all stations with bottles taken shallower than 120 m depth. Our previous study Willcox et al. (2023) indicated this would be a good proxy since the pycnocline acted as a barrier, trapping dissolved oxygen below it indicating that this water was

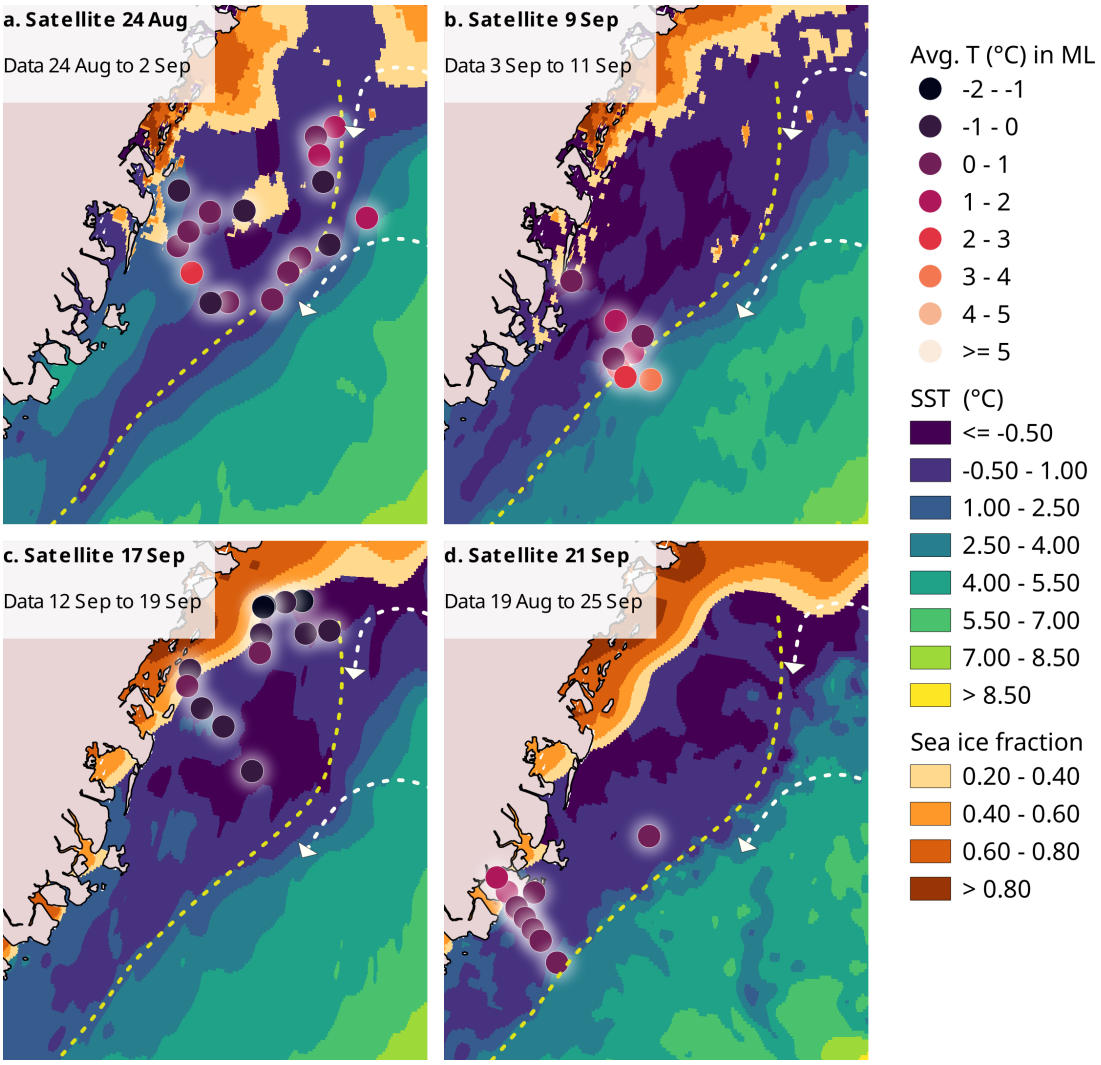

Figure 4.2: Surface conditions (sea ice fraction and sea surface temperature) on the shelf and average mixed layer depth temperature per station subdivided into four sampling periods. ESA sea surface temperature and sea ice fraction were obtained from Meteorological Office UK (2019) (Good et al., 2020). Average station mixed layer depth temperatures are the average temperature for all sampled depths above the maximum Brunt-Väisälä frequency squared (N^2)

not ventilated during the period of our study. The maximum N^2 was calculated for each CTD cast individually and depths varied between 1 and 30 m, with shallower depth closer to the coast and further north. The bottle data were normalised by the application to the data of a fitted polynomial. The polynomial captures the effects of both the sea ice melt and meteoric freshwater dilution. A full justification, including a comparison with more traditional normalisation techniques, is provided in section 3 of the Supplement associated with this manuscript.

4.3.4 Modified Z-score

Because the mean is heavily influenced by the extreme outliers in these data, parametric methods are not representative. Nonparametric methods relying on the median are more representative. The modified Z-score is one such method, it relies on the Mean Absolute Deviation (MAD). Data are marked as outliers when the modified Z-score is larger than a value D. Our choice of D (1.5) is discussed in section 4 of the Supplement.

4.4 Results and discussion

Based on previous studies, the region is expected to act as a sink for atmospheric CO_2. Periods of high drawdown are specifically thought to occur when the light returns in spring allowing for autotrophic production during phytoplankton blooms including under ice blooms (Arrigo et al., 2012; Ardyna et al., 2020), and during upwelling events in the marginal ice zone (Mundy et al., 2009). The release of CO_2 during the dark season, when no photosynthesis can occur and the region becomes (net) heterotrophic, is inhibited by extensive sea ice cover (Yager et al., 1995). This ice-covered period can be associated with CO_2 supersaturation (Duke et al., 2021). Autumn is a transition period between a summer highly stratified environment where light is available and is dominated by sea ice and meteoric freshwater flux, and a winter environment that is dark, unproductive, and influenced by sea ice growth and brine rejection. In the northern North Atlantic, autumn is

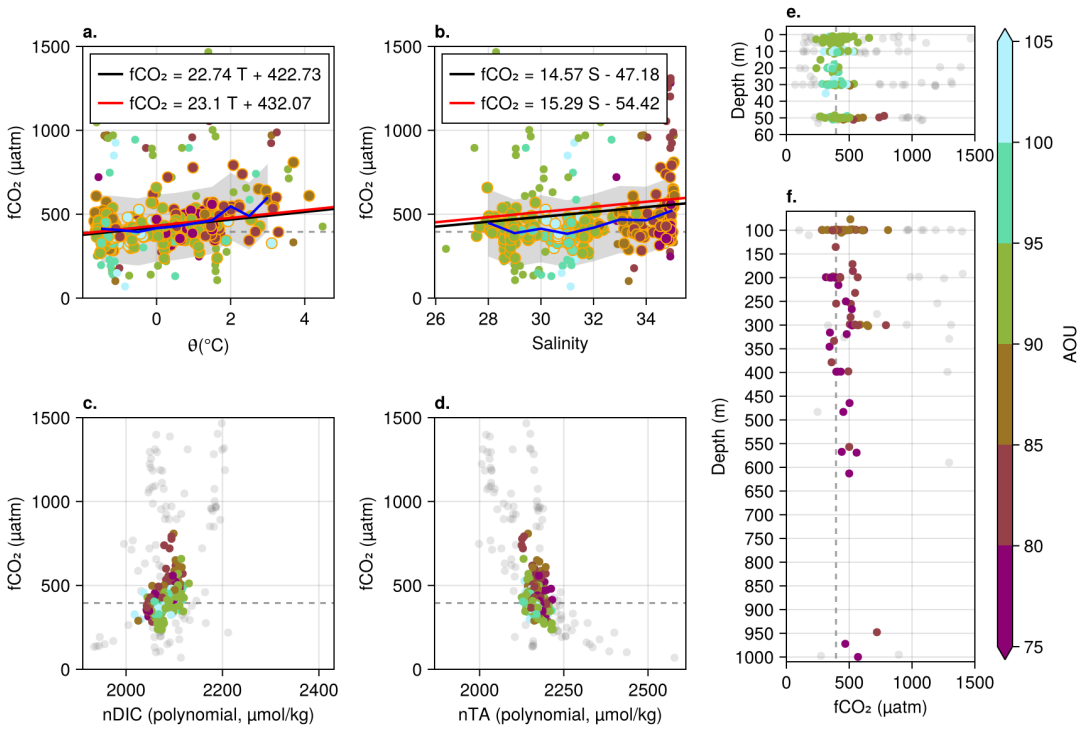

Figure 4.3: Carbon dioxide fugacity fCO_2 plotted as a function of potential temperature (a), practical salinity (b) normalised DIC (c), normalised TA (c), and with depth for shallower (e) and deeper waters (f). The orange lines in a,b are the best fit line for the median ± 200 fCO_2 for each step in controlling variable. The median for steps in salinity is shown as the blue line where values included in the median calculation (± 200) are bounded by the grey region. Data with orange stroke in a,b and in colour in c,d,e,f are values with a modified Z-score of within ± 1.5. The red line in (a,b) is the modified Z-score data best fit. All data are coloured according to the Apparent Oxygen Utilization (AOU) calculated as the difference between the TEOS-10 calculated oxygen solubility and the observed oxygen concentrations.

associated with the breakdown of stratification near the surface due to higher wind speeds and storms. This pattern is repeated in the Greenland Sea where average wind speeds tend to increase during the period of this study (days of year 240 - 256, Qu et al. (2012)), and August and September are associated with increasing concentrations of dissolved CO_2 after a seasonal low in July (Arrigo et al., 2010). The fall of 2017 had exceptionally low sea ice cover for the region (Sumata et al., 2022), allowing unpecedented access to undersampled regions of the shelf. The parameters which usually explain most of the variability in carbon dioxide fugacity (fCO_2) in the ocean surface are temperature (T), salinity (S), total alkalinity (TA), and dissolved inorganic carbon (DIC). Gas solubility is expected to increase with decreasing temperature, change with salinity as a result of variable dissociation constants through their dependence on ion activities. With increasing TA, the fCO_2 is expected to decrease since these are the ions associated with increasing the ocean buffer capacity (Zeebe and Wolf-Gladrow, 2001), and DIC is taken up by autotrophs during primary production and converted to organic matter. The data collected on the Northeast Greenland shelf in fall of 2017 do not clearly show the patterns expected (Figure 4.3). The data are scattered and outliers do not follow a discernable pattern with respect to salinity or temperature. Outliers occur during both cruises, in measurements from both labs, toward high and low TA and DIC concentrations, and at different depths. There is no clear correlation between the outliers and any variable measured. We therefore have to surmise that at this time we are missing a (set of) variable(s) and/or process(es) with which to describe the extreme values in these data, and we do not have sufficient justification to remove any of the outliers from the dataset. We cannot discard any data without a good reason to flag it as an outlier, and with this amount of variability in the dataset using linear correlations loses some efficacy. Mean values are not representative of the data therefore any attempt at statistical analysis necessarily relies on non-parametric techniques such as the modified Z-score.

Using median values of fCO_2 for steps of each controlling variable (T, S, etc.) rather than the mean and picking values for fCO_2 between which the correlation is to be made or using an extreme modified Z-score outlier flag (> D=1.5), a linear relationship can be established for temperature (Figure 4.3a). The same method fails

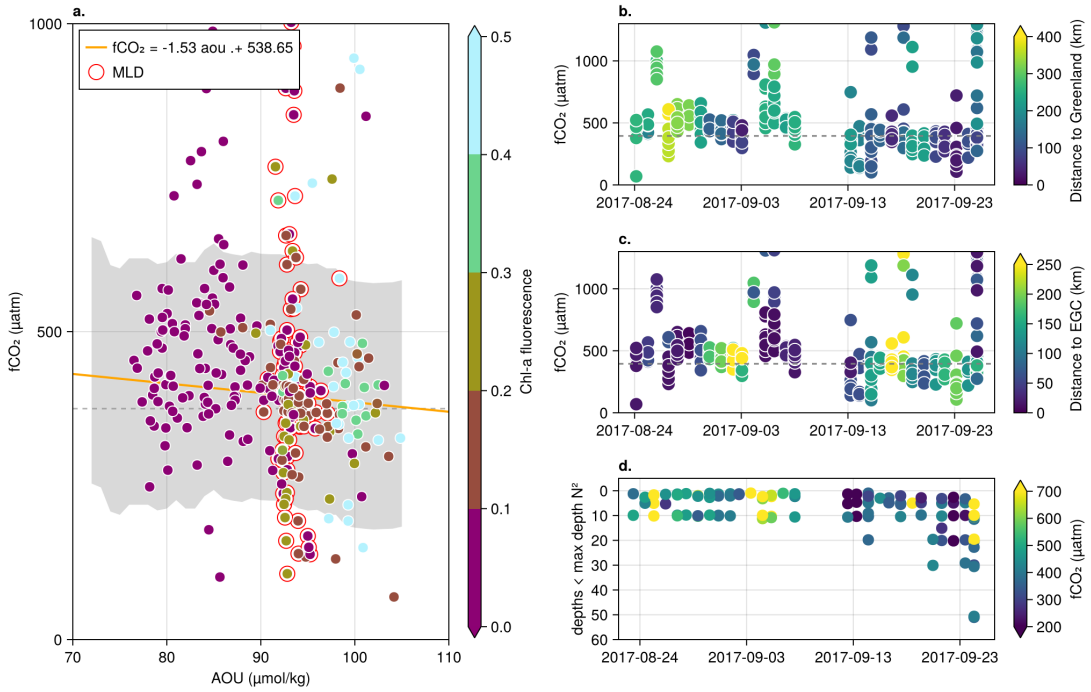

Figure 4.4: (a) the change in fCO_2 with changes in apparent oxygen utilisation (AOU). (b,c) fCO_2 changes with date, coloured respectively by distance of station to Greenland and the EGC (d) Data in the mixed layer depth (MLD) for each station by date

for salinity (Figure 4.3b) because the median fCO_2 follows a slightly polynomial shape which means the line is an overestimate compared to the values calculated from CO2SYS. The median and inter quartile range (iqr) for the mixed layer depth based on the N^2 are 410.49 and 147.58 µatm, which is above the projected atmospheric value for the region of 395 µatm based on SeaFlux (Fay et al., 2021) though this is for the entire time period which may not be representative (Figure 4.4). If we divide further by time, the period before 10 September has a median 477.66 with iqr 201.96 µatm and after this date the median goes down to 367.89 with iqr 110.66 µatm. This indicates a change in conditions, either between the sampling period or the sampling locations where the region turns from a source to a sink. For samples taken near the surface, the apparent oxygen utilisation is under 95% indicating either its use in biochemical processes, or the active ventilation of or mixing with waters with even lower dissolved oxygen concentrations. In case of the former, this may also be responsible for the some of the higher concentrations in surface layer fCO_2 though we have no additional evidence to show active remineralisation.

One of the reasons that the relationships between fCO_2 and temperature and salinity respectively is unpredictable and highly variable is that water types with different histories found on the Northeast Greenland shelf can have similar end-member values for certain parameters. For example, meteoric freshwater from the longer fjords has had time to heat up before being advected onto the shelf, with air temperatures in summer as high as 10 to 12 °C (Rysgaard et al., 2003). Atlantic Water (AW) from the return current also has temperatures of over 4 °C and a salinity of 35. Eurasian Basin Atlantic Water (EBAW) i.e. Arctic Atlantic Water that has circumnavigated the Eurasian Basin and lost heat is cold but has a salinity of 34.8. This is very close to AW salinity (34.8/35 = 0.99). The proportionality of the difference in TA between AW is similar to that in salinity, e.g. 0.98 for a EBAW TA of 2274 (Jones et al., 2008) and an AW TA of 2317 (Jones et al., 2021) but the 1% difference may be indicative of additional processes rendering TA non-conservative in this layer, diluted by a large volume. The region is also known for its small diameter (5 - 10 km) but deep penetrating eddies which offshelf can reach down to over 1000 m (Gascard et al., 2002; Wadhams et al., 2002; Rudels et al., 2005) With our sampling density which has distances between stations that are frequently over 30 km such features could

create heterogeneous results for neighbouring station locations.

At depths below the surface mixed layer, as defined by the Brunt-Väisälä frequency squared (N^2), the AOU and fCO_2 are inversely correlated (Figure 4.3 e). This ranges from the remnant of the winter mixed layer which is supersaturated with respect to dissolved oxygen, AOU > 100 %, and the median fCO_2 is lower than atmospheric values at 383.39 with an iqr of 130.40 µatm, to depths where AOU < 80 % and the fCO_2 has a median of 453.32 with an iqr of 119.61 µatm. The maximum AOU corresponds with higher chloropyll *a* fluorescence in the remnant winter mixed layer which indicates that the dissolved bioactive gas concentrations in this layer are at least partially driven by the presence of a Deep Chlorophyll Maximum (DCM) (Figure 4.4 a). While surface conditions were variable during the sampling period in terms of sea ice fraction and temperature (Figure 4.2), the region off-shelf, to the east of the EGC, is generally associated with warmer temperatures and higher salinity, while waters across the shelf itself have colder surface temperatures. Sea ice is most persistent in the north. The first part of the sampling period had warmer surface temperatures on the shelf itself, especially in the south along the coast (Figure 4.2 a). In addition, this period (before 13th September) had more stations further from land (Figure 4.4 b) and closer to the EGC (Figure 4.4 c), and generally exhibit higher fCO_2.

During the sampling period, the surface temperature cools and the sea ice in the north becomes more consolidated (Figure 4.2 b,c,d). The fCO_2 during the later period are much lower and trend below atmospheric saturation, potentially indicating a seasonal shift (Figure 4.4 b,c). The increasing Mixed Layer Depth (MLD) near the end of the study (Figure 4.4 d) could support this though this could also be attributable to another process such as the presence of a front. A comparison of mixed layer values ignoring temporal variability is included in section 6 of the Supplement.

The algorithms established by Arrigo et al. (2010) to determine TA and DIC for the North Atlantic (surface layer) fit our data well for TA, albeit with considerable scatter (Figure 4.5 a). This is not entirely surprising since the dataset used for the algorithm was in part obtained from measurements of the northern part of the

Northeast Greenland shelf (Wallace, Minnett, et al., 1995). To determine the best fit for DIC, they removed values for nearshore waters proximal to riverine meteoric freshwater sources from the dataset due to those measurements being lower than the algorithmically predicted values. Our measurements are also lower than the values predicted using their algorithm even though they are not directly near a meteoric freshwater source (Figure 4.5 b). Similar linear regressions were fitted by Nondal et al. (2009) and Olsen (2009). The former do not provide an accurate reflection of our data and the second have a similar slope but a lower intercept. The Arrigo et al. (2010) equation is therefore the best predictor for TA on the shelf.

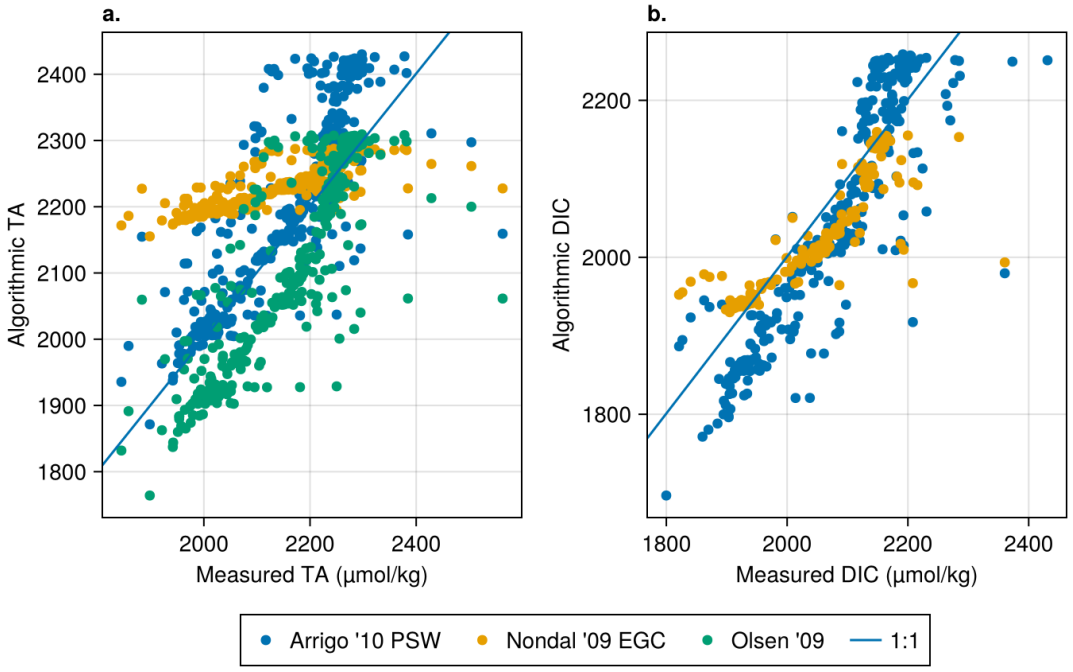

Figure 4.5: Measured concentrations of TA (a) and DIC (b) compared to values predicted using the algorithms from Arrigo et al. (2010), Nondal et al. (2009), and Olsen (2009). Since NO_3^- concentrations were only available for the last two weeks of the cruise, these are the only data shown for the Nondal et al. (2009) fit in (b)

The difference between TA and DIC drives much of the fCO_2 variability calculated using CO2SYS, and increases (on average) between the first and second parts of the cruise (Figure 4.6 a,b) as a result of a reduction in DIC. The average TA in the mixed layer remains the same throughout the study period. The reduction in mixed

layer DIC relative to mixed layer TA is most pronounced at the lower latitudes in the southernmost transect near Young Sound (Figure 4.6 c). As previously described in Henson et al. (2024), the depth-dependence of carbonate chemistry on the Northeast Greenland shelf is non-linear. Whether the surface mixed layer will act as a sink or a source of CO_2 with respect to the atmosphere seems to vary though it is clear that the region is not as strong a sink as previously expected and may be a net source. Increases in freshwater, both meteoric as well as sea ice melt, are associated with more corrosive surface waters near the coast in the region (Henson et al., 2023) but this can be compensated for by high productivity stimulated by nutrient input from local ice melt (Wallace, Behrens, et al., 1995; Fransson et al., 2023). If this is the case this may be another reason for the extreme variability of results we obtained. The mixed layer at the surface on the Northeast Greenland shelf that is advected in from the Arctic Ocean is already severely nitrogen depleted (Tuerena et al., 2022) which impacts opportunities for local primary producers to exist at the surface away from areas where local features such as eddies or actively melting sea ice might contribute nutrients to the surface water. Where sea ice melting, glacier melting, or potentially even iceberg fertilisation contribute nutrients to the surface, primary productivity can be quickly stimulated and the associated removal of DIC would allow for increased buffering by the TA and result in a lower fCO_2 in these areas. Sea ice and iceberg melt can be patchy and major continental meteoric freshwater contributions directly onto the shelf happen primarily at the termini of the 79N glacier and Zachariaea Isstrom, therefore the extent of surface primary productivity influencing the carbon system is likely limited during the sampling period. The rest of the shelf receives local freshwater input from long fjords where all the nutrients added in the surface have likely already been fully utilised before they reach the shelf (Holding et al., 2019). This means that primary productivity is necessarily limited to a deep chlorophyll maximum (DCM) below the nitracline. During years of more extensive sea ice cover primary production may occur closer to the surface and stimulate more direct uptake of CO_2 from the atmosphere. Higher benthic productivity has been observed closer to the EGC which, with strong benthic-pelagic coupling in the region, indicates higher productivity at the surface near the slope (Bodur et al., 2024) and an associated higher uptake of CO_2. In the absence of sea ice melt it is possible that this is stimulated by along-shelf upwelling or by

EGC-associated eddies which are particularly prominent in areas where the density of the warm Atlantic and the cool Polar Water are the same (Bashmachnikov et al., 2020).

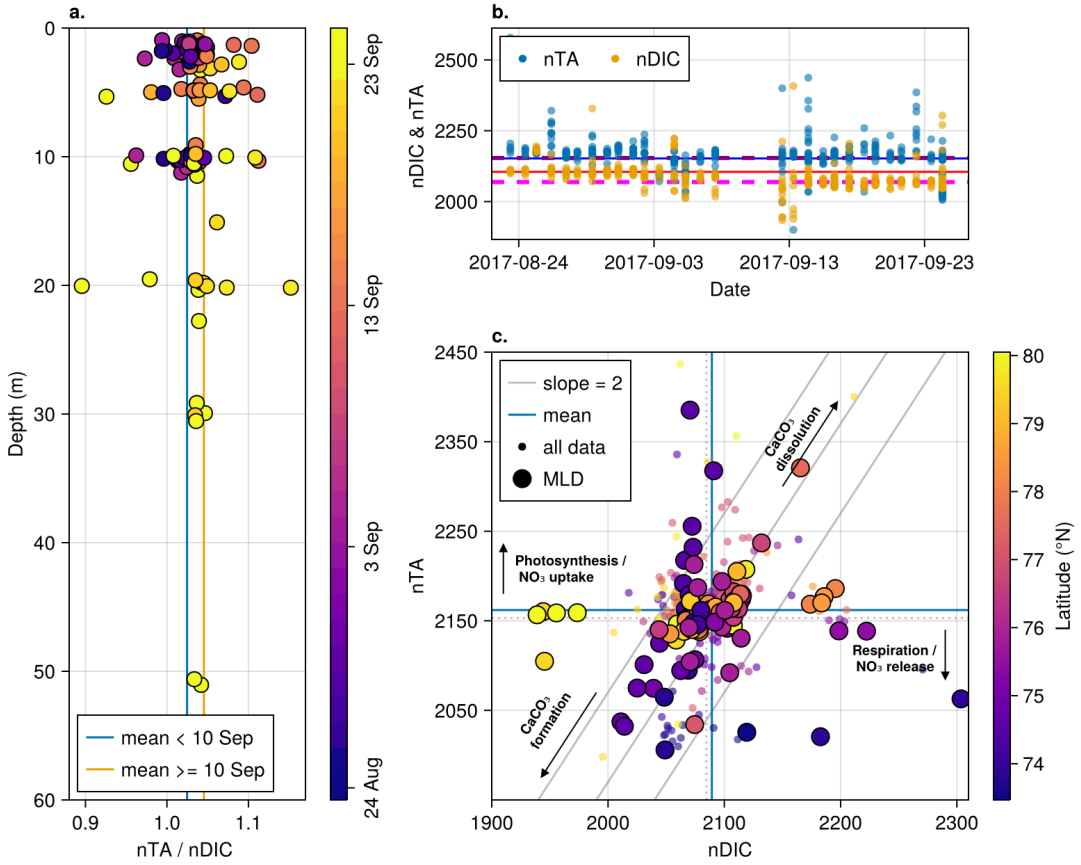

Figure 4.6: (a) Mixed layer nTA/nDIC with depth for the surface mixed layer. (b) nTA and nDIC respectively by measurement date. Blue line is TA and orange line DIC best fit between 24 Aug - 10 Sep. Dashed lines are for dates after 10 Sep. (c) nTA against nDIC

4.5 Summary

We present the first full depth carbon system observations of the area of the Northeast Greenland shelf between 75 and 79 °N, with additional measurements outside of Young Sund and in the region of the Northeast Water Polynya. Our total alkalinity

(TA) measurements correspond well to the predictive algorithm created by Arrigo et al. (2010), whereas the dissolved inorganic carbon (DIC) measurements are lower than predicted by these authors. We find that the shelf does not act as a consistent sink as expected per the calculated fugacity of carbon dioxide (fCO_2) from samples of TA and DIC. Using non-parametric methods due to the large number of outliers in the dataset, we find that the surface of the region can act as either a sink or source of CO_2 with respect to the atmosphere. The highest uptake is associated with a maximum in apparent oxygen utilisation (AOU) and chlorophyll within the remnant of the winter mixed layer where there is both light and nutrient availability. This water is not actively ventilated and therefore cannot contribute directly to atmospheric carbon exchange. The middle of the study period saw an apparent breakdown in stratification based on an increase in mixed layer depth as determined by the maximum Brunt-Väisälä frequency squared (N^2). This was associated with a reduction in surface layer fCO_2 to median values below the expected atmospheric concentration, apparently due to a corresponding reduction in DIC. The many outliers in fCO_2, particularly in the surface mixed layer, are not clearly associated with any known process or measured variable. It is likely that the shelf is characterised by influences at smaller scales than the sampling density of this study. August and September 2017 were extraordinary in terms of low sea ice cover, which was the reason that opportunistic sampling of this previously unsampled area could take place. Our results may therefore not represent a baseline for the region when ice covered but rather may act as an example of the response of the region to future increases in oceanic and atmospheric heat and reductions in sea ice.

4.6 Supplement S1

4.6.1 Goal of this supplement

The ability of the ocean to dissolve carbon dioxide (CO_2) gas is primarily affected by temperature, salinity, the buffer capacity of the ocean (measured as titrated alkalinity) and the amount of total dissolved inorganic carbon (the sum of all inorganic

carbon species in solution once released as CO_2 gas and measured by coulometric titration). To analyse the carbon chemistry from bottle data they are commonly normalised to remove the effect of salinity (S) (Broecker and Peng, 1992; Friis et al., 2003; Yamamoto-Kawai et al., 2005) or temperature (Takahashi et al., 2002; Takahashi et al., 2009). This allows the analysis of the influence of other processes on the carbon system. Generally, the four main abiotic influences on the carbonate system are temperature, salinity, total alkalinity (TA), and dissolved inorganic carbon (DIC) where the TA is generally considered to be conservative with salinity and the DIC is influenced primarily by autotrophic production and remineralisation (Zeebe and Wolf-Gladrow, 2001). When normalising data with respect to salinity in environments where TA is conservative with salinity, analyses can focus on the biology. For surface water transported to higher latitudes from low and mid latitudes, the increase in gas solutbility is is associated with the decrease in temperature (Weiss, 1970; Li and Tsui, 1971; Millero, 2013). For an isochemical water mass, the relationship was established by Takahashi et al. (1993) as shown in Equation eq. 4.1 for water taken from the North Atlantic.

$$(\partial lnpCO_2/\partial T) = 0.0423 \pm 0.0002°C^{-1} \tag{4.1}$$

The Northeast Greenland shelf is a unique high latitude coastal environment with more possible influences on the carbonate system than in lower latitude open ocean environments. The environment can not be expected to be isochemical, nor is the surface water all cooled. Water found at the surface and originating in the Arctic Ocean will be exposed to increasing atmospheric temperatures with decreasing latitude in summer which would reduce the solubility of CO_2, while the return Atlantic Water might either heat or cool depending on conditions on the e astern side of Fram Strait, the season during which it arrives on the shelf, and the amount of (melting) sea ice it encounters. Similarly, the other main variables measured to calculate the CO_2 have different sources or are subject to complex processes on the shelf.

This supplement is intended to highlight some details which are relevant to but not directly part of the study. The first is a discussion surrounding the use of water mass

tracers on the Northeast Greenland shelf and the errors associated with it. The second is a justification for our choice of using a polynomial fit to normalise the data rather than using more common methods. Finally we provide some detail regarding our use of the modified Z-score, a comparison between our data and that found in the SOCAT and CARINA databases, and overview maps for several integrated mixed layer depth observations.

4.6.2 Water mass fractions on the shelf

In an idealised estuarine environment there is a single freshwater source with which incoming ocean water is diluted. This source can be glacial or riverine, and precipitation is considered either negligible or as part of the same catchment. The TA of the freshwater source can be obtained by performing a linear regression between total alkalinity and salinity and finding the TA at S = 0. In a northern latitude fjord environment dilution of the surface layer by sea ice melt is an additional process. This makes the analysis more complex since sea ice retains TA in the form of the hydrated mineral ikaite ($CaCO_3 \cdot 6\ H_2O$) and so is no longer conservative with the salinity, both in the meltwater influenced layer as well as the underlying water into which the salty but TA-depleted water is mixed. In an idealised fjord with a single meteoric freshwater source and local sea ice formation and melting the sea ice melt influence can be approximated by performing a water mass fraction analysis. This is most frequently done by using a system of linear equations where 2 tracers are used to obtain 3 unknown water mass fractions. The most commonly used tracers are salinity and stable water oxygen isotopic composition ($\delta^{18}O$), which are independent from one another both for meteoric as well as sea ice freshwater sources, for end-members of Atlantic Water, Meteoric freshwater, and sea ice melt as shown in Equations 4.2, 4.3, and 4.4.

$$f_{sim} + F_{mw} + F_{aw} = 1 \tag{4.2}$$

$$\delta^{18}O_{sim} + \delta^{18}O_{mw} + \delta^{18}O_{aw} = \delta^{18}O_{obs} \tag{4.3}$$

$$S_{fsim} + S_{mw} + S_{aw} = S_{obs} \tag{4.4}$$

where subsripts sim, mw, and aw refer to sea ice melt, meteoric freshwater and Atlantic Water end members and obs to the observed (measured) values.

The Northeast Greenland shelf is not an idealised northern latitude fjord, it is a complex broad Arctic continental shelf which receives multiple advected watermasses and receives additional local inputs. The water advected onto the shelf is not a pure Atlantic Water end member, it is instead comprised of return Atlantic Water, directly from the West Spitsbergen Current and Eurasian Basin sourced Arctic Atlantic Water which is much colder and may have been subject to processes specific to the Arctic that the return current has not including such things as dense water cascades or sedimentary interactions. The upper water which includes the cold halocline layer and the surface water is influenced by sea ice melt and by the input of 10-11% of global meteoric river discharge (Shiklomanov et al., 2021). Each of the 6 major rivers discharging into the Arctic Ocean has its own average TA and $\delta^{18}O$ values which also vary seasonally (Cooper et al., 2008), Due to these complexities we can't assume that TA is conservative with salinity.

The method using 3 linear equations and solving for 1 unknown that is commonly used to determine the water mass fractions is sensitive to the choice of the salinity and $\delta^{18}O$ for sea ice. Sea ice $\delta^{18}O$ can vary depending on the water from which it was frozen, whether or not it is covered in snow, and on its age (first year versus multiyear ice) (Mellat et al., 2024). For end member values AW (S=35.0, $\delta^{18}O$=0.3‰), MW (S=0, $\delta^{18}O$=-20‰) and sea ice melt with S = 2 set to $\delta^{18}O$ of -4, -1, and 0.2‰ respectively entered into the system of linear equations, the lowest negative meteoric meltwater fraction (so an indicator of the size of the introduced error) in our data are -9.9%, -8.2%, -7.8% respectively. It is less sensitive to the salinity of the sea ice.

For a $\delta^{18}O$ of 0.3‰ , S = 4 results in a maximum negative freshwater fraction of -7.7% and remains the same (when rounded to 2 significant figures) at S = 0.

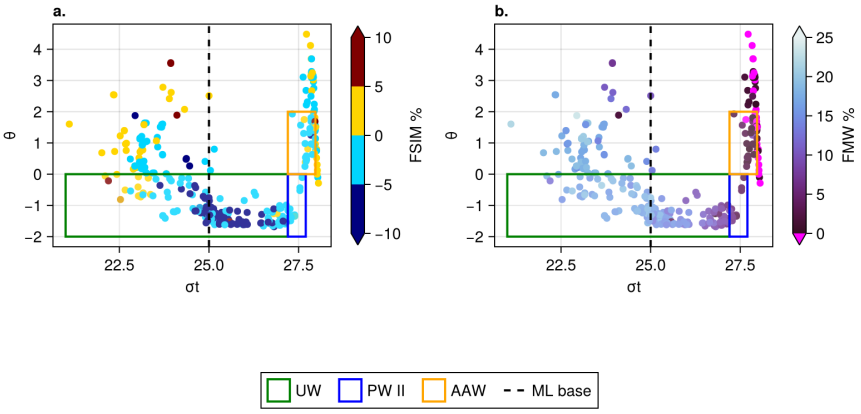

Figure 4.7: Density against temperature with fractions of sea ice melt (a) and meteoric water (b). Water mass boundaries (Rudels et al, 2022) in colour and the remnant of the winter mixed layer in the black dashed line. Acronyms UW is Upper Water, PW II is Polar Water 2 which refers to the low er halocline & winter mixed layer in the upstream Nansen Basin. Note that the Atlantic Water sea ice melt fraction is close to 0 while simulta neously, the upper water mixes from high in brine (negative melt) to high in sea ice melt crossing through 0 sea ice melt. Meteoric freshwater (FMW) has negative fractions, primarily at high densities which is clearly in error since meteoric freshwater input can't be negative. It is therefore apparent that the system of linear equations with which the water fractions are calculated is lacking the end-members or end-member values required to properly assign these fractions at each data point, likely due to the high variability of input sources.

For representative end-member values of AW (S=35.0, $\delta^{18}O$=0.3 ‰), MW (S=0, $\delta^{18}O$=-20 ‰), and for SIM S=2 and the mean $\delta^{18}O$ value of sea ice collected and melted during the second cruise: $\delta^{18}O$ = -2.34 ‰ (Willcox et al., 2023). It can be seen that the Cold Halocline Layer (CHL, from the base of the winter mixed layer at σt=25 to the Polar Water II at σt=27.2) is most influenced by negative sea ice melt (generally interpreted as brine) and all other water, the more dense Polar II and Arctic Atlantic Water as well as the surface water have meltwater fractions of 0 ± 5 %. For the surface water this is not a problem since the meteoric freshwater and Atlantic Water fractions are not below 0. It does pose a problem for the higher

density waters (σt > 27.2) where the freshwater and/or Atlantic Water fractions are unrealistically < 0 % (magenta in Figure 4.7 b) and the sea ice meltwater fraction is lower than those erroneously negative fractions. When Atlantic Water enters the Arctic Ocean, it eventually forms the lower halocline when the warm water is rapidly cooled, by loss of heat to the atmosphere, but also through the melting of sea ice and a meltwater signature in these denser waters could be correct and can not be simply discarded. This issue can't be easily resolved without the use of additional tracers such as the ^{236}U and ^{129}I anthropogenic radionuclides which can differentiate between different Atlantic Waters based on their time spent in transit.

Table 4.1: End member values used to determine water mass fractions. Meteoric water values for δ^{18}O and TA are those of the Lena river according to (Cooper et al., 2008). Sea ice melt values for δ^{18}O and TA are from own measurements on the shelf

	Salinity	δ^{18}O (‰ VSMOW2)
Sea ice melt	2	-2.344 ± 0.746
Meteoric	0	-20.5
Atlantic	35.0	0.3

4.6.3 Salinity normalisation of carbonate chemistry

The TA of return Atlantic Water that has sea ice melted directly into it may be different (say a TA of 2330 diluted with a mean shelf sea ice concentration of ~204 µmol/kg) to the TA of Arctic Atlantic Water that has a similar salinity but may have had brine and meltwater added during multiple years spent in the Arctic Ocean. Simply correcting with the sea ice meltwater fraction therefore may not be sufficient to describe local processes.

The simplest formulation of the salinity normalisation of marine inorganic carbon system data is given by Equation eq. 4.5 where the reference salinity normalised to is often 35 (Peng et al., 1987). Several modifications to this have been proposed

with time including those which involve corrections for nutrients (Broecker and Peng, 1992).

$$nX = \frac{X_{meas}}{S_{meas}} \cdot S_{ref} \tag{4.5}$$

where X is the variable to be corrected for, e.g. TA and/or DIC, S is the salinity, and the *meas* and *ref* subscripts stand for the field measurements and the reference value respectively.

Whether the resulting normalised data are entirely independent of freshwater flux has been questioned (Robbins, 2001). Later iterations were developed specifically for higher latitudes including corrections for a TA estimated by linear regression at the point S = 0 (Friis et al., 2003), and for the calculated sea ice melt fraction (Yamamoto-Kawai et al., 2005). Each of these corrections has associated issues and errors and may not provide useful information, especially where there are multiple low salinity sources for TA such as shelf environments host to catchments with differing geology. Although there is an official description of what a reference salinity is (Wright et al., 2010), it is often either chosen to be 35 or a regionally obtained variable, often the mean salinity. This makes any comparison between different geographical regions with different dominant water masses and therefore chosen reference salinity incomparable. This complexity primarily impacts mixed layer depths (Friis et al., 2003) where the meteoric-influenced layer is highest or multiple different sources such as precipitation, riverine inputs, and sea ice melt, contribute to the dilution. If these normalizations rely on other assumptions such as those underlying the calculation of sea ice melt fraction from δ^{18}O, any error in these assumptions will be propagated into any subsequent application using the normalized data.

The processes controlling the water mass composition and the associated shelf salinity and alkalinity are complex. In addition, fraction calculations suffer from the ambiguities discussed in the previous subsection, therefore these data might best be normalized with respect to salinity by the simple removal of a polynomial-predicted value from the data, rather than attempting to correct for the assumed

representative values for the Northeast Greenland shelf which contains such vastly variable sources in unknown relative quantities.

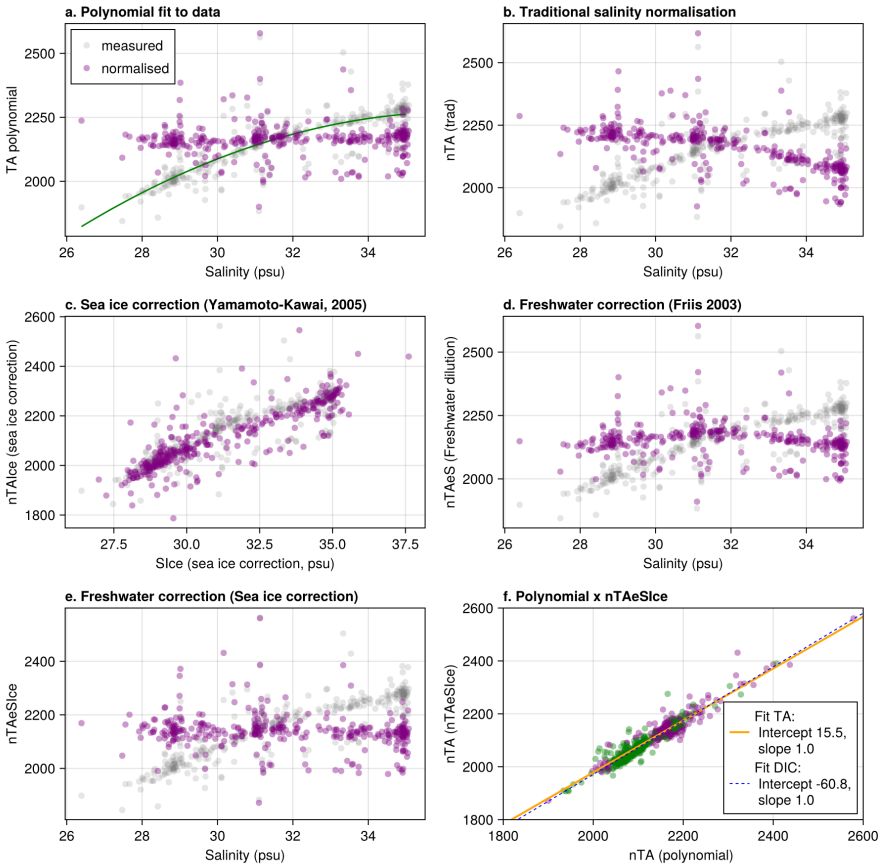

Figure 4.8: Comparison of normalisation techniques. Application by polynomial fit using the green line with equation TA = -3631.43 + 324.03 S - 4.45 S^2 (a), traditional salinity normalisation (b), Sea ice correction (c), Meteoric freshwater correction (d), Meteoric correction applied to sea ic e corrected data (e) and finally a comparison between sea ice + freshwater corrections and the polynomial correction indicating a slope of 1 b etween them.

For purposes of comparison and to choose the best representative method for the salinity normalisation of the carbonate system data, four different salinity corrections were applied (Figure 4.8). The first (Figure 4.8 a) is the direct application of the polynomial in Equation 4.6:

$$X_{pred} = X_{obs} - X_{poly} + X_{meanS} \tag{4.6}$$

where *pred* is the salinity-normalised value estimated by the equation, *obs* is the observational data, *poly* is the value predicted by the polynomial fit (green line in Figure 4.8 a), and X_{meanS} the mean salinity for the dataset. This method therefore still relies on an arbitrary choice of reference salinity but it reduces the number of assumptions made about external influences on the data such as the calculated fraction of sea ice melt although these have results that are comparable enough to be used interchangeably (Figure 4.8 f).

4.6.4 Modified Z-scores

Modified Z-scores rely on the Absolute Median Deviation (MAD) rather than the mean of a dataset and thus allow for the labeling of outliers in datasets where the mean is too sensitive to outliers. This modified Z-score is calculated according to Equations 4.7 and 4.8.

$$MAD = median_i(|x_i - \tilde{x}|) \tag{4.7}$$

$$M_i = \frac{0.6745(x_i - \tilde{x})}{MAD} \tag{4.8}$$

Data can then be flagged as an outlier if $|M_i| > D$. Although Iglewicz and Hoaglin (1993) suggest a D of 3.5, this doesn't adequately flag all outliers in our data. To make sure all outliers based on visual inspection are flagged as such we require D = 1.5.

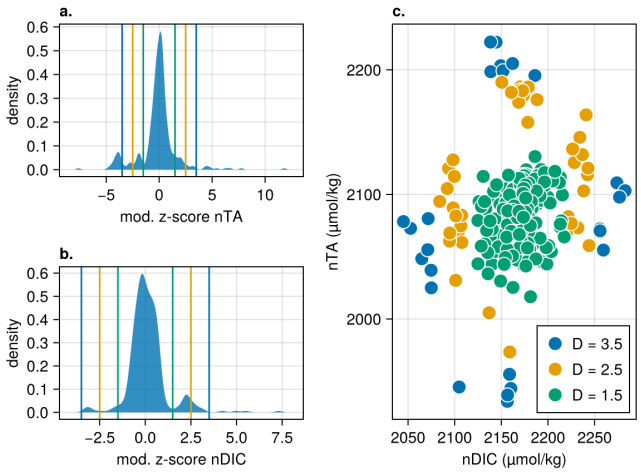

Figure 4.9: Density plots of the modified Z-scores of normalised TA and DIC (a,b) and of the data not flagged as outliers based on different choice of D

4.6.5 Comparison with SOCAT and CARINA data

Limited Surface Ocean CO_2 Atlas (SOCAT) carbon dioxide fugacity measurements and and full depth CARbon dioxide IN the Atlantic Ocean (CARINA) total alkalinity (TA) and dissolved inorganic carbon (DIC) data are available for the region of this study, however it is both geographically (1 a. main text) as well as temporally limited (Figure 4.10). For the time period (late August and September) of our study in late fall, there is only SOCAT data available from 2009 and CARINA data from 1994 and 2003 and therefore these data are not ideal for comparative purposes.

4.6.6 Mixed layer variability

Integrated values for measurements obtained at depths shallower than the depth of the maximum Brunt-Väisälä frequency squared (N^2) are shown in Figure 4.11. Due to the high variability in conditions during the sampling period, these observations cannot be treated as a single snapshot of conditions on the shelf. Since it does not represent the temporal diversity adequately, this figure has been omitted from the main text but is included here for reference.

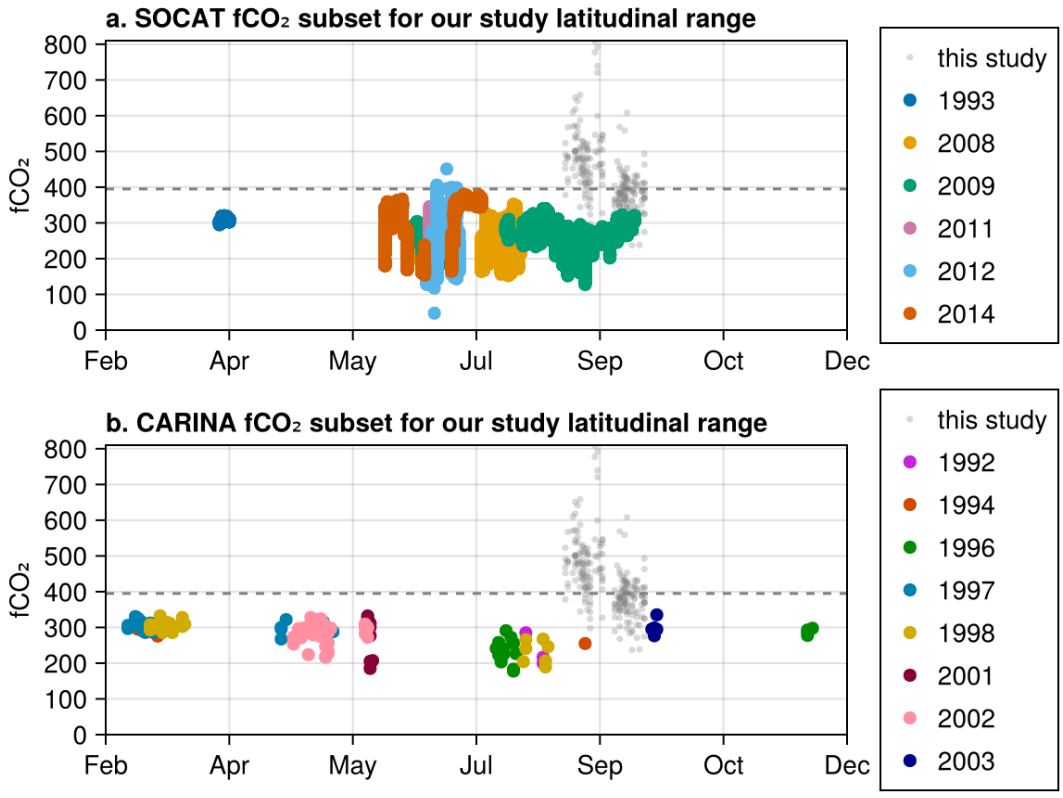

Figure 4.10: SOCAT measured fCO_2 (a) and CARINA CO2SYS calculated fCO_2 (b) for geographical area on and around the Northeast Greenland shelf compared to data from our study where D = 1.5. The grey dashed line is at 395 µatm, which is representative for the time of our study per Fay et al. (2021)

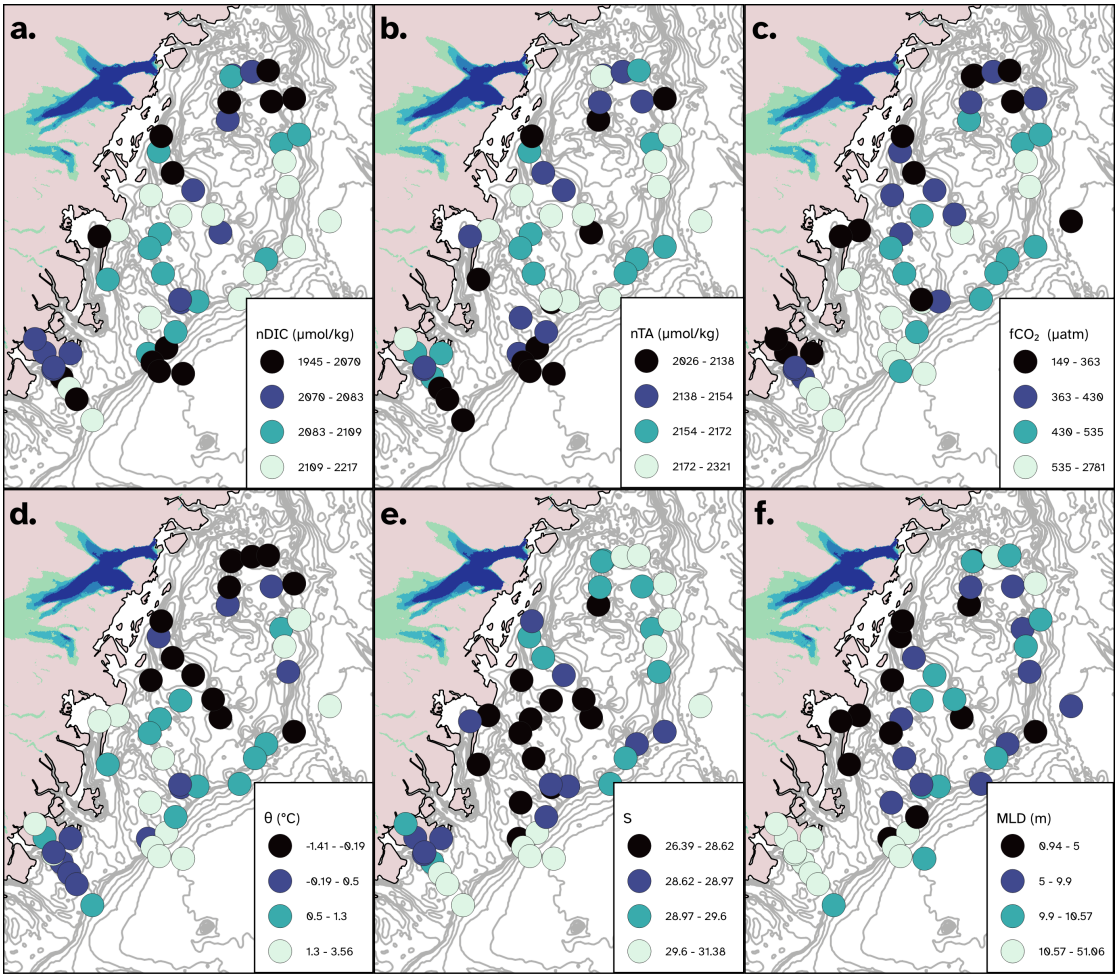

Figure 4.11: Mixed layer depth values for normalised DIC (a), normalised TA (b), fCO_2 (c), temperature (d), salinity (e). The mixed layer depth itself (p er depth of maximum N^2) is shown in f.

References

Anderson LG, Andersson PS, Björk G, Peter Jones E, Jutterström S, Wåhlström I. 2013. Source and formation of the upper halocline of the Arctic Ocean. *Journal of Geophysical Research: Oceans* **118**(1): 410 – 421. doi: 10.1029/2012JC008291

von Appen W-J, Waite AM, Bergmann M, Bienhold C, Boebel O, Bracher A, Cisewski B, Hagemann J, Hoppema M, Iversen MH, et al. 2021. Sea-ice derived meltwater stratification slows the biological carbon pump: Results from continuous observations. *Nature Communications* **12**(1): 7309. doi: 10.1038/s41467-021-26943-z

Ardyna M, Mundy CJ, Mayot N, Matthes LC, Oziel L, Horvat C, Leu E, Assmy P, Hill V, Matrai PA, et al. 2020. Under-Ice Phytoplankton Blooms: Shedding Light on the "Invisible" Part of Arctic Primary Production. *Frontiers in Marine Science* **7**: 608032. doi: 10.3389/fmars.2020.608032

Arrigo KR, van Dijken GL. 2015. Continued increases in Arctic Ocean primary production. *Progress in Oceanography* **136**: 60 – 70. doi: 10/f7mdc6

Arrigo KR, Pabi S, van Dijken GL, Maslowski W. 2010. Air-sea flux of CO2 in the Arctic Ocean, 1998 – 2003. *Journal of Geophysical Research* **115**(G4): G04024. doi: 10.1029/2009jg001224

Arrigo KR, Perovich DK, Pickart RS, Brown ZW, Van Dijken GL, Lowry KE, Mills MM, Palmer MA, Balch WM, Bahr F, et al. 2012. Massive Phytoplankton Blooms Under Arctic Sea Ice. *Science* **336**(6087): 1408 – 1408. doi: 10.1126/science.1215065

Bakker DCE, Alin SR, Bates N, Becker M, Feely RA, Gkritzalis T, Jones SD, Kozyr A, Lauvset SK, Metzl N, et al. 2023. Surface Ocean CO2 Atlas Database Version 2023 (SOCATv2023) (NCEI Accession 0278913). NOAA National Centers for Environmental Information. doi: 10.25921/R7XA-BT92

Bashmachnikov IL, Kozlov IE, Petrenko LA, Glok NI, Wekerle C. 2020. Eddies in

the North Greenland Sea and Fram Strait From Satellite Altimetry, SAR and High-Resolution Model Data. *Journal of Geophysical Research: Oceans* **125**(7): e2019JC015832. doi: 10.1029/2019JC015832

Bates NR, Mathis JT, Cooper LW. 2009. Ocean acidification and biologically induced seasonality of carbonate mineral saturation states in the western Arctic Ocean. *Journal of Geophysical Research* **114**(C11): C11007. doi: 10.1029/2008jc004862

Bauch D, Hölemann J, Willmes S, Gröger M, Novikhin A, Nikulina A, Kassens H, Timokhov L. 2010. Changes in distribution of brine waters on the Laptev Sea shelf in 2007. *Journal of Geophysical Research* **115**(C11): C11008. doi: 10.1029/2010JC006249

Bignami F, Hopkins TS. 1997. The water mass characteristics of the Northeast Water Polynya: Polar Sea data 1992 – 1993. *Journal of Marine Systems* **10**(1-4): 139 – 156. doi: 10.1016/S0924-7963(96)00079-6

Bodur YV, Renaud PE, Lins L, Da Costa Monteiro L, Ambrose WG, Felden J, Krumpen T, Wenzhöfer F, Włodarska-Kowalczuk M, Braeckman U. 2024. Weakened pelagic-benthic coupling on an Arctic outflow shelf (Northeast Greenland) suggested by benthic ecosystem changes. *Elem Sci Anth* **12**(1): 00005. doi: 10.1525/elementa.2023.00005

Broecker WS. 1997. Thermohaline Circulation, the Achilles Heel of Our Climate System: Will Man-Made CO $_2$ Upset the Current Balance? *Science* **278**(5343): 1582 – 1588. doi: 10.1126/science.278.5343.1582

Broecker WS, Peng T-H. 1992. Interhemispheric transport of carbon dioxide by ocean circulation. *Nature* **356**(6370): 587 – 589. doi: 10.1038/356587a0

Budéus G, Schneider W. 1995. On the hydrography of the Northeast Water Polynya. *Journal of Geophysical Research* **100**(C3): 4287. doi: 10.1029/94jc02024

Budéus G, Schneider W, Kattner G. 1997. Distribution and exchange of water masses in the Northeast Water polynya (Greenland Sea). *Journal of Marine Systems* **10**(1): 123 – 138. doi: 10.1016/s0924-7963(96)00074-7

Carmack E, Wassmann P. 2006. Food webs and physical – biological coupling on pan-Arctic shelves: Unifying concepts and comprehensive perspectives. *Progress in Oceanography* **71**(2-4): 446 – 477. doi: 10.1016/j.pocean.2006.10.004

Chang BX, Devol AH. 2009. Seasonal and spatial patterns of sedimentary denitrification rates in the Chukchi sea. *Deep Sea Research Part II: Topical Studies in Oceanography* **56**(17): 1339 – 1350. doi: 10.1016/j.dsr2.2008.10.024

Cooper LW, McClelland JW, Holmes RM, Raymond PA, Gibson JJ, Guay CK, Peterson BJ. 2008. Flow-weighted values of runoff tracers (d18O, DOC, Ba, alkalinity) from the six largest Arctic rivers. *Geophysical Research Letters* **35**(18): L18606. doi: 10.1029/2008gl035007

De Steur L, Sumata H, Divine DV, Granskog MA, Pavlova O. 2023. Upper ocean warming and sea ice reduction in the East Greenland Current from 2003 to 2019. *Communications Earth & Environment* **4**(1): 261. doi: 10.1038/s43247-023-00913-3

Dickson AG. 1990. Standard potential of the reaction: AgCl(s) +iH,(g) = Ag(s) + HCl(aq), and and the standard acidity constant of the ion HSOh in synthetic sea water from 273.15 to 318.15 K. *Journal of Chemical Thermodynamics* **22**: 113 – 127. doi: 10.1016/0021-9614(90)90074-Z

Dickson AG, Millero FJ. 1987. A comparison of the equilibrium constants for the dissociation of carbonic acid in seawater media. *Deep Sea Research Part A Oceanographic Research Papers* **34**(10): 1733 – 1743. doi: 10.1016/0198-0149(87)90021-5

Duke PJ, Else BGT, Jones SF, Marriot S, Ahmed MMM, Nandan V, Butterworth B,

Gonski SF, Dewey R, Sastri A, et al. 2021. Seasonal marine carbon system processes in an Arctic coastal landfast sea ice environment observed with an innovative underwater sensor platform. *Elementa: Science of the Anthropocene* **9**(1): 00103. doi: 10.1525/elementa.2021.00103

Ericson Y, Fransson A, Chierici M, Jones EM, Skjelvan I, Omar A, Olsen A, Becker M. 2023. Rapid fCO2 rise in the northern Barents Sea and Nansen Basin. *Progress in Oceanography* **217**: 103079. doi: 10.1016/j.pocean.2023.103079

Farmer JR, Hönisch B, Haynes LL, Kroon D, Jung S, Ford HL, Raymo ME, Jaume-Seguí M, Bell DB, Goldstein SL, et al. 2019. Deep Atlantic Ocean carbon storage and the rise of 100,000-year glacial cycles. *Nature Geoscience* **12**(5): 355 – 360. doi: 10.1038/s41561-019-0334-6

Fay AR, Gregor L, Landschützer P, McKinley GA, Gruber N, Gehlen M, Iida Y, Laruelle GG, Rödenbeck C, Roobaert A, et al. 2021. SeaFlux: Harmonization of air – sea CO2 fluxes from surface pCO2 data products using a standardized approach. *Earth System Science Data* **13**(10): 4693 – 4710. doi: 10.5194/essd-13-4693-2021

Fransson A, Chierici M, Granskog MA, Dodd PA, Stedmon CA. 2023. Impacts of glacial and sea-ice meltwater, primary production, and ocean CO2 uptake on ocean acidification state of waters by the 79 North Glacier and northeast Greenland shelf. *Frontiers in Marine Science* **10**: 1155126. doi: 10.3389/fmars.2023.1155126

Friis K, Körtzinger A, Wallace DWR. 2003. The salinity normalization of marine inorganic carbon chemistry data: THE SALINITY NORMALIZATION OF MARINE INORGANIC CARBON CHEMISTRY DATA. *Geophysical Research Letters* **30**(2). doi: 10.1029/2002gl015898

Gascard J-C, Watson AJ, Messias M-J, Olsson KA, Johannessen T, Simonsen K. 2002. Long-lived vortices as a mode of deep ventilation in the Greenland Sea. *Nature* **416**(6880): 525 – 527. doi: 10.1038/416525a

Henson HC, Holding JM, Meire L, Rysgaard S, Stedmon CA, Stuart-Lee A, Bendtsen J, Sejr M. 2023. Coastal freshening drives acidification state in Greenland fjords. *Science of The Total Environment* **855**: 158962. doi: 10.1016/j.scitotenv.2022.158962

Henson HC, Sejr MK, Meire L, Sørensen LL, Winding MH, Holding JM. 2024. Resolving heterogeneity in CO2 uptake potential in the Greenland coastal ocean. doi: 10.22541/essoar.171052503.36306724/v1

van Heuven S, Pierrot D, Rae J, Lewis E, Wallace DWR. 2011. Program Developed for CO2 System Calculations. Oak Ridge, TN: Carbon Dioxide Information Analysis Center, Oak Ridge National Laboratory, U.S. DoE.

Holding JM, Markager S, Juul-Pedersen T, Paulsen ML, Møller EF, Meire L, Sejr MK. 2019. Seasonal and spatial patterns of primary production in a high-latitude fjord affected by Greenland Ice Sheet run-off. *Biogeosciences* **16**(19): 3777 – 3792. doi: 10.5194/bg-16-3777-2019

Hunt GL, Drinkwater KF, Arrigo K, Berge J, Daly KL, Danielson S, Daase M, Hop H, Isla E, Karnovsky N, et al. 2016. Advection in polar and sub-polar environments: Impacts on high latitude marine ecosystems. *Progress in Oceanography* **149**: 40 – 81. doi: 10.1016/j.pocean.2016.10.004

Iglewicz B, Hoaglin DC. 1993. *Volume 16: How to Detect and Handle Outliers*. La Vergne: ASQ Quality Press.

Jones EM, Chierici M, Menze S, Fransson A, Ingvaldsen RB, Lødemel HH. 2021. Ocean acidification state variability of the Atlantic Arctic Ocean around northern Svalbard. *Progress in Oceanography* **199**: 102708. doi: 10.1016/j.pocean.2021.102708

Jones EP, Anderson LG, Jutterström S, Swift JH. 2008. Sources and distribution of fresh water in the East Greenland Current. *Progress in Oceanography* **78**(1): 37

– 44. doi: 10.1016/j.pocean.2007.06.003

Li Y-H, Tsui T-F. 1971. The solubility of CO $_2$ in water and sea water. *Journal of Geophysical Research* **76**(18): 4203 – 4207. doi: 10.1029/JC076i018p04203

Martin J, Dumont D, Tremblay J-É. 2013. Contribution of subsurface chlorophyll maxima to primary production in the coastal Beaufort Sea (Canadian Arctic): A model assessment: CONTRIBUTION OF SCM IN BEAUFORT SEA. *Journal of Geophysical Research: Oceans* **118**(11): 5873 – 5886. doi: 10.1002/2013JC008843

Mehrbach C, Culberson CH, Hawley JE, Pytkowicx RM. 1973. Measurement of the apparent dissociation constants of carbonic acid in seawater at atmospheric pressure. *Limnology and Oceanography* **18**(6): 897 – 907. doi: 10.4319/lo.1973.18.6.0897

Mellat M, Brunello CF, Werner M, Bauch D, Damm E, Angelopoulos M, Nomura D, Welker JM, Schneebeli M, Granskog MA, et al. 2024. Isotopic signatures of snow, sea ice, and surface seawater in the central Arctic Ocean during the MOSAiC expedition. *Elem Sci Anth* **12**(1): 00078. doi: 10.1525/elementa.2023.00078

Michel C, Hamilton J, Hansen E, Barber D, Reigstad M, Iacozza J, Seuthe L, Niemi A. 2015. Arctic Ocean outflow shelves in the changing Arctic: A review and perspectives. *Progress in Oceanography* **139**: 66 – 88. doi: 10.1016/j.pocean.2015.08.007

Millero FJ. 2013. *Millero, Frank J - Chemical Oceanography, Fourth Edition-CRC Press (2013).pdf*. Fourth. Boca Raton, FL: CRC Press.

Mundy CJ, Gosselin M, Ehn J, Gratton Y, Rossnagel A, Barber DG, Martin J, Tremblay J-É, Palmer M, Arrigo KR, et al. 2009. Contribution of under-ice primary production to an ice-edge upwelling phytoplankton bloom in the Canadian Beaufort Sea. *Geophysical Research Letters* **36**(17): 2009GL038837. doi: 10.1029/2009GL038837

Nakaoka S-I, Aoki S, Nakazawa T, Hashida G, Morimoto S, Yamanouchi T, Yoshikawa-Inoue H. 2006. Temporal and spatial variations of oceanic pCO_2 and air − sea CO_2 flux in the Greenland Sea and the Barents Sea. *Tellus B: Chemical and Physical Meteorology* **58**(2): 148. doi: 10.1111/j.1600-0889.2006.00178.x

Nitishinsky M, Anderson LG, Hölemann JA. 2007. Inorganic carbon and nutrient fluxes on the Arctic Shelf. *Continental Shelf Research* **27**(10-11): 1584 − 1599. doi: 10.1016/j.csr.2007.01.019

Nondal G, Bellerby RGJ, Olsen A, Johannessen T, Olafsson J. 2009. Optimal evaluation of the surface ocean CO2 system in the northern North Atlantic using data from voluntary observing ships. *Limnology and Oceanography: Methods* **7**(1): 109 − 118. doi: 10.4319/lom.2009.7.109

Olafsson J, Olafsdottir SR, Takahashi T, Danielsen M, Arnarson TS. 2021. Enhancement of the North Atlantic CO_2 sink by Arctic Waters. *Biogeosciences* **18**(5): 1689 − 1701. doi: 10.5194/bg-18-1689-2021

Olsen A. 2009. Nordic Seas total alkalinity data in CARINA. *Earth System Science Data* **1**(1): 77 − 86. doi: 10.5194/essd-1-77-2009

Olsen A, Brown KR, Chierici M, Johannessen T, Neill C. 2008. Sea-surface CO2 fugacity in the subpolar North Atlantic. *Biogeosciences* **5**(2): 535 − 547. doi: 10.5194/bg-5-535-2008

Overland J, Dunlea E, Box JE, Corell R, Forsius M, Kattsov V, Olsen MS, Pawlak J, Reiersen L-O, Wang M. 2019. The urgency of Arctic change. *Polar Science* **21**: 6 − 13. doi: 10.1016/j.polar.2018.11.008

Peng T-H, Takahashi T, Broecker WS, Olafsson J. 1987. Seasonal variability of carbon dioxide, nutrients and oxygen in the northern North Atlantic surface water: Observations and a model*. *Tellus B* **39B**(5): 439 − 458. doi: 10.1111/j.1600-0889.1987.tb00205.x

Polyakov IV, Pnyushkov AV, Alkire MB, Ashik IM, Baumann TM, Carmack EC, Goszczko I, Guthrie J, Ivanov VV, Kanzow T, et al. 2017. Greater role for Atlantic inflows on sea-ice loss in the Eurasian Basin of the Arctic Ocean. *Science* **356**(6335): 285 – 291. doi: 10.1126/science.aai8204

Polyakov IV, Rippeth TP, Fer I, Alkire MB, Baumann TM, Carmack EC, Ingvaldsen R, Ivanov VV, Janout M, Lind S, et al. 2020. Weakening of Cold Halocline Layer Exposes Sea Ice to Oceanic Heat in the Eastern Arctic Ocean. *Journal of Climate* **33**(18): 8107 – 8123. doi: 10.1175/JCLI-D-19-0976.1

Qu B, Gabric AJ, Zhu J, Lin D, Qian F, Zhao M. 2012. Correlation between sea surface temperature and wind speed in Greenland Sea and their relationships with NAO variability. **5**(3).

Rajasakaren B, Jeansson E, Olsen A, Tanhua T, Johannessen T, Smethie WM. 2019. Trends in anthropogenic carbon in the Arctic Ocean. *Progress in Oceanography* **178**: 102177. doi: 10.1016/j.pocean.2019.102177

Richter-Menge J, Overland JE, Mathis JT, Osborne E, Brown R, Mudryk L, Luojus K, Helfrich S. 2017. Arctic Report Card 2017.

Robbins PE. 2001. Oceanic carbon transport carried by freshwater divergence: Are salinity normalizations useful? *Journal of Geophysical Research: Oceans* **106**(C12): 30939 – 30946. doi: 10.1029/2000JC000451

Rudels B, Björk G, Nilsson J, Winsor P, Lake I, Nohr C. 2005. The interaction between waters from the Arctic Ocean and the Nordic Seas north of Fram Strait and along the East Greenland Current: Results from the Arctic Ocean-02 Oden expedition. *Journal of Marine Systems* **55**(1-2): 1 – 30. doi: 10.1016/j.jmarsys.2004.06.008

Rysgaard S, Bendtsen J, Pedersen LT, Ramløv H, Glud RN. 2009. Increased CO2 uptake due to sea ice growth and decay in the Nordic Seas. *Journal of Geophysical Research* **114**(C9): C09011. doi: 10.1029/2008JC005088

Rysgaard S, Vang T, Stjernholm M, Rasmussen B, Windelin A, Kiilsholm S. 2003. Physical Conditions, Carbon Transport, and Climate Change Impacts in a Northeast Greenland Fjord. *Arctic, Antarctic, and Alpine Research* **35**(3): 301 – 312. doi: 10.1657/1523-0430(2003)035[0301:PCCTAC]2.0.CO;2

Sejr MK, Krause-Jensen D, Rysgaard S, Sørensen LL, Christensen PB, Glud RN. 2011. Air—sea flux of CO_2 in arctic coastal waters influenced by glacial melt water and sea ice. *Tellus B: Chemical and Physical Meteorology* **63**(5): 815 – 822. doi: 10.1111/j.1600-0889.2011.00540.x

Serreze MC, Barry RG. 2011. Processes and impacts of Arctic amplification: A research synthesis. *Global and Planetary Change* **77**(1-2): 85 – 96. doi: 10.1016/j.gloplacha.2011.03.004

Shiklomanov A, Déry S, Tretiakov M, Yang D, Magritsky D, Georgiadi A, Tang W. 2021. River freshwater flux to the arctic ocean. In: Yang D, Kane DL, editors. *Arctic Hydrology, Permafrost and Ecosystems*. Cham: Springer International Publishing. p. 703 – 738. doi: 10.1007/978-3-030-50930-9₂4

Smethie JWM, Fine RA. 2001. Rates of North Atlantic Deep Water formation calculated from chlorofluorocarbon inventories. : 27.

Stroh JN, Kirillov S, Panteleev G, Francis O, Yaremchuk M, Bloshkina E, Lebedev N. 2019. Changes in Arctic Ocean Climate Evinced through Analysis of IPY 2007 – 2008 Oceanographic Observations. In: Kanao M, Kakinami Y, Toyokuni G, editors. *Arctic Studies - A Proxy for Climate Change*. IntechOpen. doi: 10.5772/intechopen.80926

Sumata H, De Steur L, Gerland S, Divine DV, Pavlova O. 2022. Unprecedented decline of Arctic sea ice outflow in 2018. *Nature Communications* **13**(1): 1747. doi: 10.1038/s41467-022-29470-7

Takahashi T, Olafsson J, Goddard JG, Chipman DW, Sutherland SC. 1993. Seasonal

variation of CO_2 and nutrients in the high-latitude surface oceans: A comparative study. *Global Biogeochemical Cycles* **7**(4): 843 – 878. doi: 10.1029/93GB02263

Takahashi T, Sutherland SC, Chipman DW, Goddard JG, Ho C, Newberger T, Sweeney C, Munro DR. 2014. Climatological distributions of pH, pCO2, total CO2, alkalinity, and CaCO3 saturation in the global surface ocean, and temporal changes at selected locations. *Marine Chemistry* **164**: 95 – 125. doi: 10.1016/j.marchem.2014.06.004

Takahashi T, Sutherland SC, Sweeney C, Poisson A, Metzl N, Tilbrook B, Bates N, Wanninkhof R, Feely RA, Sabine C, et al. 2002. Global sea – air CO2 flux based on climatological surface ocean pCO2, and seasonal biological and temperature effects. *Deep Sea Research Part II: Topical Studies in Oceanography* **49**(9-10): 1601 – 1622. doi: 10.1016/s0967-0645(02)00003-6

Takahashi T, Sutherland SC, Wanninkhof R, Sweeney C, Feely RA, Chipman DW, Hales B, Friederich G, Chavez F, Sabine C, et al. 2009. Climatological mean and decadal change in surface ocean pCO2, and net sea – air CO2 flux over the global oceans. *Deep Sea Research Part II: Topical Studies in Oceanography* **56**(8-10): 554 – 577. doi: 10.1016/j.dsr2.2008.12.009

Tuerena RE, Mahaffey C, Henley SF, De La Vega C, Norman L, Brand T, Sanders T, Debyser M, Dähnke K, Braun J, et al. 2022. Nutrient pathways and their susceptibility to past and future change in the Eurasian Arctic Ocean. *Ambio* **51**(2): 355 – 369. doi: 10.1007/s13280-021-01673-0

Wadhams P, Holfort J, Hansen E, Wilkinson JP. 2002. A deep convective chimney in the winter greenland sea. *Geophysical Research Letters* **29**(10). doi: 10.1029/2001GL014306

Wallace DWR, Behrens WJ, Hopkins TS, Kinder C, Deming J, Smith WO, Top Z, Walsh ID. 1995. Collaborative research on the Northeast Water Polynya: NEWP92 hydrographic data report. USCGC Polar Sea cruise, July 15 – August 15, 1992.

Report No.: BNL – 61923, 102497. doi: 10.2172/102497

Wallace DWR, Minnett PJ, Hopkins TS. 1995. Nutrients, oxygen, and inferred new production in the Northeast Water Polynya, 1992. *Journal of Geophysical Research* **100**(C3): 4323. doi: 10.1029/94JC02203

Weiss RF. 1970. The solubility of nitrogen, oxygen and argon in water and seawater. *Deep Sea Research and Oceanographic Abstracts* **17**(4): 721 – 735. doi: 10.1016/0011-7471(70)90037-9

Willcox E, Bendtsen J, Mortensen J, Mohn C, Lemes M, Pedersen T-J, Holding J, Møller EF, Sejr MK, Seidenkrantz M-S, et al. 2023. An Updated View of the Water Masses on the Northeast Greenland Shelf and Their Link to the Laptev Sea and Lena River. *Journal of Geophysical Research: Oceans* **128**(4): e2022JC019052. doi: 10.1029/2022JC019052

Wright DG, Pawlowicz R, McDougall TJ, Feistel R, Marion GM. 2010. Absolute Salinity, "Density Salinity" and the Reference-Composition Salinity Scale: Present and future use in the seawater standard TEOS-10. All Depths/Operational Oceanography/All Geographic Regions/Temperature, Salinity and Density Fields. doi: 10.5194/osd-7-1559-2010

Yager PL, Wallace DWR, Johnson KM, Smith WO, Minnett PJ, Deming JW. 1995. The Northeast Water Polynya as an atmospheric CO_2 sink: A seasonal rectification hypothesis. *Journal of Geophysical Research* **100**(C3): 4389. doi: 10.1029/94JC01962

Yamamoto-Kawai M, Tanaka N, Pivovarov S. 2005. Freshwater and brine behaviors in the Arctic Ocean deduced from historical data of δ18O and alkalinity (1929 – 2002 A.D.). *Journal of Geophysical Research: Oceans* **110**(C10). doi: 10.1029/2004JC002793

Yasunaka S, Siswanto E, Olsen A, Hoppema M, Watanabe E, Fransson A, Chierici M,

Murata A, Lauvset SK, Wanninkhof R, et al. 2018. Arctic Ocean CO2 uptake: An improved multiyear estimate of the air − sea CO2 flux incorporating chlorophyll a concentrations. *Biogeosciences* **15**(6): 1643 − 1661. doi: 10.5194/bg-15-1643-2018

Zeebe RE, Wolf-Gladrow DA. 2001. *CO_2 in Seawater: Equilibrium, Kinetics, Isotopes*. Amsterdam ; New York: Elsevier. (Elsevier oceanography series; Vol. 65).

Zhuang Y, Jin H, Cai W-J, Li H, Jin M, Qi D, Chen J. 2021. Freshening leads to a three-decade trend of declining nutrients in the western Arctic Ocean. *Environmental Research Letters* **16**(5): 054047. doi: 10.1088/1748-9326/abf58b

Zhuang Y, Jin H, Cai W-J, Li H, Qi D, Chen J. 2022. Extreme Nitrate Deficits in the Western Arctic Ocean: Origin, Decadal Changes, and Implications for Denitrification on a Polar Marginal Shelf. *Global Biogeochemical Cycles* **36**(7): e2022GB007304. doi: 10.1029/2022GB007304

5 A year of hydrographic variability in a fjord in Northeast Greenland

Co-authors: Lise Lotte Sørensen, Eugenio Ruiz Castillo, Wieter Boone, Søren Rysgaard

preparing to publish

5.1 Abstract

The Arctic Ocean receives about 11% of the world's river runoff. This, combined with freshwater from increasing melting of sea ice and Greenland's glaciers, is leading to rapid freshening of the region. This accumulation of freshwater alters the physical and biogeochemical dynamics of the ocean and can potentially disrupt the thermohaline circulation, which plays a critical role in regulating global climate. Freshening also affects marine ecosystems, but predicting the overall impact is difficult due to the complexity of the processes involved. Here we present a year long multi-disciplinary dataset from a fjord in Northeast Greenland collected through the Greenland Integrated Observing System (GIOS) comprising of an oceanographic mooring, a water sampler, and a weather station. Together these data show that peak freshwater is achieved in late September at 11 m while at 50 m it is reached in mid-October. This indicates that there is a month difference or delay between the freshwater export in the different layers within the Polar (Surface) Water. Landfast ice covers the fjord from 09 November, as indicated by a lack of scatter in the upward facing altimeter data. The salinity steadily increases throughout winter

though the water column remains stratified between 11 and 50 m depth. Two high salinity events occur in winter and have durations of 9 and 6 days respectively. We hypothesize that these events are caused by advection from an as yet unknown event. The stable water isotope data do not support brine formation as the most likely origin of the salinity increase and therefore this water must be transported from elsewhere.

Piteraq, katabatic winds that form from higher density air masses resulting from cooling across the ice sheet and can reach high speeds, dominate the wind system from October to April. Between May and August there is a shift to along-shelf and along-shore wind prevalence. Ice break-up occurs on 2 July and is associated with increased wind speed. We expect that the highly stratified fjord water observed will be exported onto the shelf and contribute to the overall stratification and freshening of the region.

5.2 Introduction

Fjords in Northeast Greenland are experiencing rapid change. Not only is the Greenland Ice Sheet experiencing accelerated mass loss (Rignot et al., 2008; Velicogna, 2009), but waters advected into the fjords from the shelf are subject to changes in Arctic freshwater discharge (Shiklomanov et al., 2021), increased North Atlantic heat content (Polyakov et al., 2023) and sea ice melt (Polyakov et al., 2017) Northeast Greenland coastal shelf waters are experiencing significant coastal freshening on decadal scales as a result (Sejr et al., 2017). These processes influence the freshwater hydrography and dynamics inside Northeast Greenland fjords in response to climate change.

In general, freshwater is added at the head of the fjords in summer by glacial discharge and rivers, and sea ice melting along the entire fjord surface. In winter freshwater input is reduced to only subglacial discharge from friction and pressure melting (Benn and Evans, 2014) while sea ice is formed at the surface and removes

freshwater from the system. As a result of this change in forcing, shelf waters,~consisting mainly of Arctic Ocean derived water that is heavily influenced by freshwater input from Arctic rivers (Paffrath et al., 2021; Willcox et al., 2023; Gjelstrup et al., 2024) , are transported into the fjords (Fraser et al., 2018; Jackson et al., 2018).

The waters surrounding Greenland are associated with several of the major climate tipping points (CTPs) identified by the IPCC (IPCC, 2023) and others (Armstrong McKay et al., 2022; Wunderling et al., 2024). Each of the proposed tipping point events is connected to the presence of freshwater in the system: the slowing of the Atlantic Meridional Overturning Circulation (AMOC) through enhanced stratification at the Irminger and Labrador sea convection areas where overturning relies on an initial weak stratification at the surface (De Jong et al., 2018), the collapse and melting of the Greenland ice sheet resulting in global sea level rise (Aschwanden et al., 2019), and reductions in the extent and thickness of Arctic sea ice through the impact of freshwater on stratification and the associated trapping of heat (Jackson et al., 2010; Polyakov et al., 2013; Brown et al., 2020) and the amount of salty brine that is exported to depth. Northeast Greenland fjord systems lie at the intersection of these processes, necessitating improved monitoring.

The interactions between these different freshwater sources within Northeast Greenland fjords have not been described in detail. Much of the existing research in the region focuses either on the innermost fjord in a fjord complex where terrestrial input dominates the dynamics (Rooijakkers, 2024), or on the coast where shelf water has a larger influence (Sutherland and Cenedese, 2009; Fraser et al., 2018; Jackson et al., 2018; Rysgaard et al., 2024). Even when investigations span the length of a fjord system, they frequently focus on the summer and fall seasons when they can be accessed (Sejr et al., 2017; Holding et al., 2019). Questions remain regarding the behaviour and residence time of locally produced freshwater and how seasonal dynamics impact stratification.

The data we present in this study are the first full year of high resolution data (August 2022 to July 2023) from a container monitoring system developed as part of the long-term Greenland Integrated Observing System (GIOS) study (Rysgaard et al., 2022). This container is located at Ella Ø in Northeast Greenland (Figure 5.1)

which lies at the intersection between inland fjords (north and west) and those connected directly to the shelf (south and east). We focus on the seasonal variability of surface (0-50 m) freshwater. We highlight an increase in freshwater discharge during summer and late autumn, followed by its slow removal during the winter season interspersed by several high salinity events.

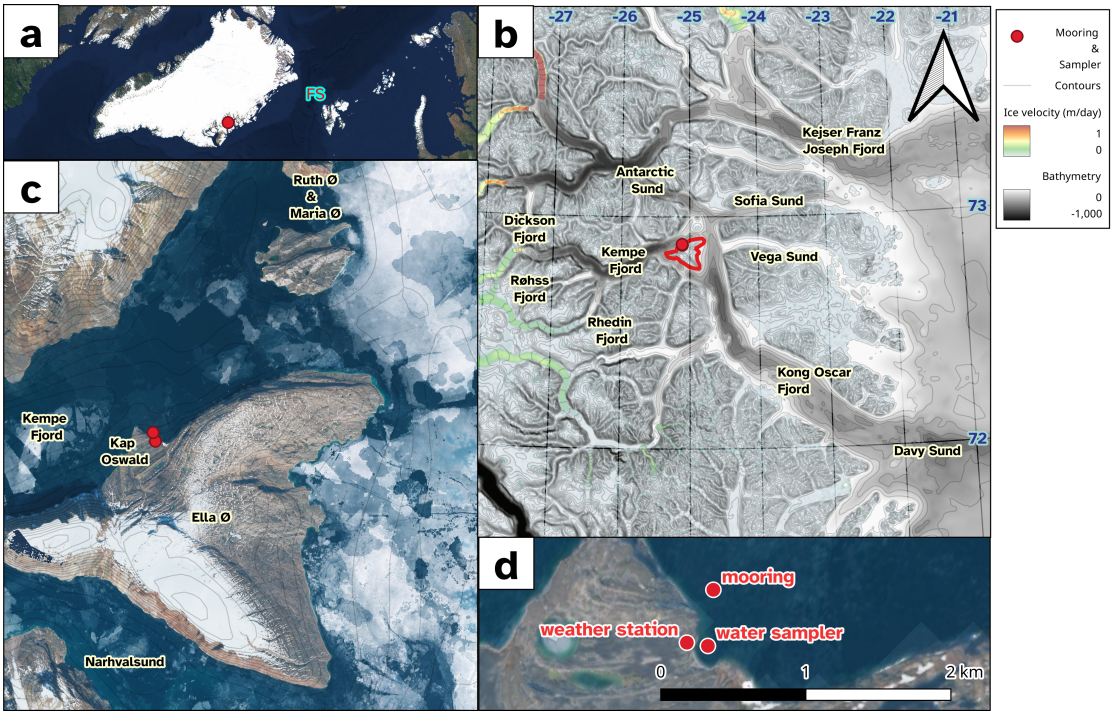

Figure 5.1: Mooring and water sampler location(s), a. In Greenland (FS is Fram Strait), b. in the fjord system, c. Ella Ø and its direct surroundings, d. Precise location of equipment. The ice velocity, contours, terrestrial hydrology, and bathymetry (a,b) are from QGreenland (Moon et al., 2022), and satellite image is from EOX IT Services GmbH (2022)

5.3 Background

Ella Ø is located at the intersection between several fjords. In the south to south-east direction is Kong Oscar Fjord (Figure 5.1) which is directly connected to the Northeast Greenland continental shelf via Davy Sund. Kong Oscar Fjord lacks the shallow sill that can be found in some fjord environments (Pickard and Stanton,

1980; Bao and Moffat, 2024). Without this depth restriction, more shelf water is able to enter. Other fjords that are connected to the shelf from where water could be advected to Ella Ø and up-fjord into Kempe fjord and have connections to the shelf are more restricted in depth; Antarctic Sund to ~300 m at its head, Sofia Sund and Vega Sund to ~200 m in the main fjords and ~100 m at the mouth. Water found at deeper depths, particularly that with Atlantic Water characteristics, is therefore most likely sourced from the deeper silled Kong Oscar Fjord though no existing observations have explicitly confirmed this. Shelf water has a multilayered structure as a result of meteoric input and the annual sea ice melt-freeze cycle in the upstream Arctic Ocean consists primarily of the denser and deeper Atlantic Water (AW) and more buoyant Pacific Water (PW) (Willcox et al., 2023; Rysgaard et al., 2024). The former includes water from both the Arctic Ocean and from the West Spitsbergen Current (WSC). PW includes all water with densities equal to or lower than that of the lower halocline at 1027.2 kg m^{-2} (Rudels, 2022). The majority of PW follows the freezing line in the form of the Cold Halocline Layer (CHL) to the density of the Surface Mixed Layer (SML) which has a thickness (and temperature) that varies seasonally (Peralta-Ferriz and Woodgate, 2015). The summer SML on the Northeast Greenland shelf varies from 10 to 30 m thickness below which the CHL extends to between 70 and 100 m depth (Budéus and Schneider, 1995; Willcox et al., 2023).

The input of deeper water, particularly AW, from Kong Oscar Fjord to the mooring location is limited by the bathymetry surrounding Ella Ø. The maximum depths are ~ 200 m between the smaller islands (Maria Ø and Ruth Ø) to the north-east and through the Narhvalsund channel to the west with depths restricted to 222 m. Antarctic Sund to the north is connected to Isfjord and Kjerulf Fjord, each of which receive glacial input, and a more distant connection to the shelf via Kejser Franz Joseph Fjord. To the east are Sofia Sund (~240 m), and Vega Sund (~10 m). The main up-fjord influence on the mooring location is Kempe fjord to the west and its source fjords (Dickson, Røhss, and Rhedin). Kempe fjord is deep with maximum depths of ~820 m. Dickson fjord is also deep (~700 m) and receives freshwater from a tidewater glacier at its head. The two others are shallower (~30 and ~200 m respectively) and have riverine hydrology at their heads. Though Rhedin valley contains a land-terminating glacier, Røhss does not.

Fjord hydrography in idealized fjords is thought to be a function of outflowing surface water driving a two layer estuarine circulation in an along-fjord direction (Stigebrandt, 1981; Farmer and Freeland, 1983) that depends on the width of the fjord and the depth of the sill at the entrance. Whether cross-fjord circulation plays a role is thought to depend on the Rossby radius or on secondary flow dynamics (Valle-Levinson, 2010). In Arctic fjords, katabatic wind forcing can play a large role in fjord circulation during periods of open water (Cottier et al., 2010).

The summer hydrography in Dicksonfjorden, upstream of the mooring location, is typical of that seen in other Greenland fjords (Rysgaard et al., 2003; Rooijakkers, 2024). At the surface there is a layer of locally discharged freshwater and sea ice melt of ~ 10 m thick (the summer SML) which overlies a sub-surface water structure similar to that found on the shelf, including PW and AW. (Gjelstrup et al., 2022; Willcox et al., 2023). Basin Water is likely present but there has been no study of the full depth of the surrounding fjords with which to verify this. The halocline associated with the CHL-AW boundary occurs a depth of ~ 100 m and a salinity of ~ 32.5. Salinities at depths below this increase until they stabilize near 34.8 with temperatures increasing up to 1 °C, indicating this is Transformed AW from the Arctic Ocean rather than recirculating AW sourced from the WSC (Rooijakkers, 2024). Kong Oscar fjord downstream also shows superposition of water masses associated with the Northeast Greenland shelf including the CHL. The range of salinities at freezing temperatures that form the CHL may be increasing and has been associated with increased freshening of the surface layer during the previous decades. In 2018 the hydrography included an eroded LHW at S ~ 34, and a boundary between the SML and the top of the CHL (remnant of the winter mixed layer) at S ~ 32 (Gjelstrup et al., 2022), where during low sea ice years it has been measured to be as low as 31.4 on the Northeast Greenland shelf (Willcox et al., 2023).

We have only sparse measurements of the stratification in Northeast Greenland fjords during winter (Rysgaard et al., 2003; Dmitrenko et al., 2015; Boone et al., 2017; Boone et al., 2018) and can't observe the circulation below the landfast ice in winter from satellites.

5.4 Methods

5.4.1 Data collection

5.4.1.1 Ocean

This study includes two moorings and a weather station. A cabled observatory was installed in the seasonally ice-covered Kempe fjord near Ella Ø ($72°52.907'N$, $25°06.779'W$). The observatory consists of an inductive link and sensors, an anchor, acoustic release, dyneema lines and buoyancy floats. The inductive link had a topside and subsea inductive modem (Develogic) interlinked with an inductive cable (horizontal length: 1 km, vertical: 16 m) and a swivel. The interfaced sensors, connected to the subsea inductive modem, consisted of a multiparameter ocean sensor and an upward-looking acoustic doppler current profiler (ADCP). Various instrumentation can be attached to the inductive link. In the present setup we selected a Nortek Signature 500 kHz ADCP instrument to be deployed at 36 m depth in a protective buoy for telemetering hourly averaged velocity profiles and for 12 hourly derived ice keel and drift measurements. The RBRconcerto CTD instrument deployed at 50 m depth was selected for conductivity, temperature, and depth (pressure) recordings. Both sensors streamed serial data to the subsea unit which forwarded the data to the topside unit where it was stored until the topside unit was interrogated by the marine container telemetry software for data submission to the servers. The mooring setup further consisted of a 200 kg steel H-bar connected to an acoustic release (Edgetech Port LF) and 2 trawlers (1 3.2 kg + 1 8.4 kg) which functioned as buoyancy. The nodes were connected via dyneema lines of 7.95 mm. More details on the setup are provided by (Rysgaard et al., 2022). The water sampler mooring that was deployed nearer the coast ($72°52.710'N$, $25°06.543'W$) contained a Sea-bird SBE37SM MicroCAT with RS-232 interface CTD and an automatic water sampler (Poulsen et al., n.d.) deployed at a depth of 11 m and sampling weekly. The stable hydrogen and oxygen isotope concentrations in the collected water samples were determined using a Cavity Ringdown Spectrometer, L2130-i Isotopic sH20

(Picarro Inc., USA). All instruments were factory calibrated prior to deployment. Sensors and accuracies are provided in Table Table 5.1.

Table 5.1: Sensor details for the moorings deployed near Ella Ø. RBR Concerto and Seabird SBE 911 plus CTDs and the Nortek Signature 500 ADCP

device	**sensor**	**range**	**initial accuracy (+/-)**	**unit**
rbr concerto	temperat-ures	-5 to 35	0.002	°C
	conductivity	0 to 85	0.003	mS/cm
	pressure	20 - 740 (dbar)	0.05	%
sbe 37SM	temperature	-5 to 45	0.002	°C
	conductivity	0 to 7	0.0003	S/m
	pressure	0 - 7000 (m)	0.1 of full scale range	%
sig. 500	temperature	-4 to 40	0.1	°C
	compass		2° for tilt < 30	Hz
	tilt		0.2° for tilt < 30	Hz
	pressure	0 to 500 (m)	0.1	%
	velocity	0.5 to 70	0.3 +/- 0.3cm	%

5.4.1.2 Atmosphere

Instruments for measurements of climatology, meteorology and surface fluxes were collected from a 6-meter mast close to the moorings (72°52.688N, 25°06.8W). The ambient relative humidity and air temperature were measured with a HMP155 Humidity and Temperature probe manufactured by Vaisala Oyj, Finland. Skin temperature was measured with an Infrared Radiometer, model SI-100-SS manufactured by Apogee Instruments, Utah, USA. The sensor was mounted on top of the mast in an angle to measure the skin temperature of the fjord. PAR was measured with Quantum Sensor, model LI-190/R from Li-Cor Bioscience, Nebraska, USA. The PAR sensor was mounted on the mast at 6 m height above ground on an aluminium-boom pointing towards east. Net radiation was measured with a Net Radiometer model NR

Lite 2 manufactured by Kipp & Zonen B.V., The Netherlands. The global radiation was measured with a CMP 10 pyranometer manufactured by Kipp & Zonen B.V., The Netherlands. All radiation instruments, temperature and humidity sensors were connected to a Campbell datalogger, model CR1000X for data collection. Data was stored each 5 minutes. The datalogger was connected to a server in the marine container with an 30 m long cable where data was stored and transmitted via Iridium satellite together with the marine data.

5.4.1.3 ERA5 atmospheric re-analysis data

ERA5 hourly pressure level gridded re-analysis data were downloaded for the 1000 hPa pressure level from the Copernicus climate data store. The data has a 0.25° x 0.25° horizontal resolution and where shown here are data from the cell at longitude -25.38° and latitude 72.98°.

5.4.2 Data analysis

After collection the raw data (as .ad2p files) were processed. The ad2p data file format contains flags for whether data are considered valid by the instrument. Each data file was converted to two (dual profile) NetCDF files using the Dolfyn module in the MHKiT-Python package (Pauly et al., 2024). The Dolfyn module performs corrections such as frame rotation, and declination and motion correction which were applied. The correlation filter threshold was set to 50%. The declination was set for the mooring coordinates. The produced NetCDF files were concatenated using Memory Mapped IO and further analysed in the Julia programming language.

Raw data from the CTDs, weather station, and automatic water sampler were read into Julia directly from CSV. All data are presented unless stated otherwise. Time averaged dataframes were created for all data excluding the weekly automatic water samples using TimeArrays.jl for running mean averaged hourly, daily, and weekly time intervals. Unless otherwise specified, hourly averaged data is used in this manuscript. The averaging process also removed any outliers.

Tides were analysed using the Utide (Codiga, 2011) python package both for the CTD pressure gauges and for u,v ADCP velocity data.

5.4.2.1 Notes on the data

Some issues with the data were identified. This includes an issue of lower battery voltage during winter affecting the weather station, leading to a loss of some data during the winter season. A separate issue affected the storage of all but 50 measurements of salinity at the deeper CTD after 31/04/2023.

The start and end of persistent land-fast sea ice cover was identified by a sudden loss of scatter in the leading edge altimeter data. During the open water season, as verified by satellite imagery not included in this study, the sea ice draft measured through this method was 0.5 m. Since the visual spectrum satellite data did not show any sea ice or mélange cover at this time, the source of this discrepancy can not been explained. Only during the period of the freshwater peak in late autumn, the sea ice draft goes to 0 m. It is possible that a 0.5 m freshwater lens was present at the surface with such a density difference that it acted as a strong reflector to the altimeter which was subsequently broken down during the period of peak freshwater, but there is no way to verify that this was the case. The thickness observation of 0.5 m ice draft resumes directly after ice break up in spring and will require further analysis in future data collection.

5.5 Results

The container deployment at Ella Ø includes a weather station and two moorings in a remote climate sensitive area downstream the major outlet of the Arctic Ocean. The data here represent the first year of deployment from September 2022 to early August 2023. Vertical lines in all timeseries plots are as follows: fw1 and fw2 are peaks in freshwater during September, lfo is landfast ice onset, br1 and br2 are increased salinity events during the period of fast ice cover, and sp1 and sp2 are events in spring associated with melting.

5.5.1 Hydrography

The hydrography near Kap Oswald north of Ella Ø follows a seasonal pattern in terms of temperature and salinity (Figure 5.2). During autumn, water temperatures nearer the surface are high (~ 3 °C) and salinities are low (~ 28). The peak in freshwater observed at the 11 m CTD occurs at fw1 on 25 September 2022, prior to which a temperature increase is observed. Directly after this peak the temperature at 11 m drops swiftly and continues to do so at a rate of (on average) -0.06 °C per day until December 1st when it approaches freezing temperatures. Freshening and an increase in temperature away from the freezing line occur simultaneously at the 50 m CTD starting at fw1, and reaching its peak at 13 October 2022 (fw2) after which it follows cooling at a similar rate to the CTD at 11 m.

Freeze-up is associated with a sudden decrease in scatter in the hourly averaged leading edge altimeter distance (Figure 5.2 c) and occurs on 09 November 2022 (lfo). Salinities at both CTDs continue to increase after this date. Two events occur at 11 m during winter, at 06 January 2023 (br1), and 22 February 2023 (br2) respectively when the salinity increases to similar values as the 50 m CTD. These events are associated with a simultaneous increase in temperature. Nonetheless, the system recovers and remains stratified until spring. The maximum ice thickness in winter is estimated at 1.5 m and is achieved in late April.

Observations of $\delta^{18}O$ (Figure 5.2 d) display some scatter, especially in autumn when the values are on average increasing. The fluctuations display a weekly periodicity during this time of more and less negative values. At event br1, the $\delta^{18}O$ jumps almost 1 ‰ to values near -2.5 ‰. The slope around which the $\delta^{18}O$ fluctuates is also reduced. On 21 June 2023 there is a sudden decrease in $\delta^{18}O$ of around 1 ‰. The system takes an additional three weeks to recover back to values near -2.5 ‰. This is also when the temperature at the 11 m CTD starts to increase.

Ice breakup, identified by a sudden increase in scatter in the leading edge altimeter distance (Figure 5.2 c) occurs at 07 July 2023 (sp2). Water temperatures at 11 m depth do not start approaching 0 °C until a week later. The leading ice edge thickness prior to the first freshwater event and after sea ice melt of 0.5 m is not

interpreted as sea ice or melange, nor as the surface, but as open water which acts as a strong reflector, potentially due to extreme differences in salinity. The lack of sea ice and melange cover was verified by using satellite imagery. The disappearance of this reflector is interpreted as the breakdown of what was creating the strong reflector. The reflector immediately resumes in spring after sea ice melt.

Tides at Ella Ø are semi-diurnal. Utide predicted extrema (-1.05, 0.85 m), i.e. spring tides, based on the 11 m CTD depth observations match well to the extrema in the observations (-1.05 to 0.98 m) at the 11 m CTD. Neap tide heights are around 0.3 m. Tidal frequencies, amplitudes, phases, and signal to noise ratios are shown in Table 5.2. The semi-diurnal lunar tide (M2) is the dominant tidal harmonic constituent and is responsible for almost 0.5 m of the tide height. The solar diurnal constituent (S2) is responsible for an additional 0.2 m of amplitude.

Table 5.2: Tides as calculated from the pressure gauge in the 11 m CTD mounted on the water sampler. The name refers to the two character acronym for the tidal constituent, e.g. M2 is principal lunar and S2 is principal solar. Amplitude refers to vertical distance to the centre line (mean tide level), the frequency is the inverse of the period of the wave, and the phase refers to the horizontal phase shift of the wave.

Name	Frequency	Amplitude (m)	Phase (°)
M2	0.081 ± 0.0	0.497±0.001	333.3±0.12
S2	0.083 ± 0.0	0.195±0.001	46.13±0.29
N2	0.079 ± 0.0	0.097 ±0.001	293.2±0.61
K1	0.042 ± 0.0	0.085±0.001	97.0 ±0.73
O1	0.039 ± 0.0	0.084±0.001	33.78±0.64
K2	0.084 ± 0.0	0.055±0.001	46.22±0.91

5.5.2 Winds and currents

The dominant wind directon during winter is from west to southwest starting in October and ending in April Figure 5.3.. After this the wind direction is from the

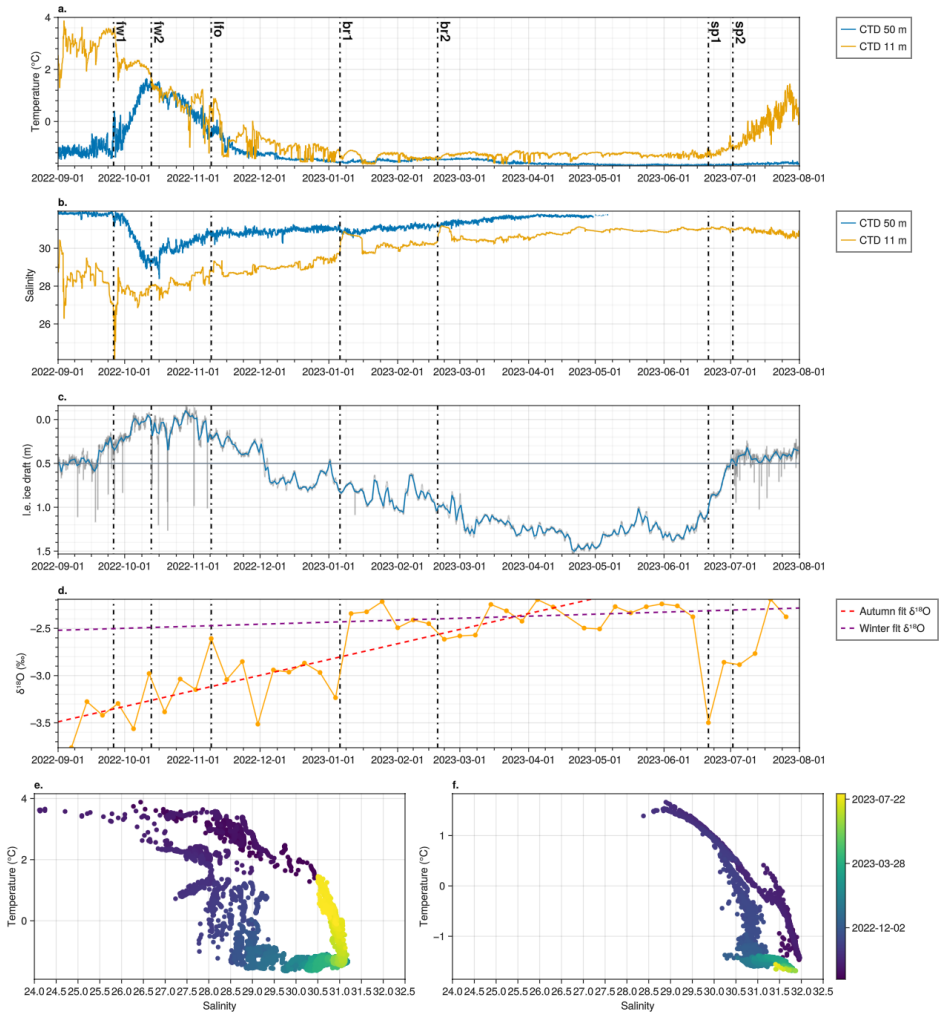

Figure 5.2: Hydrographic parameters. a. Water temperature for both deplyed CTDs, b. Practical salinity c. ice draft (pressure - leading edge altitude), d. stable oxygen isotopes (w.r.t. VSMOW2) with a linear fit for dates up to event br1 and from event br1 up to to event sp1, d. and e. are *TS* diagrams for the CTDs deployed at 11 and 50 m respectively

northeast until August when it starts to shift back. Wind speeds are highest during the period with the fewest measurements in January and February.

Current roses show water primarily flowing southeast though from May onward there are more frequent currents toward the west. Overall, the current speeds increase during the first two months of observations. Increased speeds precede both freshwater peak events, and is particularly pronounced prior to fw1. Both are also associated with a change in direction to ~ 270°. During winter the highest current speeds occur in the first week in February. Both increased salinity events (br1 and br2) are associated with a change in current direction. From May onward current speeds are low.

5.5.3 Atmospheric changes

Incoming radiation, air temperature, relative humidity, and local air pressure are shown in Figure 5.4. In terms of incoming radiation and PAR there is a clear seasonal pattern with receding daylight during autumn, a dark winter, and increasing incoming radiation in spring which reaches a maximum at midsummer. Both spring events, though particularly the second (sp2), are associated with very prominent drops in incoming radiation.

The air temperature drops in autumn from around 10°C, and remains on average just above freezing during late September and early October. In the second week of October, the temperature drops but starts to rise at the time of the second freshwater event (fw2) to a maximum of 10 °C almost one week later. By the last week of October temperatures have dropped to average below freezing. They remain low until the third week of May. Local measurements in March and April, and during the first spring event (sp1) are lower than those in the ERA5 re-analysis data. During the second spring event (sp2) the temperature jumps briefly to over 10 °C.

The average relative observed humidity is 70.86 ± 17.4 % though at the first freshwater event in autumn (fw1) drops down to below 20 %. Conversely, the second event is associated with an increase to 80 % immediately followed with another drop to around 30 %. Re-analysis and local measurements are fairly similar until

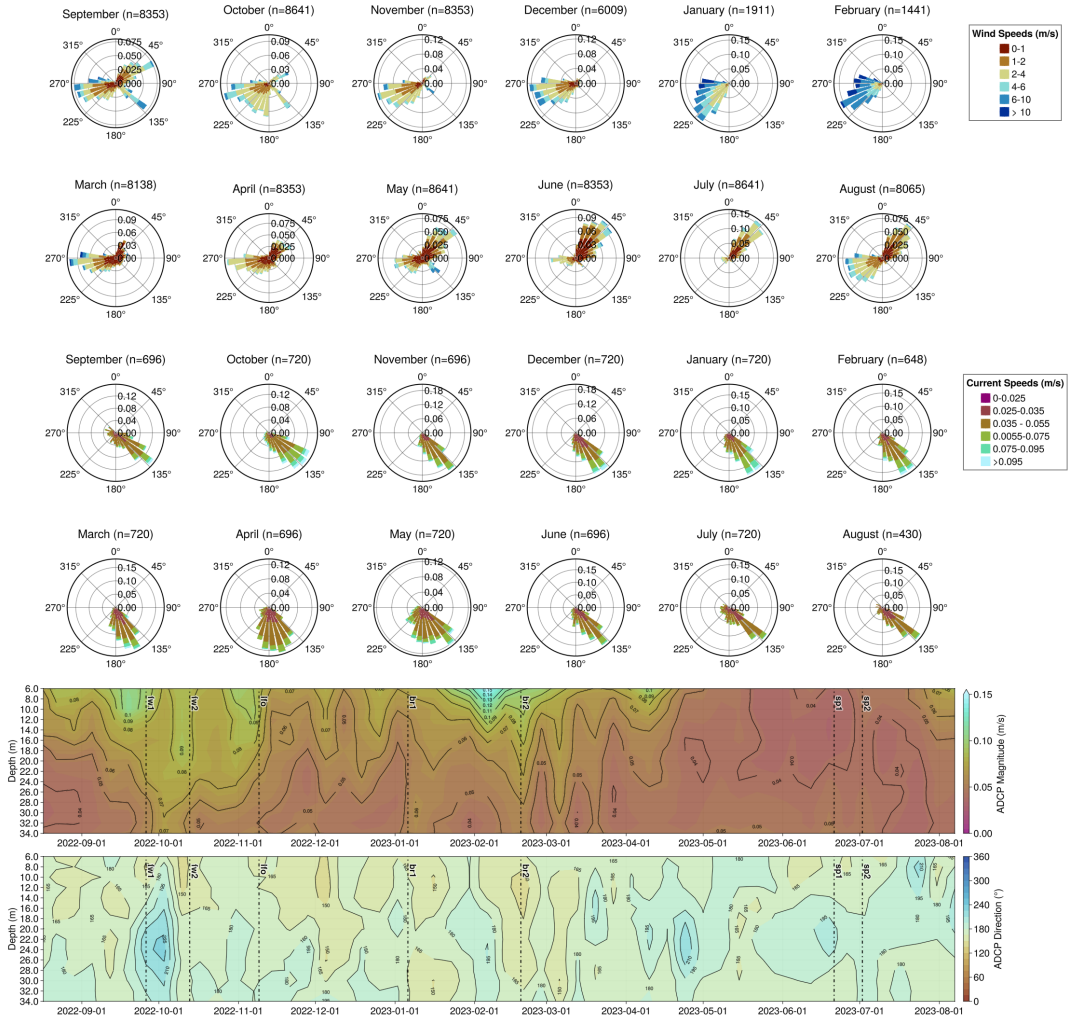

Figure 5.3: Wind roses (top 2 rows) for each month including the number of datapoints available (n) for the weather station, ADCP hourly current roses (rows 3 and 4) second for the 6 - 8 m depth bin, and ADCP weekly averaged current speed (fifth row) and direction (bottom row) for Ella Ø between September 2022 and August 2023

spring. Although little data is available during the increased salinity events (br1 and 2), ERA5 data indicate that both events are associated with a drop in relative humidity though this only persists for a week just after the first. During the two events in spring, weather station relative humidity drops, though only in the second event by as much as 60%.

Air pressure tends to be over 100 kPa throughout the measurement period. The second freshwater event (fw2) is associated with a change in atmospheric pressure from ~ 100 kPa to 104 kPa. This occurs simultaneously to the increase in air temperature at this time. After the onset of landfast sea ice (lfo) local observations of pressures show an increase in amplitudes generally. One events stands out, in the second week of December where air pressures of > 105 hPa are observed. This is again associated with an increase in temperatures to > 0 °C followed by a drop in air pressure that is associated with cooling of below -20 °C. Air pressure increases in late March and remains high throughout April and into May. In spring, the second event (sp2) sees an increase in atmospheric pressure and warm air.

5.6 Discussion

We present a year of observations of the water column and atmosphere just north of Ella Ø in East Greenland. The island is located at the intersection of several fjords, some fed by glaciers and rivers and others connected to the East Greenland shelf. During the year from August 2022 to August 2023 the system remained salinity-stratified and the seasonal deepening of the mixed layer never leads to a permanently homogeneous water column in terms of both temperature and salinity between the two moored CTDs during the winter season. There are two events during winter (br1 and br2) that show potential mixed layer deepening and last 9 and 6 days respectively. These are discussed in more depth in sec. 5.6.2.

The lack of substantial mixed layer deepening is counter to conventional expectations which suggest substantive deepening of the mixed layer during the autumn and winter months as a result of convection forced by seasonal increases in wind speed,

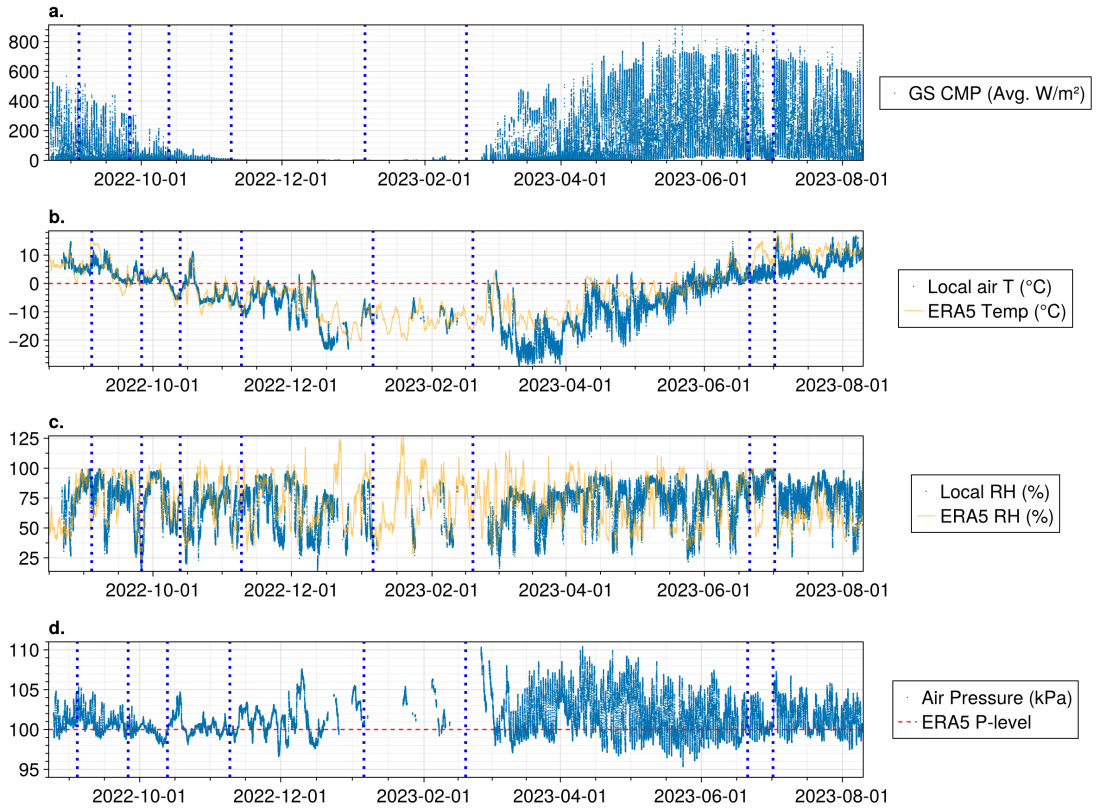

Figure 5.4: Atmospheric observations from the weather station and for b. and c. from ERA5 hourly reanalysis data for the coordinates of Ella Ø and for a fixed pressure of 100 kPa. The gaps in data during the dark season where the battery was depleted are apparent from the lack of scatter in d. and e. Subplots of a. Radiation, b. Air temperature, c. Relative humidity, and d. Air pressure.

rapid cooling of the surface, and the formation of frazil ice crystals. Our data is insufficient to determine whether a freshwater lens remains at depths above 11 m. Increasing salinity at both observed depths during the winter season do indicate a steady disappearance of freshwater during winter, also discussed in more detail below. Our previous research on the Northeast Greenland shelf has shown a remnant of the winter SML at a depth of ~ 30 m (Willcox et al., 2023) potentially indicating that this is not just a local phenomenon but a regional inability to seasonally overcome stratification. The stable water isotopes roughly follow the trend set by salinity but show a lot of fluctuation. The lower values -2.5 ‰ likely indicate the presence of terrestrial discharge as a water mass fraction though this could be from rivers and glaciers, or from snow melt.

The annual *TS* diagrams at 11 and 50 m (Figure 5.2 d,e) depth show a clear seasonal pattern that is reminiscent of those found in Young Sound (Boone et al., 2018). Since our moorings are shallower in the water column, the observed salinities are lower and the variability more extreme. For 2022, the water at 50 m stays cold (near the freezing line) until it is affected by freshwater in September. This is most likely to be discharge from land. Based on the 2023 data, freshening starts earlier at 11 m, around the time of the first spring event (sp1).

The tidal amplitude has a maximum of about 1 m during spring flood and a minimum of about 0.3 m (not shown). The dominant constituent is the semi-diurnal lunar component M2 with an amplitude of 0.49 m, and the second and third most important constituents are S2 and N2 with amplitudes of 0.19 m and 0.09 m respectively (Table 1). This is in accordance with observations from current-meter moorings in the East Greenland Current system at 75 °N where analysis of currents in the water column showed a similar relative importance of the tidal constituents (Woodgate et al., 1999).

Wind speeds and direction indicate that the period between October and April is dominated by piteraq (katabatic wind) from the direction of Kempe fjord. Outside of this period more wind comes from the northeast and east, in the direction of Vega Sund and Sofia Sund indicating a more along-shelf dominated wind regime. The winds are guided by the steep-walled topography of the fjords surrounding Ella Ø.

Along-valley wind-channelling, gap winds, and other processes are complex topic and beyond the scope of this paper.

The current near the surface is consistently toward south-southeast, including during winter when it is decoupled from the atmosphere by land-fast sea ice cover. The period from April to August, is associated with more water directed toward the south and south-west. This corresponds to the period of along-shelf winds. This is also the case during the period of land-fast ice cover. This implies that the water currents may be correlated to wind though not necessarily locally driven.

The air temperature generally reduces in autumn with a loss of incoming shortwave radiation in the area though there are some clear deviations from this trend that are associated with similar changes in atmospheric pressure and relative humidity, such as those around the second freshwater event (fw2) and sea ice breakup (sp2). These atmospheric events occur for periods of a week or longer.

5.6.1 Autumn

The anti-correlated peaks in salinity and temperature in autumn at fw1 and fw2 (Figure 5.2 a,b) are interpreted as peaks of terrestrial freshwater transported to the mooring location north of Ella Ø. The freshwater peak at 11 m depth is preceded by an increase in current speed near the surface. This is in September when the current direction is south-east. Given the orientation of Kapp Oswald (Figure 5.1) we assume that this freshwater at 11 m is most likely sourced from Kempe fjord to the west rather than the east. This first freshwater event (fw1) followed by a change in current direction towards the west centred at a depth of 24 m, after this the near-surface current speeds are again increased. Since we have no data for the current direction below the ADCP depth at ~ 36 m, including at the depth of the lower CTD, we cannot verify the source location of the freshwater spike at the second freshwater event (fw2). The deepest point between the islands of Maria and Ruth Ø and the north shore of Kempe fjord is around 75 m. Between these islands and Ella Ø it is deeper. It is therefore as plausible that the freshwater spike at 50 m is advected from Antarctic Sund and/or Kong Oscar fjord to the east as it is from

Kempe fjord to the west. This will depend on the stratification and external forcing both locally and upstream of the moorings.

The peak in freshwater at 11 m depth (fw1) is associated with very low relative humidity (20%). Some lows in relative humidity are associated with a simultaneous increase in local temperature, even though the ERA5 temperature decreases. This implies that in the case of a wind driven event, it may be a foehn wind, associated with melt events in Northeast Greenland, rather than a piteraq which would cause a drop in temperature instead (Mattingly et al., 2023).

If, as an example, we take a surface speed at the higher end of our observations, say ~ 10 cm/s, water could travel 1 km in around 27 hours. The distance from the mooring to the head of Kempe fjord, where it is formed at the intersection of the Rhedin, Rohss, and Dickson fjords, is around 40 km, leading to a transport time of around 45 days of advection time. Even longer from the heads of the three upstream fjords. The distances from the heads of these three fjords to the head of Kempe fjord are ~ 40 km for Dickson, ~ 12 km for Røhss, and ~ 18 km for Rhedin fjord. For Dickson fjord then, the time it could take for water to be discharged from the tidewater glacier at the head of Dickson fjord if we exclude any retention or recirculation and the current speed does not vary, would be around 80 days, placing the date where the freshwater peak was discharged on the 7th of July, 15-17 days after midsummer.

This example is subject to many assumptions but does support upstream glacial discharge as a plausible source for the freshwater peaks seen in late September and early October. In other fjords in Greenland, including Young Sound in Northeast Greenland (Sejr et al., 2017; Boone et al., 2018) , and Godthabsfjord in Southwest Greenland (Mortensen et al., 2014) seasonal peaks with a maximum in autumn are also observed and associated with freshwater discharge at fjord heads.

The onset of fast ice cover (lfo) occurs when incoming radiation has ceased and air temperatures drop to -10 °C. Water temperatures fluctuate around this period (from a week before until a week after) between ±0.6 °C. The two largest increases in temperature are associated with a simultaneous increase in salinity of almost 1.

These events are interpreted as periods of active freezing and frazil ice formation. After freeze-up there is a reduction in current speeds near the surface.

5.6.2 Winter

The start of the winter period is characterized by increasing ice draft and a steady increase in salinity, particularly at the 11 m CTD (Figure 5.2 a,b). Current speeds remain between 0.05 and 0.07 m/s until January when they increase coincident with several other changes. January wind speeds are higher than those in the preceding months. On the first of January there is a drop in sea ice draft (Figure 5.2 c). This coincides with an initial drop in $\delta^{18}O$ of 0.2 ‰. Directly after the ice draft recovers, growing from 0.5 m to 0.8 m, there is a sharp salinity and temperature increase (br1) at the 11m CTD, and an increase in $\delta^{18}O$ of 1 ‰. Another increase in ice draft associated with a drop in $\delta^{18}O$ occurred on 1st December 2022, which does not result in as large an increase in salinity while having higher water temperatures. Whereas the anomalous salinity and temperature during br1 recover after a period of nine days, the $\delta\ ^{18}O$ remains high, potentially a sign that the freshwater in the system no longer consists of local discharge but has been replaced by PW with a salinity of 30. Although there are only few recorded atmospheric observations around this event, it is clear that fluctuations in air temperature and a dramatic drop in relative humidity occur at br1.

The atmospheric observations are too sparse to determine whether this is also the case at the second enhanced salinity event (br2) in the third week of February. February does have the highest recorded wind speeds and the first and second week of the month are marked by the highest surface current speeds measured, of up to 0.15 m/s at a depth of 6 m (Figure 5.3). At the end of the first week the ice draft reduces by almost 50 cm (from 1.1 m to 0.6 m). The recovery is slower than during br1, but like br1 the increase in salinity occurs when the ice draft reaches the same thickness (1.1 m). The temperature does increase but this is less pronounced than in br1 and the $\delta^{18}O$ decreases by 0.1 ‰. The duration of the salinity increase associated with events br1 and br2 are 9 and 6 days respectively.

The two winter events, br1 and br2, are similar in some ways (increased salinity, reduction, and recovery of ice draft, increased temperature), and different in others (change in $\delta^{18}O$), with several unknowns (atmospheric parameters). The determination of the precise driver(s) of these events is therefore necessarily hypothetical. One possibility is simply that an increase in air temperature changed the heat balance at the air-ice interface leading to melting, and the subsequent growth of the ice after cooling increased the salinity directly below the ice. Another is that water was advected from elsewhere with the properties observed, or that advected water eroded the base of the ice, through heating, increased salinity, or current shear stress. In addition there is the possibility that any changes in ice draft are unrelated to the observations at 11 m. The 11 m CTD is on the water sampler mooring rather than the mooring with the ADCP that records the ice draft. Ice draft can be highly heterogeneous. After br2 the salinity steadily continues to increase until spring.

The best fit scenario for these two events is that there is a polynya that periodically opens up in an upstream location to the mooring, which generates a temperature and salinity signature that is similar to that observed during the initial freeze-up (lfo). The water that is generated is advected to the mooring location with a duration determined by the polynya open water period. We have not been able to locate cloud-free satellite imagery for these dates, therefore future work will be required to determine whether this hypothesis is true.

An alternative hypothesis could be that (tidal) cracking of sea ice, once it has gained a certain thickness or brittleness, releases brine into the surface layer through lateral drainage. This brine would have a higher density than its surroundings, and show up in the data as a period of high salinity, dependent on the porosity of the ice, for the duration of the drainage event. At this time there is no information available of such a process and this will require further investigation. Satellite data in the region from spring shows a few cracks from Ella Ø to the opposite shore across Kempe fjord though we can not determine when or how they were initially formed from our available data.

The air temperatures rise in the last week of February and the first week of March, increasing to just above the freezing point, both for local observations as well as in

the ERA5 reanalysis data. After this the local temperature recorded is much colder than that in ERA5, from March to April local temperatures are below -20 °C. The sea ice reaches its maximum thickness at the end of April and maintains this for almost two weeks before it starts to thin, even though air temperatures are already increasing.

From the onset of land-fast ice cover (lfo) to the start of spring (sp1), the salinity of the water column increases by around 2 at 11 m depth and around 1 at 50 m depth. The two layers remain stratified with the exception of the two events br1 and br2 during which both depths have the same salinity. After the end of April, when the wind changes from piteraq to shelf winds, current speeds are lower at around 0.4 m/s, possibly due to geographic restrictions in the direction of Maria and Ruth Ø.

5.6.3 Spring and summer

In May the air temperatures increase to above freezing more frequently. Temperatures over above freezing become consistent at the start of June. Water temperatures at 11 m start to increase in the third week of June. This is directly followed by a negative spike in $\delta^{18}O$ (sp1) on 21 June 2023. This event is associated with high relative humidity and low incoming radiation. This spike is not associated with a simultaneously registered change in salinity by the 11 m CTD mounted just above it which complicates its interpretation. Since $\delta^{18}O$ and S are conservative properties, this is peculiar. The observed decrease in $\delta^{18}O$ is 0.9 ‰ from -2.6 to -3.5 ‰. For a terrestrial snow value of $\delta^{18}O$ = -20 ‰, this represents a 35 % change. An equivalent change in salinity for a terrestrial snow value of 0 would certainly be observed.

It is possible that the water sampler bottle results sample a different volume of water. For example, if there were negative $\delta^{18}O$ snow crystals suspended in the water column, this would not contribute to the signal in salinity as recorded by the CTD. Though if captured in a bottle, they would displace water and once retrieved would lower both the salinity and the $\delta^{18}O$ recorded for the bottle sample. Since the ADCP is 100 m away from the water sampler, the suspended snow crystals would not

necessarily be observed unless very large or efficiently transported to the deeper mooring. Since the water samples are limited in volume, the sample salinity was not measured independently.

One week after sp1, there is another longer period of low incoming radiation that lasts several days. This is associated with land-fast sea ice breakup on 2 July (sp2) which is directly followed by a sharp increase in temperature, atmospheric pressure, and associated drop in relative humidity. July experiences only along-shore shelf winds.

The drop in incoming radiation and the changes in the other atmospheric parameters associated with sea ice break up make a storm, or other atmospheric event transporting warm (~ 10 °C) and dry (RH ~ 40 %) air into the region, the main contender as the driver of sea ice breakup in spring/summer 2023 at Ella Ø.~Water temperatures at the 11 m CTD reach 0 °C in the second week of July and continue to increase to a maximum of 2 °C. The influence of freshwater discharge at this time is likely negligible, only a reduction in salinity of around 0.2 is observed. The temperature increase is attributed to increasing spring and summer shortwave radiation and the increase in temperature is likely due to local runoff from Ella Ø and sea ice melt.

5.7 Summary

We provide a year long time-series (August 2022 to July 2023) of interdisciplinary (surface hydrological and meteorological) data from an East-Greenland fjord connecting the Greenland ice sheet to the (North-)East-Greenland shelf. We observe the peaks in autumn discharge at different depths, with 24 as the lowest salinity recorded at 11 m depth in the surface mixed layer on 26 September 2022 and a lowest salinity at 50 m in the polar (surface) water of 28.5 occurring almost two weeks later. The discharge corresponds to a period of increased current activity from the up-fjord direction in Kempe fjord.

Water temperatures at 11 m depth during autumn are high, up to 3.8 °C. Atmospheric temperatures during the warmest period average at around 10 °C with peaks up to 15 °C. Temperatures drop in response to reductions in insolation during winter. The wind system is dominated by piteraq transported through Kempe fjord from the west during winter and by shelf winds through Sofia Sund in the northeast in summer, most prominently during May, June, and July. The observed current speeds are reduced in response to fast sea ice cover.

Winter is marked by a steady increase in salinity and water temperatures that are near freezing. Two events of 9 and 6 days respectively are associated with increases in salinity of around 1. We make the assumption that there is open water somewhere to generate this water type though this will require further verification when data from future years is available. At the end of the winter the water at 11 m depth would be classified as Polar (Surface) Water or remnant winter water due to its increased salinity of 31 and a temperature of -0.6 °C once it reached the shelf.

The break up of the fast-ice in spring is driven by changes in atmospheric conditions and may have been expedited by a storm. It is unclear why the discrepancy exists between the extremely negative spike in $\delta^{18}O$ compared to the lack of such a spike in the salinity data. This will require further data and subsequent analysis.

We expect the water we observe inside the fjord will make its way out onto the shelf where it will contribute to the observed freshening of the region. Freshwater associated stratification of the surface layer has already been implicated in the cessation of deep water mixing in winter in the Greenland Sea and forming a new intermediate watermass (Strehl et al., 2024). With sufficient increased freshwater from locations, including Northeast Greenland fjords, to overcome mixing in the Labrador Sea, a similar change could occur in that region, with broad geochemical consequences for the deep and intermediate North Atlantic Ocean.

The GIOS observatory network provides unprecedented access for the observation and analysis of fjords in Northeast Greenland their role in connecting the Greenland Ice Sheet to the shelf.

References

Armstrong McKay DI, Staal A, Abrams JF, Winkelmann R, Sakschewski B, Loriani S, Fetzer I, Cornell SE, Rockström J, Lenton TM. 2022. Exceeding 1.5°C global warming could trigger multiple climate tipping points. *Science* **377**(6611): eabn7950. doi: 10.1126/science.abn7950

Aschwanden A, Fahnestock MA, Truffer M, Brinkerhoff DJ, Hock R, Khroulev C, Mottram R, Khan SA. 2019. Contribution of the Greenland Ice Sheet to sea level over the next millennium. *Science Advances* **5**(6): eaav9396. doi: 10.1126/sciadv.aav9396

Bao W, Moffat C. 2024. Impact of shallow sills on circulation regimes and submarine melting in glacial fjords. *The Cryosphere* **18**(1): 187 – 203. doi: 10.5194/tc-18-187-2024

Benn D, Evans DJA. 2014. *Glaciers and Glaciation, 2nd Edition*. 0th ed. Routledge. doi: 10.4324/9780203785010

Boone W, Rysgaard S, Carlson DF, Meire L, Kirillov S, Mortensen J, Dmitrenko I, Vergeynst L, Sejr MK. 2018. Coastal Freshening Prevents Fjord Bottom Water Renewal in Northeast Greenland: A Mooring Study From 2003 to 2015. *Geophysical Research Letters*: 8. doi: 10.1002/2017GL076591

Boone W, Rysgaard S, Kirillov S, Dmitrenko I, Bendtsen J, Mortensen J, Meire L, Petrusevich V, Barber DG. 2017. Circulation and fjord-shelf exchange during the ice-covered period in Young Sound-Tyrolerfjord, Northeast Greenland (74°N). *Estuarine, Coastal and Shelf Science* **194**: 205 – 216. doi: 10.1016/j.ecss.2017.06.021

Brown KA, Holding JM, Carmack EC. 2020. Understanding Regional and Seasonal Variability Is Key to Gaining a Pan-Arctic Perspective on Arctic Ocean Freshening. *Frontiers in Marine Science* **7**: 606. doi: 10.3389/fmars.2020.00606

Budéus G, Schneider W. 1995. On the hydrography of the Northeast Water Polynya. *Journal of Geophysical Research* **100**(C3): 4287. doi: 10.1029/94jc02024

Codiga DL. 2011. Unified tidal analysis and prediction using the UTide Matlab functions, in press. Graduate School of Oceanography, University of Rhode Island. doi: 10.13140/RG.2.1.3761.2008

Cottier FR, Nilsen F, Skogseth R, Tverberg V, Skarhamar J, Svendsen H. 2010. Arctic fjords: A review of the oceanographic environment and dominant physical processes. *Geological Society, London, Special Publications* **344**(1): 35 – 50. doi: 10.1144/SP344.4

De Jong MF, Oltmanns M, Karstensen J, De Steur L. 2018. Deep Convection in the Irminger Sea Observed with a Dense Mooring Array. *Oceanography* **31**(1): 50 – 59. doi: 10.5670/oceanog.2018.109

Dmitrenko IA, Kirillov SA, Rysgaard S, Barber DG, Babb DG, Pedersen LT, Koldunov NV, Boone W, Crabeck O, Mortensen J. 2015. Polynya impacts on water properties in a Northeast Greenland fjord. *Estuarine, Coastal and Shelf Science* **153**: 10 – 17. doi: 10.1016/j.ecss.2014.11.027

EOX IT Services GmbH. 2022. Sentinel-2 cloudless - https://s2maps.eu (Contains modified Copernicus Sentinel data 2022).

Farmer DM, Freeland HJ. 1983. The physical oceanography of Fjords. *Progress in Oceanography* **12**(2): 147 – 219. doi: 10.1016/0079-6611(83)90004-6

Fraser NJ, Inall ME, Magaldi MG, Haine TWN, Jones SC. 2018. Wintertime Fjord-Shelf Interaction and Ice Sheet Melting in Southeast Greenland. *Journal of Geophysical Research: Oceans* **123**(12): 9156 – 9177. doi: 10.1029/2018JC014435

Gjelstrup CVB, Myers PG, Lee CM, Azetsu-Scott K, Stedmon CA. 2024. Connectivity between Siberian river runoff and the lower limb of the Atlantic Meridional

Overturning Circulation. *Limnology and Oceanography* **69**(11): 2680 – 2687. doi: 10.1002/lno.12696

Gjelstrup CVB, Sejr MK, De Steur L, Christiansen JS, Granskog MA, Koch BP, Møller EF, Winding MHS, Stedmon CA. 2022. Vertical redistribution of principle water masses on the Northeast Greenland Shelf. *Nature Communications* **13**(1): 7660. doi: 10.1038/s41467-022-35413-z

Holding JM, Markager S, Juul-Pedersen T, Paulsen ML, Møller EF, Meire L, Sejr MK. 2019. Seasonal and spatial patterns of primary production in a high-latitude fjord affected by Greenland Ice Sheet run-off. *Biogeosciences* **16**(19): 3777 – 3792. doi: 10.5194/bg-16-3777-2019

IPCC. 2023. *Climate Change 2021 – The Physical Science Basis: Working Group I Contribution to the Sixth Assessment Report of the Intergovernmental Panel on Climate Change*. 1st ed. Cambridge University Press. doi: 10.1017/9781009157896

Jackson JM, Carmack EC, McLaughlin FA, Allen SE, Ingram RG. 2010. Identification, characterization, and change of the near-surface temperature maximum in the Canada Basin, 1993 – 2008. *Journal of Geophysical Research* **115**(C5): C05021. doi: 10.1029/2009JC005265

Jackson RH, Lentz SJ, Straneo F. 2018. The Dynamics of Shelf Forcing in Greenlandic Fjords. *Journal of Physical Oceanography* **48**(11): 2799 – 2827. doi: 10.1175/JPO-D-18-0057.1

Mattingly KS, Turton JV, Wille JD, Noël B, Fettweis X, Rennermalm ÅK, Mote TL. 2023. Increasing extreme melt in northeast Greenland linked to foehn winds and atmospheric rivers. *Nature Communications* **14**(1): 1743. doi: 10.1038/s41467-023-37434-8

Moon TA, Fisher M, Harden L, Shimonoko H, Stafford T. 2022. QGreenland (v2.0.0).

Mortensen J, Bendtsen J, Lennert K, Rysgaard S. 2014. Seasonal variability of the circulation system in a west Greenland tidewater outlet glacier fjord, Godthåbsfjord (64°N): Godthåbsfjord. *Journal of Geophysical Research: Earth Surface* **119**(12): 2591 – 2603. doi: 10.1002/2014JF003267

Paffrath R, Laukert G, Bauch D, Rutgers van der Loeff M, Pahnke K. 2021. Separating individual contributions of major Siberian rivers in the Transpolar Drift of the Arctic Ocean. *Scientific Reports* **11**(1): 8216. doi: 10.1038/s41598-021-86948-y

Pauly R, Olson S, Klise K, Ruehl K, Chris-Ivanov, Keester A, Coe R, McVey J, Ströfer CAM, Boyd M, et al. 2024. MHKiT-Software/MHKiT-Python: V0.9.0. Zenodo. doi: 10.5281/ZENODO.3924683

Peralta-Ferriz C, Woodgate RA. 2015. Seasonal and interannual variability of pan-Arctic surface mixed layer properties from 1979 to 2012 from hydrographic data, and the dominance of stratification for multiyear mixed layer depth shoaling. *Progress in Oceanography* **134**: 19 – 53. doi: 10.1016/j.pocean.2014.12.005

Pickard GL, Stanton BR. 1980. Pacific Fjords - A Review of Their Water Characteristics. In: Freeland HJ, Farmer DM, Levings CD, editors. *Fjord Oceanography*. Boston, MA: Springer US. p. 1 – 51. doi: 10.1007/978-1-4613-3105-6_1

Polyakov IV, Ingvaldsen RB, Pnyushkov AV, Bhatt US, Francis JA, Janout M, Kwok R, Skagseth Ø. 2023. Fluctuating Atlantic inflows modulate Arctic atlantification. *Science* **381**(6661): 972 – 979. doi: 10.1126/science.adh5158

Polyakov IV, Pnyushkov AV, Alkire MB, Ashik IM, Baumann TM, Carmack EC, Goszczko I, Guthrie J, Ivanov VV, Kanzow T, et al. 2017. Greater role for Atlantic inflows on sea-ice loss in the Eurasian Basin of the Arctic Ocean. *Science* **356**(6335): 285 – 291. doi: 10.1126/science.aai8204

Polyakov IV, Pnyushkov AV, Rember R, Padman L, Carmack EC, Jackson JM. 2013. Winter Convection Transports Atlantic Water Heat to the Surface Layer in the

Eastern Arctic Ocean*. *Journal of Physical Oceanography* **43**(10): 2142 – 2155. doi: 10.1175/JPO-D-12-0169.1

Poulsen E, Melvad P, Melvad C, Rysgaard S. n.d. Rugged, low-cost, and lightweight rosette water sampler for ocean profiling and mooring deployment (Submitted). *HardwareX*, in press.

Rignot E, Box JE, Burgess E, Hanna E. 2008. Mass balance of the Greenland ice sheet from 1958 to 2007. *Geophysical Research Letters* **35**(20): 2008GL035417. doi: 10.1029/2008GL035417

Rooijakkers FJ. 2024. Department of Applied Physics Master Thesis [Master of {{Science}}]. [Delft]: TU Delft.

Rudels B. 2022. The circulation and transformations of Atlantic water in the Arctic Mediterranean Sea. In: *The Physical Oceanography of the Arctic Mediterranean Sea*. Elsevier. p. 211 – 276. doi: 10.1016/B978-0-12-816930-8.00010-4

Rysgaard S, Bjerge K, Boone W, Frandsen E, Graversen M, Thomas Høye T, Jensen B, Johnen G, Antoni Jackowicz-Korczynski M, Taylor Kerby J, et al. 2022. A mobile observatory powered by sun and wind for near real time measurements of atmospheric, glacial, terrestrial, limnic and coastal oceanic conditions in remote off-grid areas. *HardwareX* **12**: e00331. doi: 10.1016/j.ohx.2022.e00331

Rysgaard S, Mortensen J, Haxen M, Gillard LC, Risgaard-Petersen N. 2024. Summer Hydrography Conditions at Proglacial Fjord Entrances Along East Greenland. *Journal of Geophysical Research: Oceans* **129**(7): e2023JC020665. doi: 10.1029/2023JC020665

Rysgaard S, Vang T, Stjernholm M, Rasmussen B, Windelin A, Kiilsholm S. 2003. Physical Conditions, Carbon Transport, and Climate Change Impacts in a Northeast Greenland Fjord. *Arctic, Antarctic, and Alpine Research* **35**(3): 301 – 312. doi: 10.1657/1523-0430(2003)035[0301:PCCTAC]2.0.CO;2

Sejr MK, Stedmon CA, Bendtsen J, Abermann J, Juul-Pedersen T, Mortensen J, Rysgaard S. 2017. Evidence of local and regional freshening of Northeast Greenland coastal waters. *Scientific Reports* **7**(1): 13183. doi: 10.1038/s41598-017-10610-9

Shiklomanov A, Déry S, Tretiakov M, Yang D, Magritsky D, Georgiadi A, Tang W. 2021. River freshwater flux to the arctic ocean. In: Yang D, Kane DL, editors. *Arctic Hydrology, Permafrost and Ecosystems*. Cham: Springer International Publishing. p. 703 – 738. doi: 10.1007/978-3-030-50930-9₂4

Stigebrandt A. 1981. A mechanism governing the estuarine circulation in deep, strongly stratified fjords. *Estuarine, Coastal and Shelf Science* **13**(2): 197 – 211. doi: 10.1016/S0302-3524(81)80076-X

Strehl A-M, Våge K, Smedsrud LH, Barreyre T. 2024. A 70-year perspective on water-mass transformation in the Greenland Sea: From thermobaric to thermal convection. *Progress in Oceanography* **227**: 103304. doi: 10.1016/j.pocean.2024.103304

Sutherland DA, Cenedese C. 2009. Laboratory Experiments on the Interaction of a Buoyant Coastal Current with a Canyon: Application to the East Greenland Current. *Journal of Physical Oceanography* **39**(5): 1258 – 1271. doi: 10.1175/2008JPO4028.1

Valle-Levinson A. 2010. *Contemporary Issues in Estuarine Physics*.

Velicogna I. 2009. Increasing rates of ice mass loss from the Greenland and Antarctic ice sheets revealed by GRACE. *Geophysical Research Letters* **36**(19): 2009GL040222. doi: 10.1029/2009GL040222

Willcox E, Bendtsen J, Mortensen J, Mohn C, Lemes M, Pedersen T-J, Holding J, Møller EF, Sejr MK, Seidenkrantz M-S, et al. 2023. An Updated View of the Water Masses on the Northeast Greenland Shelf and Their Link to the Laptev Sea and Lena River. *Journal of Geophysical Research: Oceans* **128**(4): e2022JC019052.

doi: 10.1029/2022JC019052

Woodgate RA, Fahrbach E, Rohardt G. 1999. Structure and transports of the East Greenland Current at 75°N from moored current meters. *Journal of Geophysical Research: Oceans* **104**(C8): 18059 – 18072. doi: 10.1029/1999JC900146

Wunderling N, Von Der Heydt AS, Aksenov Y, Barker S, Bastiaansen R, Brovkin V, Brunetti M, Couplet V, Kleinen T, Lear CH, et al. 2024. Climate tipping point interactions and cascades: A review. *Earth System Dynamics* **15**(1): 41 – 74. doi: 10.5194/esd-15-41-2024

6 Summary and Conclusions

The research presented in this thesis provides a novel look at the water surrounding Northeast Greenland. The Northeast Greenland shelf was first subjected to a detailed investigation during the NEWP92/93 cruises in the 1990s (Wallace et al., 1995) as part of the International Arctic Polynya Program (Deming and The NEWATER Steering Committee and Principle Investigators, 1993). There was a further programme on the Niogerhalvfjersbrae (79N glacier) and its associated ice shelf by the Geological Survey of Denmark and Greenland from 1996 to 1998 (Thomsen et al., 1997) which included remote work on the influence of sea ice using remote satellite imagery (Reeh et al., 2001).

Due to the inaccessibility of the region, much of the focus remained on the Northeast Water Polynya area (Belgica Trough, Norske Trough, and Westwind Trough) rather than the shelf in its entirety (An et al., 2021; Huhn et al., 2021; Fransson et al., 2023; McPherson et al., 2023; Bennett et al., 2024; Wekerle et al., 2024). This thesis extends the latitudes for which observations have been described. The work highlights how dynamic the Northeast Greenland shelf is due to the unique superposition of water masses and changes associated with their respective source regions all interacting on the shelf, including regions beyond the Northeast Water Polynya. This can have surprising and unpredictable (non-linear) consequences in terms of the physical and chemical interactions on the shelf.

In this work, I primarily focus on the freshwater source fractions in the surface waters on the Northeast Greenland shelf, and consequentially the carbon dynamics in the surface water, and show that they can not be easily described by the application of existing models. This is the most important contribution of this work. I further investigate hydrographical changes inside a fjord system that is connected to the

Northeast Greenland shelf, an important pre-requisite to be able to separate local and upstream contributions to the freshwater system. A more detailed breakdown of the contributions made by this work is done in section 6.1, and its potential application to further work in section 6.2. Finally, some closing comments are put forward in section 6.3.

My research provides clear evidence that the water from an individual 'great river' (in our case the Lena) located on the other side of the Arctic Ocean can be identified in the surface water on the Northeast Greenland shelf. This means that the region may also be influenced by other changes in chemistry, such as that associated with permafrost melt or transported pollutants. I also show that the seasonal rectification hypothesis, where sea ice cover inhibits the release of CO_2 to the atmosphere on the Northeast Greenland shelf, can be false in low sea ice years. It is surprising that temperature is not strongly correlated with dissolved CO_2 in this regions as it is elsewhere. This will require further investigation.

6.1 Summary of major contributions

6.1.1 Contribution 1: Revised the hydrography of the Northeast Greenland shelf; Surface freshening, maximum winter mixed layer depths, and shelf-edge mixing

We describe the hydrography of the entirety of the Northeast Greenland shelf for the first time in chapter 3. We find a similar water mass structure present to that observed in the 1990s, with the characteristic superposition of Lower Halocline Water (LHW) with Cold Halocline Layer (CHL) and Surface Mixed Layer (SML), though with some poignant differences. At the base of the Surface Mixed Layer (SML), there is an unventilated water type, as determined by supersaturation of O_2, which is not depleted in NO_3^- like the overlying Surface Mixed Layer (SML). This water type was observed in older studies but at a higher salinity (with a density of 26 in Bignami and Hopkins (1997) instead of our observation of Northeast Greenland Winter Water (NGWW) $\rho = 25$), indicating significant freshening of the Cold Halocline

Layer (CHL), which corresponds to the known increase in river discharge into the Arctic Ocean. Since this layer is not ventilated, and the Cold Halocline Layer (CHL) is intact, we interpret this layer as the deepest depth at which winter mixing has occured. This is corroborated by its stability (per the Brunt-Väisälä frequency squared). The Surface Mixed Layer (SML) above this is geochemically distinct and strongly influenced by sea ice melt.

Due to the number of observations and their extension to previously unstudied latitudes between Belgica Trough (77 °N) and Young Sound (74 °N), on the shelf proper as well as along the shelf edge, different regions could be identified by their CTD profile. The main shelf is characterised by the presence of Polar Surface Water (PSW), where closer to the shelf edge Return Atlantic Water (RAW) is more prominent and closer to the surface and is associated with mixing processes. Mixing occurs along the shelf edge, and the polynya region is hydrographically distinct due to its lack of a clear Lower Halocline Water (LHW).

The approach taken in chapter 3 of grouping *TS* profiles by their shape and then determining their geographical location is novel and led to the finding of geographical patterns that would otherwise have been missed, such as the Cold Halocline Layer (CHL) in certain regions having a higher temperature than in others (Slope two and main groups in e.g. Figure 3.3). This directly addresses objective 1 as set forward in section 1.2.

6.1.2 Contribution 2: Established a direct connection between water on the Northeast Greenland shelf and Siberian river runoff using chemical tracers

Not only the hydrographical change in the salinity-driven density of the Northeast Greenland Winter Water (NGWW) water type is associated with riverine inflow. In chapter 3 we use several different tracers to show, independently, that the water found in the Cold Halocline Layer (CHL) is primarily sourced from the Laptev Sea. The data also explicitly excludes the presence of Pacific Water (PW) and Upper

Halocline Water (UHW) from the Northeast Greenland shelf region during the sampling period in August/September 2017.

Previous research commonly associated any increase in the NO_3/PO_4 tracer specifically with the Chukchi Sea, where already nutrient depleted water is mixed across denitrified sediments during winter full depth convection and creates a strong biogeochemical denitrification signature. This water is then transported across the East Siberian Sea and into the Transpolar Drift (TPD). Once it has crossed the Arctic Ocean it encounters the 'switchyard' in the Lincoln Sea which separates the water from the TPD into that transported into Nares Strait and that which exists the Arctic through Fram Strait. We show that this signal as seen on the Northeast Greenland shelf maps directly onto denitrification signals from the Laptev Sea. Other tracers, such as the ratio of the stable water isotopes ($\delta^{18}O/\delta^{2}H$) and the PO_4^{3-} and SiO_4 to AOU ratios support this finding, showing a much stronger connection to the Laptev Sea than to the East Siberian or Chukchi Seas. Although it is unclear whether this connection was specific to the year 2017 or whether Laptev Sea water has been misinterpreted as Pacific Water (PW) in the past is unclear and requires further study. This finding addresses objective 1 as set forward in section 1.2.

6.1.3 Contribution 3: Advanced the understanding of the carbon mechanics on the Northeast Greenland shelf and show it can be a source rather than a sink for atmospheric CO_2

In terms of the carbon system in Northeast Greenland, prior research in the region was the foundation of the frequently referenced *seasonal rectification hypothesis* which suggests that sea ice cover in cold water regions can inhibit the seasonal release of CO_2 to the atmosphere during the times of year when there is net respiration. We show in chapter 4 that this outflow shelf can act as a source of CO_2 during late summer and early autumn prior to freeze-up.

In addition, contrary to in the Canadian Arctic, the Northeast Greenland shelf CO_2 does not show any clear correlation to temperature. There is a roughly linear relationship between AOU and CO_2 in the layers below the Surface Mixed Layer

(SML). This is interpreted to be due to a severe lack of nitrate (NO_3^-) which inhibits primary production at shallower depths only allowing primary productivity at deeper depths. Primary productivity maxima in a water type that is not in contact with the atmosphere means that no CO_2 uptake from the atmosphere occurs either. Between a lack of uptake from the atmosphere and the lack of sea ice inhibition, we shed doubt on the applicability of the seasonal rectification hypothesis during the late summer and early autumn season of 2017.

When mixing starts to break down stratification in the latter part of the dataset, dissolved CO_2 is reduced, interpreted as an effect of active ventilation. Vertical mixing as a dominant control on atmospheric CO_2 exchange with surface waters, having a larger impact than for example temperature, is a major finding and will influence future interpretation of the carbon system on the Northeast Greenland shelf. Since vertical mixing can occur at such small spatiotemporal scales in the region, for example due to the small diameter of deep eddies, this will require higher density sampling than exists in currently available data and will inform the planning of future carbon research in the region. This chapter directly addresses objective 2 in section 1.2.

6.1.4 Contribution 4: Novel approach to salinity normalising carbon data that will simplify future analyses

Carbon data is commonly normalised to remove the effects of dilution by freshwater. The top several hundred meters of the Arctic Ocean contain large fractions of freshwater, both as meteoric freshwater input from rivers and precipitation as well as through the dilution effect of repeated sea ice freezing (exporting salt to deeper water) and melting. Since these are different sources with different alkalinity at a salinity of 0, the accurate normalisation of these data tends to require two steps, one for the normalisation with respect to meteoric freshwater, and one with respect to the effect of sea ice melt dilution.

Through the application of known methods for the salinity normalisation of carbon data and superimposing the most commonly used Arctic freshwater and sea ice

normalisations concurrently, we show that this is equivalent to the simple application of a polynomial to the data. This is discussed in chapter 4.6. The previous normalisation procedures require known or approximated values for both the end members with respect to which the normalisation is being performed, which leads to the requirement of an additional measurement, for example $\delta^{18}O$. The simple polynomial technique removes this requirement and thereby simplifies the normalisation procedure. This is a methodological contribution and does not directly relate to any objective directly.

6.1.5 Contribution 5: A year of mooring and novel water isotope sampler data for a Northeast Greenland fjord, potential for locally forming Polar Surface Water (PSW)

Mooring data from Northeast Greenland fjords is relatively rare and frequently associated with long term monitoring programs and larger fjords such as Young Sund or Scoresby Sund. Having combined wind and mooring data is rarer still, and we provide the first look at weekly data from an automated water sampler in chapter 5. We show that the maximum in terrestrial discharge at the site, advected from upstream sources, is in Autumn around a week after the first freezing air temperatures are recorded. The peak in discharge at 50 m depth occurs later than that at 11 m depth, though whether this is a result of shear or differing behaviour in different layers cannot be concluded from our dataset since we do not have Acoustic Doppler Current Profiler (ADCP) data for the lower CTD. The discharge maxima are associated with an increase in current speeds and a change in wind direction from the summer dominant along shelf direction to the winter dominant piteraq (katabatic winds). Once land-fast sea ice cover is established the current speeds reduce which implies that high current speeds during the previous period were at least partially caused by wind.

Throughout winter the salinity increases and as the slope of the salinity flattens (at around 31), there is also a change in the slope of the $\delta^{18}O$. The salinity is close to that found for the Northeast Greenland Winter Water (NGWW) on the Northeast

Greenland shelf in chapter 3, while the $\delta^{18}O$ is lighter than that of the Northeast Greenland Winter Water (NGWW) (around -3 ‰). If this difference remains in subsequent studies, this result can be used to distinguish between local and remotely formed winter water. This would allow measurements at downstream locations to parameterize the contribution of the Greenland Ice Sheet to observed Polar Surface Water (PSW). This finding contributes to objective 1 in section 1.2.

6.1.6 Contribution 6: Novel observations of two high salinity events during winter and hypothesis regarding their cause

During winter there are two extended periods of increased salinity, with durations of 9 days and 6 days respectively. We assume that these events are driven by open water nearby, increasing the salinity through sea ice formation, with the salty water then advected to the region. This is supported for the second event in particular which is preceded by a period of higher current speeds.

There are several possibilities regarding open water in the region. Open water can be generated by polynyas that act as ice factories or by landfast ice cracking under tidal tension and releasing the brine inside. We have been unable to locate any polynyas in the region due to the lack of adequate satellite coverage. Long cracks across the fjord are apparent from satellite data though the mechanism of brine release from these has not been studied and therefore their potential contribution is unknown and will depend on the porosity and brine salinity.

These events are of interest due to their particular characteristics, but also because the system recovers to a stratified state afterward, which is evidence that the environment is so highly stratified that even prolonged events do not influence it from a seasonal perspective. This finding contributes to objective 1 in section 1.2.

6.2 Limitations of study & future work

The data we discuss in this work are the first ever observations for many of the sampled locations and times, both for the Northeast Greenland shelf as well the year of data north of Ella Ø. The data used for chapter 3 and chapter 4 were obtained opportunistically. This was made possible by extraordinary low ice conditions for the region and season. The two moorings and novel water sampler in chapter 5 are the first data from the Greenland Integrated Observing System (GIOS) which facilitates the long-term deployment of container moorings across the region.

Sea ice and weather conditions in Northeast Greenland are frequently such that idealised itineraries made while on land have to be abandoned in favour of alternative plans. Moorings can be displaced as a result of iceberg keel dragging, and finding locations suitable for long term deployment can therefore be difficult, especially for the collection of near-surface data. Satellite data in visible and thermal spectra of high enough resolution to determine fjord-scale processes, is frequently either unavailable due to infrequent coverage, or the data that is present is difficult to use or unusable as a result of polar night, shadow from low sun angles, cloud cover, and fog. It is therefore important to see the limitations described below as an ideal, rather than a, at this time, realistically attainable goal, although future projects such as the deployment of additional container moorings, planned field campaigns, and a cube satellite in an orbit specifically chosen to monitor the region will go a long way to addressing them.

From a statistical point of view, the incredible dynamism of the region requires relatively high resolution sampling. This is particularly true when it comes to the geochemistry, since there are so many additional factors to consider in this environment compared to a less dynamic region with fewer input sources. The most basic mass balance model for geochemical parameters is a division into 1) advection to a coordinate, 2) production, modification, and/or destruction at the coordinate, and 3) advection away from the coordinate. In the open ocean, away from coastal input and limited to primary productivity associated with the recycling of nutrients, many of the parameters associated with such a mass balance model

can be measured or obtained by a conservative relationship to another variable, most frequently salinity. Unlike other oceans, the Arctic Ocean has high freshwater content from terrestrial sources and is dominated by broad continental shelves.

Each of the major and minor rivers generates its own seasonal geochemical nutrient signal. These signals mix on the shelves and are transported into the Arctic Ocean where the Transpolar Drift (TPD) transports them to Fram Strait and onto the Northeast Greenland shelf. During transport, geochemical components in the SML are modified by a sequence of seasonal sea ice growth and decay. The geochemical signature is therefore already complex, potentially with a seasonal signal, on arrival in Northeast Greenland. On the shelf itself additional processes take place that will mix the incoming water in potentially unpredictable ways. There is the addition of Return Atlantic Water (RAW) at latitudes at and below 79 °N, which directly interacts with Polar Surface Water (PSW) and Arctic Atlantic Water (AAW) coming from the Arctic Ocean via the EGC. Our own observations in chapter 3 show that mixing occurs along the shelf edge, which has consequences for the retention of any conservative water mass property, even ignoring the existence of eddies and terrestrial input from the Greenland Ice Sheet.

High statistical power tends to be difficult to achieve in field environments, even more so in those that are remote and challenging. To increase statistical power, in the absence of knowing the effect size since these are the first studies of their kind, only the sample size can be increased. Chapter 3 utilised several different tracers to determine the source location for the freshwater component in the PSW found on the Northeast Greenland shelf.

The two most well known tracers used, the () and $\delta^{18}O$, are not able to clearly distinguish between riverine input sources when used in mass balance equations with salinity, especially after modification of the water type by sea ice and/or brine. The determination of the source river (Lena) was made possible through the use of river geochemical data from the different Arctic source regions. Although these data are collected systematically as part of ArcticGRO (Arctic Great Rivers Observatory), their collection in marine environments is far more sparse. An increase in the availability of tracers across spheres and with a similar ability to distinguish between

riverine input sources as δ^2H:$\delta^{18}O$ both locally and at upstream locations would have strengthened our conclusion that the Laptev Sea was the dominant source of freshwater on the Northeast Greenland shelf in late summer 2017.

For chapter 4, increased spatial resolution in particular would have improved our analysis. The scatter in the data was large and there was no clear reason to discard any of the data, leading to our use of the Median Absolute Deviation (MAD) instead of a mean-based statistic to determine any relationships between the carbon data. The calculated fCO_2 from dissolved carbon parameters was much higher than was seen in previous data from the area (1994, 2003, and 2009 in CARINA and SOCAT databases per Figure 4.10 in chapter 4.6), especially data collected in August. Since no procedural or systemic issues were distinguishable between the two labs who processed the data, it is assumed that the scatter is related to in situ processes. Geographically, higher fCO_2 in the SML seems to be associated with (Figure 4.11 in chapter 4.6) mixed layer depth and the fraction of RAW present in a sample. The latter is difficult to distinguish from AAW from conservative geochemical properties, which would be required to really understand the causes leading to the extraordinarily high values of fCO_2.

The main limitation for chapter 5 is that the lower Conductivity Temperature Depth device (CTD) is not covered by a second Acoustic Doppler Current Profiler (ADCP). This means that where there is a discrepancy between the CTD signal at 11 m and that at 50 m, it is impossible to determine whether these layers of water are being advected from the same direction or different ones. Additional measurements of *TS* between the ADCP and 11 m would also have been beneficial to determine a more precise vertical density profile. The addition of such devices would allow a more detailed determination of seasonal changes inside the PSW and their drivers, and the local contribution(s) to this layer. Determining the fractions of locally produced PSW versus that advected from the Arctic Ocean at different depths would link the Greenland Ice Sheet to longer term ocean circulation, including the water formed seasonally in the Labrador Sea.

Having more temporally diverse data for the Northeast Greenland shelf would be an additional benefit. The two consecutive cruises that provided data for chapter 3 and

chapter 4 were both during a low ice year that allowed ships without ice breaking capacity to sample the region safely. These exceptional conditions were a great laboratory for a future period with less ice, but are less successful at providing a baseline by which to measure change. Whether this can realistically be achieved considering the logistical requirements is another matter.

Finally, any work in Northeast Greenland would benefit from a known estimate of Transpolar Drift (TPD) surface water transport times as well as residence times, both on the shelf (chapter 3 and chapter 4), as well as inside the fjords (chapter 5). These data are not available at this time but all work on the Northeast Greenland shelf would benefit if the temporal dimension of the circulation was more constrained. This would create a contextual framework for the interpretation of these observations thereby aiding in the broader applicability of the results.

6.3 Closing comments

This thesis presents a set of observations that primarily highlights how little we know about this important Arctic ouflow shelf and its associated fjord systems. Our study of the hydrography of the Northeast Greenland shelf provides additional detail compared to previous observations, such as the direct link to the Laptev Sea region, rather than a more ephemeral 'Eurasian river water' descriptor. This helps because it will allow us to map source region changes as compared to the period of study that is covered by the observations in this work. For example the (re-)emergence of Pacific Water (PW) and Upper Halocline Water (UHW) on the shelf through tracers that more accurately reflect the Pacific sector of the Siberian Arctic shelf seas, such as silicate (SiO_4) or dissolved inorganic carbon DIC.

Light is also shed on along-shelf mixing, with evidence pointing toward water mass modification along the shelf edge between areas where Return Atlantic Water (RAW) is at or near the surface versus the Polar Surface Water (PSW) dominated shelf waters. There is even the potential for Return Atlantic Water (RAW) melting sea ice along the shelf edge and at the polar front and the formation of local Lower

Halocline Water (LHW). This is an exciting prospect and will require extensive additional study.

In terms of CO_2 exchange, our work highlights the importance of high density sampling in the region, particularly those areas associated with the interactions between different geochemical end-members, such as sea ice, Return Atlantic Water (RAW), Polar Surface Water (PSW), and glacial input. One area may not be representative of another on the Northeast Greenland shelf and this has consequences for future sampling campaigns. The nutrient-depleted sea ice melt influenced surface layer and its inhibition of atmospheric gas exchange, compared to our previous assumption where exchange was inhibited during winter and not during summer, changes our perspective on the entire region as a net CO_2 sink.

In conclusion, this work provides a thorough base for future work on the Northeast Greenland shelf and the fjords surrounding Ella Ø. It has increased our understanding of the oceanography of Northeast Greenland.

References

An L, Rignot E, Wood M, Willis JK, Mouginot J, Khan SA. 2021. Ocean melting of the Zachariae Isstrøm and Nioghalvfjerdsfjorden glaciers, northeast Greenland. *Proceedings of the National Academy of Sciences* **118**(2): e2015483118. doi: 10.1073/pnas.2015483118

Bennett MG, Renfrew IA, Stevens DP, Moore GWK. 2024. The Northeast Water Polynya, Greenland: Climatology, Atmospheric Forcing and Ocean Response. *Journal of Geophysical Research: Oceans* **129**(5): e2023JC020513. doi: 10.1029/2023JC020513

Bignami F, Hopkins TS. 1997. The water mass characteristics of the Northeast Water Polynya: Polar Sea data 1992 – 1993. *Journal of Marine Systems* **10**(1-4): 139 – 156. doi: 10.1016/S0924-7963(96)00079-6

Deming J, The NEWATER Steering Committee and Principle Investigators. 1993. Northeast water polynya: Polar sea cruise results. *Eos, Transactions American Geophysical Union* **74**(16): 185 – 196. doi: 10.1029/93EO00264

Fransson A, Chierici M, Granskog MA, Dodd PA, Stedmon CA. 2023. Impacts of glacial and sea-ice meltwater, primary production, and ocean CO2 uptake on ocean acidification state of waters by the 79 North Glacier and northeast Greenland shelf. *Frontiers in Marine Science* **10**: 1155126. doi: 10.3389/fmars.2023.1155126

Huhn O, Rhein M, Kanzow T, Schaffer J, Sültenfuß J. 2021. Submarine Meltwater From Nioghalvfjerdsbræ (79 North Glacier), Northeast Greenland. *Journal of Geophysical Research: Oceans* **126**(7). doi: 10.1029/2021JC017224

McPherson RA, Wekerle C, Kanzow T. 2023 Sep. Shifts of the Recirculation Pathways in central Fram Strait drive Atlantic Intermediate Water Variability on Northeast Greenland shelf. *Journal of Geophysical Research: Oceans*: e2023JC019915. doi: 10.1029/2023JC019915

Reeh N, Thomsen HH, Higgins AK, Weidick A. 2001. Sea ice and the stability of north and northeast Greenland floating glaciers. *Annals of Glaciology* **33**: 474 – 480. doi: 10.3189/172756401781818554

Thomsen HH, Reeh N, Olesen OB, Egede Bøggilde C, Starzer W, Weidick A, Higgins AK. 1997. The Nioghalvfjerdsfjorden glacier project, North-East Greenland: A study of ice sheet response to climatic change. *Geology of Greenland Survey Bulletin* **176**: 95 – 103. doi: 10.34194/ggub.v176.5073

Wallace DWR, Behrens WJ, Hopkins TS, Kinder C, Deming J, Smith WO, Top Z, Walsh ID. 1995. Collaborative research on the Northeast Water Polynya: NEWP92 hydrographic data report. USCGC Polar Sea cruise, July 15 – August 15, 1992. Report No.: BNL – 61923, 102497. doi: 10.2172/102497

Wekerle C, McPherson R, Von Appen W-J, Wang Q, Timmermann R, Scholz P, Danilov S,

Shu Q, Kanzow T. 2024. Atlantic Water warming increases melt below Northeast Greenland’s last floating ice tongue. *Nature Communications* **15**(1): 1336. doi: 10.1038/s41467-024-45650-z

7 Contributions of Collaborating Authors

Chapter 3 and chapter 4

The two cruises from which the data for these two papers were obtained were led by M.S. Seidenkrantz and S. Rysgaard respectively. Samples were taken aboard the ship by multiple people including C. Mohn, T.-J. Pedersen, E. F. Møller, J. Holding, and S. Rysgaard. Laboratory analyses were performed by J. Marchiano Holding, M. Lemes, and M. K. Sejr. J. Bendtsen (modeling) and J. Mortensen (physical oceanography) provided valuable feedback during the initial process of the hydrographical analyses. All data analyses, programming, and interpretative work were performed by me under the guidance of S. Rysgaard. Co-author feedback was generously provided by all authors prior to paper submission.

Chapter 5

The design, creation, and deployment of the oceanographic mooring including all logistical support was performed by S. Rysgaard and W. Boone. The meteorological station was set up and run by L.L. Sørensen. Data quality control, analyses, programming, and interpretive work were performed by me under the guidance of S. Rysgaard. E.R. Castillo (physical oceanography) and L.L. Sørensen (meteorology) provided extensive feedback on graphical representaton of data and analysis prior to paper submission.

Acronyms

AAW	Arctic Atlantic Water 5, 35, 178, 179, 185
ADCP	Acoustic Doppler Current Profiler 6, 175, 179, 185
AIW	Arctic Intermediate Water 35, 185
AMOC	Atlantic Meridional Overturning Circulation 19, 185
AO	Arctic Ocean 185
AW	Atlantic Water xi, 1, 5, 12, 13, 15–17, 24–26, 35, 36, 38, 142, 143, 185
BSBW	Barents Sea Branch Water 17, 23, 185
BSO	Barents Sea Opening 13, 185
CC	Coastal Current 36, 185
CHL	Cold Halocline Layer xii, 16, 17, 19, 23, 29, 36, 37, 142, 143, 171, 172, 185
CTD	Conductivity Temperature Depth device 5, 6, 179, 185
EGC	East Greenland Current 5, 15, 178, 185
EGCC	East Greenland Coastal Current 185
FSBW	Fram Strait Branch Water 17, 35, 185
LHW	Lower Halocline Water 15–17, 19, 23, 35, 36, 171, 172, 180, 185
MIZ	Marginal Ice Zone 16, 24, 185
NAC	North Atlantic Current 13, 185
NCaC	North Cape Current 13, 185

Chemical formulae and acronyms

Notation	Description	Page List
AOU	Apparent Oxygen Utilisation. This is the difference between the fraction of dissolved oxygen that the water mass would contain if it was fully ventlilated, and that observed. Away from the surface, and by making certain assumptions, this measurement can provide clues regarding the amout of productivitythat has occurred inside the watermass since the last period and location of ventilation	173, 185
CA	Carbonate alkalinity	32, 185
$CDOM$	Coloured dissolved organic matter	34, 185
CH_4	Methane. Second largest atmospheric greenhouse gas after CO_2. It traps more heat but has a shorter lifespan than CO_2.	29, 185
CO_2	Carbon Dioxide. The most important greenhouse gas.	xii, 1–6, 13, 29–34, 173, 174, 181, 185

Notation	Description	Page List
CO_3^{2-}	Carbonate ion. Plays an important role in the ocean carbon cycle as part of the solubility pump	xii, 30–33, 185
$CaCO_3 \cdot 6H_2O$	Ikaite. Polymorph of calcium carbonate ($CaCO_3$). Other polymorphs of $CaCO_3$ include calcite, aragonite, and vaterite	32, 33, 185
$CaCO_3$	Calcium carbonate	32–34, 185
Ca^{2+}	Calcium ion. Combines with carbonate to form calcium carbonate ($CaCO_3$)	32, 33, 185
DIC	Dissolved inorganic carbon	31, 32, 34, 180, 185
DOC	Dissolved organic carbon	34, 185
DOM	Dissolved Organic Matter	34, 185
HCO_3^-	Bicarbonate ion. Plays an important role in the ocean carbon cycle as part of the solubility pump.	xii, 30–32, 185
H^+	Hydrogen ion. Also frequently referred to as a proton. If an acid is added to water, water and the acid will react to form hydronium (H_3O^+)	31, 32, 185
H_2CO_3	Carbonic acid. Frequently seen as an intermediate stage in ocean acidification since it rapidly dissociates after it is formed in ocean surface waters.	31, 32, 185
H_2O	Water	29, 31, 32, 185
NO_3^-	Nitrate. Nitrate is the main limiting nutrient in the Arctic Ocean. It is fixed by primary producers.	22–24, 171, 174, 185

Notation	Description	Page List
N_2O	Nitrous oxide. Plays a role in climate.	29, 185
O_2	Dissolved oxygen. Dissolved oxygen is mixed into seawater when it is exposed to the atmosphere by diffusion and by bubbles caused by wind mixing as well as produced by primary producers during photosynthesis. During respiration dissolved oxygen is consumed	22, 23, 171, 185
O_3	Ozone. Filters out certain wavelengths of radiation from the sun in the stratosphere, and the third most important greenhouse gas after carbon dioxide (CO_2) and methane (CH_4)	29, 185
PO_4^{3-}	Phosphate. Phosphate is a nutrient which is utilised by primary producers during photosynthesis. It is not as limiting in the Arctic Ocean as nitrate	23, 24, 173, 185
SiO_2	Silicon dioxide. Silicon dioxide is a major component of quartz minerals and is a large component of Earth's crust. The mineral is also utilised by diatoms in its hydrated form to create biogenic glass	29, 185
SiO_4	Silicate. Silica is used by diatoms and other biogenic glass producing primary producers to form silicon dioxide frustules. It can also be found in the upper mantle as part of the mineral olivine. Silicate can be a limiting nutrient in the Eurasian Basin	173, 180, 185
TA	Total alkalinity.	32–34, 178, 185
Ω	The saturation state of calcium carbonate ($CaCO_3$) in seawater	32, 33, 185

Notation	Description	Page List
$\delta^{18}O$	The $\delta^{18}O$ is a formula that relates the amount of heavier ^{18}O oxygen isotopes to the lighter ^{16}O oxygen isotopes in a sample using a standard. The formula is $\delta^{18}O = \left(\frac{\left(\frac{^{18}O}{^{16}O}\right)_s}{\left(\frac{^{18}O}{^{16}O}\right)_r} - 1 \right) x1000‰$	5, 185
$\delta^2 H$	As with oxygen, this variable relates the amount of heavier versus lighter hydrogen isotopes in a sample	5, 185

Physics notation and acronyms

Notation	Description	Page List
ΔT	Change in temperature between two water layers	15, 185
α	Coefficient of thermal expansion, the change in volume associated with changes in temperature outside of phase transitions	185
β	Coefficient of haline contraction. The change in ocean density resulting from a change in salinity	185
ρ	Density	15, 185
c	Specific heat of water	15, 185
H	Height of surface water	185
L	Latent heat	185

Glossary

TS Potential temperature x Salinity diagram. Used to separate water types by their potential temperature and salinity. Temperature is non-conservative and is associated with heating and cooling. Salinity is a conservative property which reflects the loss or gain of water compared to the salts and other consituents of seawater, including precipitation, evaporation, riverine input, and sea ice melting and freezing. When mixing occurs between end-members this is represented as points falling on a line between them. Since the density is mainly a function of temperature and salinity, lines of density can be added to such plots and will show whether mixing is isopycnal or diapycnal 5, 17, 21, 35, 36, 185

Atlantification Atlantification is the process whereby the influence of Atlantic Water is felt further and further north in the Arctic Ocean 17, 185

binary geophysical fluid A binary geophysical fluid is a term used to describe a fluid made from two components, frequently a solid dissolved in a liquid. Seawater is frequently approximated as a binary (geophysical) fluid made up of salt and pure water. This approximation is only possible due to the salt fraction of the various salts making up the salt component being relatively constant away from input regions such as coastal areas and mid ocean ridges. 21, 185

buffer capacity The buffer capacity of a solution describes its resistance to changes in pH when an acid or base is added. Within the context of Arctic surface water alkalinity, having an increased buffer capacity would allow more carbon to be dissolved without the solution becoming more acidic, thus preventing the

'other CO_2 problem', namely ocean acidification which has been associated with a negative impact on marine calcifiers. 2, 185

fast ice Fast ice is ice that is attached to land and tends to be stable and immobile compared to the pack ice. The location of the fast ice edge depends on the local conditions and is expected to be a function of river depth along the Siberian shelfs but of compression north of Alaska. As far as I am aware the mechanisms controlling fast ice in Northeast Greenland have not been investigated 20, 185

flaw lead A flaw lead is an opening in the sea ice 20, 185

haline convection Convection under the influence of the increase in density associated with the removal of water molecules from seawater. This can occur as a result of evaporation or sea ice formation. 20, 185

lead A lead is an opening (or crack) in the ice cover that is formed as a result of divergent ice flow 20, 185

Optimum Multiparameter Analysis OMP is a method to determinet he relative fraction of specific water masses (represented by a unique water type for the source region) present in a sample. It utilises a matrix of weighted end-member variables according to the equation Gx - d = R , where G is a matrix of the source water masses, x is the matrix to solve for, which contains the relative contribution of each water mass to the sample, d are observations, and R is the residual fit. 22, 185

pack ice Pack ice is ice that is not attached to land and is therefore unencombered. This ice can be moved by currents and wind. 20, 185

pH pH stands for hydrogen potential nad is defined as the $pH = -\log_{10}([H^+])$. Is is the measure by which we determine a solution in terms of its acidity (or basicity). Seawater is considered to be slightly alkaline, or basic though the pH is dropping, leading to it becoming more acidic, as a result of the uptake of

anthropogenic CO_2. This process is referred to as ”ocean acidification” or ”the other CO_2 problem”. 2, 31, 32, 185

piteraq Piteraq is the Greenlandic name for a katabatic wind that forms across the Greenland Ice Sheet. As air at high altitudes is cooled to very low temperatures across the ice sheet, it becomes more dense and less buoyant and will be transported downslope. This causes high wind speeds, particularly where funnelled through narrow channels such as fjords. 7, 185

polynya A polynya is an area of open water and/or much thinner ice cover than the surrounding area. Several different types of polynyas exist, including latent heat and sensible heat polynyas. 20, 185

water mass Water masses are geographically recognisable bodies of water with a common formation history and geographic region that results in properties, particularly in temperature and salinity, that are distinct from the surrounding water. A water mass is defined by a *TS* curve. 12, 16, 19, 21, 23, 25, 33, 171, 178, 185

water type A water type is a set of co-ordinates on a *TS* diagram that represents an end-member in *TS* space. 19, 171, 172, 174, 178, 185